Characterization of Linked Polymer Solutions (LPS)
– Influence of salinity and divalent ions

Master's thesis

Petroleum Technology – Reservoir Chemistry

Sigbjørn Fitjar Lunestad

Department of Chemistry

uni CIPR

Centre for Integrated Petroleum Research

University of Bergen

June 2011

Acknowledgements

I would like to thank my supervisor Professor Harald Høiland and co-supervisor Professor Arne Skauge, for their guidance and support during the work on my thesis.

I would like to show my gratitude to my co-supervisor Dr. Tormod Skauge for taking much interest in my work, and always being available for discussions and counselling. This thesis would not have been possible without him.

I would also like to thank Maria Nordli for letting me participate in some of her experimental work, giving me valuable experience in both the procedures and the science behind linked polymer solutions.

Furthermore, many thanks to CIPR for lending of laboratories and equipment, for providing me with an office during my two years as a master student, and for all the support and help from both their scientific and administrative staff. A special thanks to Per Arne Ormehaug and Tore Skodvin for help and counselling with the experimental equipment.

Finally, thanks to my family, my friends, and my fellow students at CIPR for believing in and supporting me through my student years.

Sigbjørn Fitjar Lunestad

Abstract

Water flooding with addition of polymers cross-linked by polyvalent ions (LPS) has proven to increase the oil recovery both in field applications and laboratory studies, but with constraints on the brine salinity. With of an offshore LPS-application on the Norwegian continental shelf in mind, this thesis aimed to characterize the pressure build-up mechanisms thought to be responsible for the oil mobilization, for LPS in solvents with high ionic strengths, containing both mono- and divalent ions.

During the present work, LPS solutions of partial hydrolysed polyacrylamide (HPAM) were solved in brines containing 0.5% NaCl, 5% NaCl, and 0.5% $CaCl_2$ + 4.21% NaCl, at a constant polymer concentration of 300ppm, cross-linked by Al^{3+} at a polymer to aluminium ratio of 30:1. The LPS solutions were characterized by viscosity measurements and filter-floods, to investigate the pressure build-up properties of the solutions under variation of injection rates and pore sizes of the filters. The concept of LPS filter-flooding with variation of the flow rates has not been previously reported, thus a new method has been developed, tested, and verified.

The new method has proven reliable and has indentified critical rates (Qc) for a sudden increase in differential pressure during filter-floods of LPS systems for increasing flow rates. Based on a proposed model for shear flow, the increased pressures cannot be explained solely by the shear thickening behaviour of LPS solutions, but is suggested also caused by the Log-Jamming effect, where intra-molecular cross-linked polymer coils accumulate at pore throats, causing local permeability reductions and flow diversion.

The Log-Jamming ability of LPS solutions seems to decrease for higher brine salinity due to enhanced coiling of the polymer molecules. Addition of 0.5% by weight $CaCl_2$ to LPS solutions under constant ionic strength seems to improve the Log-Jamming abilities, probably due to increased number of-, higher density of-, or higher affinity between the cross-linked particles.

Addition of 0.5% by weight $CaCl_2$ to a non-cross-linked polymer under constant ionic strength has proved to give equal pressure build-up properties and Log-Jamming ability as a corresponding LPS solution cross-linked by 10ppm Al^{3+} in a monovalent solvent. Addition of 1.0% by weight $CaCl_2$ under the same conditions has proven to reduce the Log-Jamming

ability, this is suggested due to repulsion between the cross-linked particles caused by oversaturation of the negative sites on the polymer molecules. This indicates that Ca^{2+} may substitute Al^{3+} as cross-linker in LPS solutions, but with a risk of lowered Log-Jamming abilities for sufficiently high Ca^{2+} concentrations.

Nomenclature

3430S	Low molecular weight HPAM polymer
3630S	High molecular weight HPAM polymer
A	Area
a	Outer radius for radial flow
AlCit	Aluminium Citrate
BPR	Back pressure regulator
c	Concentration
C	Celcius
C*	Critical overlap concentration
CBY-model	The Carreau-Bird-Yasuda model
CDG	Colloidal dispersion gel
CeB	Calcium enriched brine
CP-75	Cone plate geometry for rheometer
D	Translational diffusion coefficient
d	Diameter
d(H)	Hydrodynamic diameter
DG-26.7	Double gap geometry for rheometer
DLS	Dynamic light scattering
dP	Differential pressure
dP*	Relative differential pressure
$dP^{*\gamma}$	Shear-dependent relative differential pressure
dP/dr	Radial pressure gradient
DPT	Differential pressure transmitter
EOR	Enhanced oil recovery
HPAM	Partial hydrolysed polyacrylamide, polymer type
I	Intensity
k	Boltzmann's constant
K	Permeability
K'	Power law constant
K_b	Brine permeability
K_H	Huggins constant
LPC	Linked polymer coil
LPS	Linked polymer solutions
mD	MilliDarcy
MDa	MegaDaltons
ml/min	Millilitres per minute
n	Power law exponent
nm	Nanometre

OOIP	Oil originally in place
PDMS	Polydimethylsiloxane, fluid
PFA	Perfluoralkoxy, tubing material
PLM	The Power law model
ppm	Parts per million, mass fraction
PSD	Particle size distribution
PtC-ratio	Polymer to cross-linker-ratio, [ppm/ppm]
Q	Volumetric flow rate
Qc	Critical rate for Log-Jamming
R	Inner radius for radial flow
Rpm	Rounds per minute
RRF	Residual resistance factor
S_{or}	Residual oil saturation
SSW	Synthetic sea water
T	Absolute temperature
TDS	Total dissolved solids
u	Darcy velocity, Q/A
V_{sp}	Specific volume
x-aggregate	Int*er*-molecular cross-linked polymer molecule
x-coil	Int*ra*-molecular cross-linked polymer molecule
$\emptyset$	Porosity

Greek letters

α	Shift factor for estimation of γ_{pm}
γ	Shear rate
γ_{pm}	Shear rate in porous media
λ	Time constant in the CBY-model
μ	Newtonian- or bulk viscosity
μ_0	Zero shear viscosity
μ_∞	Infinite shear viscosity
$\mu_{(\gamma)}$	Shear dependent viscosity
$\lvert\eta\rvert$	Intrinsic viscosity
η_{sp}	Specific viscosity
τ	Shear stress

Table of contents

1. Introduction

Linked Polymer Solutions or LPS are defined as dilute aqueous solutions of cross-linked polymer molecules. In the literature, they are known as *Colloidal Dispersion Gels*[1, 2] *(CDG)*, *Intra-Molecular Cross-linked Polymers*[3], or *Microgels*[3, 4]. CDGs and microgels concerns cross-linked polymer solutions within a wide range of concentrations, intended for water shut-off by permanent permeability reduction in the near-well regions. The basic idea is that the CDGs will flow as a viscous solution above a certain differential pressure, called the transition pressure [5]. As the flow rates decreases away from the injector and the differential pressure drops below the transition pressure, the CDG will act as a gel, effectively blocking pores. Polymers used in CDG are typically high polymer weight and with a high degree of hydrolysis, to achieve the necessary gel strength for water shut off[6]. The LPS system is also made up by a polymer and a cross-linker, but has a different aim for the purpose when inside the reservoir. The LPS should not form a gel phase before injection, but form nano-sized particles that propagates through the porous media[7]. By accumulation at the pore throats, the particles generate local permeability reductions, leading to flow diversion on a microscopic level. The accumulated particles may separate and propagate through the reservoir, making LPS-injection a dynamic process. The particle accumulations may give an increased oil recovery beyond that of a non cross-linked polymer, without generating high differential pressures as with CDG injection[6]. For this thesis, the term LPS will be used for cross-linked polymer solutions with polymers concentrations ranging from 100 up to 1000 ppm (mass to mass concentrations).

When describing a LPS solution, the nomenclature *polymer concentration in ppm/ aluminium concentration in ppm / solvent NaCl concentration in percent,* will be used. For calcium enriched brines, the abbreviation *CeB* is added, followed by the concentration of $CaCl_2$ and NaCl in mass percent. Table 1.1 shows examples of both cases:

Table 1.1: *Examples of the nomenclature used to describe LPS solutions. Concentrations are given in mass to mass parts per million or percent.*

Nomenclature	**Concentration**			
	Polymer	**Al^{3+}**	**NaCl**	**$CaCl_2$**
	[ppm]	**[ppm]**	**[%]**	**[%]**
300/10/0.5	300	10	0.5	0
300/10/CeB 0.5/4.21	300	10	4.21	0.5

To distinguish between particles in polymer and LPS solution, the terms *coils* and *aggregates* will be used to describe non-cross-linked particles, while *x-coils* and *x-aggregates* refers to intra-molecular- and inter-molecular cross-linked particles, respectively. The term *brine* is used for distilled water with additions of ions, i.e. all solvents used for the LPS/polymer solutions prepared for this thesis.

1.1 Objective

The Log-Jamming effect has been proposed as the major mechanism for oil mobilization during LPS laboratory core floods[7]. This thesis aims to investigate the Log-Jamming abilities of LPS solutions of HPAM, in both high- and low salinity brines, containing both mono- and divalent ions. The Log-Jamming abilities were investigated by filter-flooding experiments under variation of the flow rate. Viscosity measurements were also applied to provide a more comprehensive foundation for interpretation of the results.

Filter-floods of LPS solutions under variation of flow rate have not been previously reported, thus the experimental work also included the development and implementation of a novel method for operational procedures and interpretation of the obtained data.

The experimental work has been performed with a constant polymer concentration of 300ppm and a polymer-to-aluminium ratio of 30:1. Two different HPAM polymer types have been used to detect the influence of polymer molecular weight. The LPS solutions have been solved in three different brines, containing 0.5% NaCl, 5% NaCl, and a calcium enriched brine containing 0.5% $CaCl_2$ + 4.21% NaCl. The two NaCl brines are applied to characterize the impact of low versus high ionic strength by monovalent ions. The calcium enriched brine has equal ionic strength as 5% NaCl, and should therefore provide information regarding pressure build-up properties for LPS under constant ionic strength, but in the presence of divalent ions.

The LPS systems have been filter-flooded for several filter sizes to investigate if the trends are reproducible for different porous media. The corresponding non-cross-linked polymer solutions have been filter-flooded for selected parts of the experimental ranges for comparison with the LPS solutions.

2 Theory and background

2.1 Linked Polymer Solutions (LPS)

The polymer molecules in a LPS are cross-linked by a polyvalent ion. For this thesis, the polymer and cross-linker of choice are partially hydrolyzed polyacrylamide (HPAM) and Aluminium Citrate (AlCit). Several other polyvalent ions like Cr^{3+}, Fe^{3+} and Zr^{4+} may be used for cross-linking, but previous work on LPS are only performed using AlCit[1, 2, 7] due to its high valence and favourable environmental classification. The cross-linking occurs between the dissociated hydrolyzed monomer on the polymer molecule, and the metal ion. One aluminium ion may react with several carboxylate groups on the same polymer molecule (Intra-molecular bonding/x-coils), or with carboxylate groups on more than one polymer molecules (Inter-molecular bonding/x-aggregates).

LPS consists of a polymer and a cross-linker. The polymer concentration is usually ranging from 100 to1000ppm, with polymer to cross-linker (PtC)-ratios ranging from 10:1 to 100:1. When dilute solutions of polymer and cross-linker are mixed, both intra-molecular and/or inter-molecular bonds may be formed.

The applied cross-linker Aluminium Citrate (AlCit) is complex with respect to its molecular structure. Depending on factors like pH, temperature and ionic concentration of the solvent, several molecular compounds may be formed, containing Al^{3+} and Cit^{2-} at different molar ratios. Figure 2.1.1 shows one of the possible molecular structures of AlCit in the solid state. The properties of the AlCit compound applied for this thesis is described in section *3.1.1 Salts.*

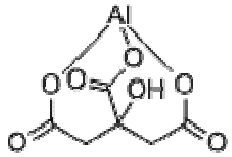

Figure 2.1.1: *Molecular structure of Aluminium Citrate (* $C_6H_5AlO_7$*) in solid state (www.chemicalbook.com).*

As the AlCit is solved in water, the compounds may disassociate into aluminium and citrate ions. It is not known whether the reactive species towards HPAM is the Al^{3+} ion or the AlCit complex. It is, however, known that the presence of the citrate ligand is a prerequisite for a slow rate of cross-linking in polymer solutions[8]. The dissociation of an AlCit compound may be described by the general (unbalanced) formula:

$$AlCit \leftrightarrow Al^{3+} + Cit^{2-} \qquad \textbf{(2.1)}$$

When mixed with a HPAM solution, the Al^{3+} ions or/and the AlCit complexes may react with the carboxylate groups on the polymer molecules, forming LPS.

$$\text{Cross-linker} + \text{HPAM} \leftrightarrow \text{LPS} \qquad \textbf{(2.2)}$$

The two proposed equilibriums shown by Formulas 2.1 and 2.2 suggest that the majority of aluminium is either in the form of an AlCit complex ion, or bound to polymer molecules. Hence, the citrate may be thought of as a "storage", ensuring a slow release of cross-linkers to the polymer solution. A rapid release of free aluminium to polymer solutions is known to cause premature and inconsistent gel formation in CDG applications[8].

Whether the LPS is dominated by intra- or inter-molecular bonds is dependent upon several factors, including polymer type and concentration, PtC-ratio, solvent salinity and cross-linking temperature[7]. Three regimes with possible mechanisms for the formation of intra- and inter-molecular bonds are shown in Figure 2.1.2.

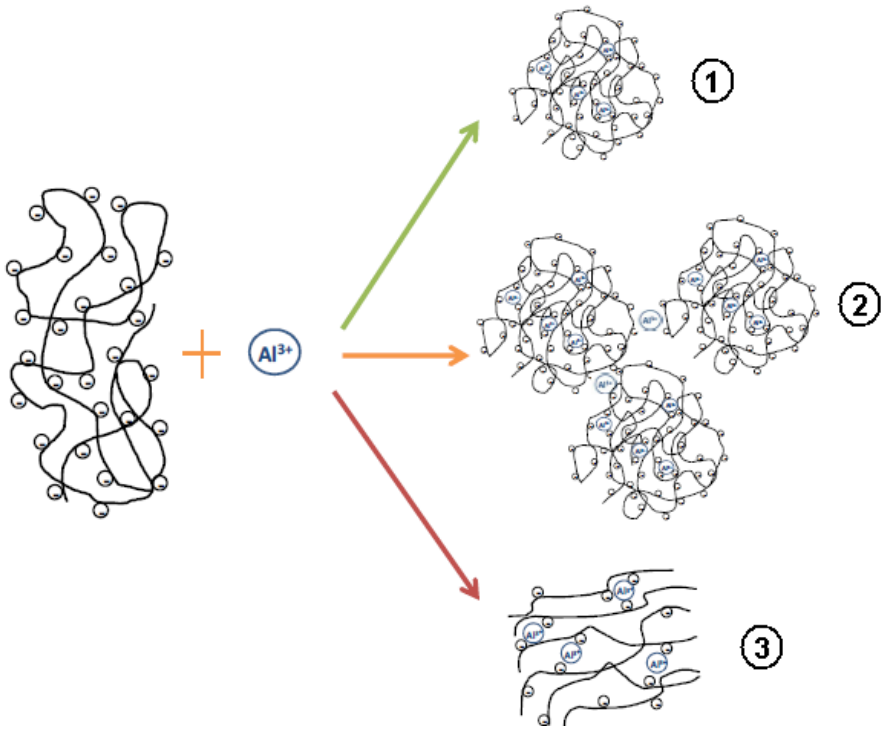

Figure 2.1.2: *Different regimes for cross-linking (Skauge et al.[6]).*

1) In dilute solutions, intra-molecular bonding is favoured, as the aluminium ion reacts with multiple carboxylate groups on the same polymer molecule. This causes the polymer molecules to coil up independently, creating dispersed particles of finite size, with no connectivity.

2) In semidilute solutions, a combination of intra- and inter-molecular bonds will dominate. The inter-molecular bonded aggregates may be made up of intra-molecular bonded coils.

3) In concentrated solutions above the critical overlap concentration, inter-molecular bonding will dominate[9], resulting in large aggregates and a continuous network may be formed. The network is created when one aluminium ion bonds with more than one polymer molecule.

LPS systems intended for reservoir flooding requires that the reaction between polymer and cross-linker predominantly forms intra-molecular bonds. Otherwise, the aggregates and gel phases may result in plugging of the reservoir and/or high injection pressures[6]. The most

important factor regarding the formation of inter- or intra-molecular bonds are the critical overlap concentration C*[10]. The C* is defined as the concentration at which below, the interactions between molecules are very small[11]. Above C* the polymer molecules tends to aggregate, while they can be seen as individual units below C*. Several additional factors have been reported to shift the equilibrium in the cross-linking reaction towards intra-molecular bonding; i) Low concentration of free aluminium ions in solution[1], ii) Low polymer concentration[1], iii) High PtC-ratio[12], iv) Lower polymer molecular weight[10], v) High temperature and brine salinity [13].

The magnitude of the PtC-ratios, and "dilute", "semidilute" and "concentrated" with respect to polymer concentrations depends on the salinity of the solvent, since the ionic strength will influence the polymer conformation and affect the critical overlap concentration. Solved in distilled water, the polymer molecule will have a free conformation, i.e. expanded, because of repulsion between the negative charged carboxylate groups. Addition of ions to the solution will screen the charges of the hydroxyl groups, thus reduce the expansion of the polymer molecule. Bjørsvik et.al.[9] measured the electrophoretic mobilities for 600 ppm HPAM solutions with a 10:1 PtC ratio solved in 0.5 and 5% by weight NaCl, and SSW respectively. All the solutions had negative mobilities, suggesting that the particles where negatively charged and that the conformation of the polymer molecules where dependent upon ions in the solvent. The higher salinity, the lower the negative mobility, since a higher concentration of counter-ions will screen more effectively. The authors also measured particle size by dynamic light scattering, before and after a dialysis that removed all added salt and excess AlCit. It appeared that the polymer coils and aggregates maintained the same size regardless of the removal of salts, suggesting that once formed, LPS particles are stable over a considerable time.

The valence of dissolved ions may also be an important factor regarding the polymer conformation and the critical overlap concentration. Addition of polyvalent ions may not only increase the ionic strength of the solution, but may also cross-link the polymer molecules without addition of a dedicated cross-linker.

2.2 LPS for Enhanced Oil Recovery (EOR)

Lake (1989) defines Enhanced Oil Recovery (EOR) as "*... oil recovery by the injection of materials normally not present in the reservoir*"[14]. Such materials can be among others polymers, which are added to the injection water to improve the mobility ratio, thereby increasing the recovery. Polymer flooding is primarily applied in very heterogeneous reservoirs, or reservoirs containing high-viscous oil.

Permeability control in the near-well (production side, radius > 50m) area by injection of CDG has proven to increase the volumetric sweep efficiency and contribute to an increased recovery[1, 15].

Studies of LPS as an aid for permeability control for water cut reduction, both in the near-well area and in-depth, have been reported since the mid-90s. Mack and Smith[1] presented the first field results from a nine year campaign on 29 oil fields in the Rocky Mountains. They defined colloidal dispersion gels (CDG) as aqueous solutions with a polymer concentration ranging from 100-1200ppm, and a polymer to aluminium ratios between of 100:1 to 20:1. At these concentrations a continuous network cannot form like in a bulk gel. Instead, a solution of separate gel bundles form, primarily due to intra-molecular cross-linking. The field results showed success in 22 of 29 projects, with an increased oil recovery (% OOIP) of 1.3 to 18.2, and reduced water production. Based on the unsuccessful cases, the authors claim that CDG systems should not be applied when the injection water exceeds 25.000 mg/L total dissolved solids.

Li et al.[10] investigated the size and the conformation of linked polymer coils (LPCs) by measuring dynamic light scattering, studying dried up drops of LPS using a scanning electron microscope and filtrating diluted LPS systems through a micro-porous membrane. The authors found that LPCs was spherical and had a more rigid conformation than coils in a normal polymer solution, giving them better abilities to plug membranes compared to a normal polymer coil. When the polymer concentration in a LPS system was below a minimum value, the hydrodynamic radius of the LPC increased with higher molecular weights of the polymer. When the molecular weight of the polymer is fixed, the radius of the LPC is determined by the polymer concentration. The radius of the LPC increases with the polymer concentration, as long as it is below the critical overlap concentration. The mean

hydrodynamic radii of the LPCs were found to range between 199 and 610 nm for different polymers at concentrations between 10 and 600 ppm**.**

A standard method for determining LPS properties is viscosity measurements. Bjørsvik et al.[16] compared 600 ppm HPAM solutions with 600 ppm LPS systems at a polymer to aluminium ratio 10:1, at different solvent salinities and as a function of time. Successful experiments were conducted with salinities ranging up to 5000 ppm NaCl. The author found that the viscosities for the LPS system where lower than that of the corresponding HPAM solutions. However, the relative viscosity differences decreased with increasing solvent salinity. After a cross-linker was added, the viscosity dropped immediately, and a continuing slow viscosity decrease was observed for 15 days before stabilizing. Since the viscosity stabilized, the decrease was not likely to be due to polymer disintegration. The authors proposed instead, that the initial cross-linking happens quickly, forming polymer coils by intra-molecular bonding. Over the following 15 days, the bonds are rearranged to form inter-molecular bonds, i.e. aggregates of polymer coils. The relative viscosity decrease over time was as expected lower for the highest salinity, since high salt concentration promotes the formation of polymer coils[11].

Arraa et al.[17] measured the particle size in 600 ppm LPS systems with a fixed aluminium concentration of 30 ppm, and with salinities between 0.2 and 5% NaCl. Three different HPAM polymers were measured, and they found the average particle size ranging from approximately 20 to 50 nm, depending on the type and solute salinity.

Wang et al.[18] measured viscosity and flow performance for the polymer concentrations 500, 600 and 700 ppm, varying the cross-linker concentration, temperature, and electrolyte composition as well as the concentration. This was performed to determine critical conditions for the formation of intra-molecular cross-linking in the LPS solutions. They found that even though both are divalent, Ca^{2+} was more likely to enhance intra-molecular bonds than Mg^{2+}. They concluded that intra-molecular bonds are more likely to be formed when the concentration of electrolytes are high, cross-linker concentration is high, and at higher gelling temperatures.

Ryles[19] investigated the effects of the presence of divalent ions in HPAM solutions. The author found that under extreme conditions, divalent ions could cause phase separation, i.e. gels or precipitates. It was also reported that high molecular weight HPAM was more

sensitive to divalent ions, and that Ca^{2+} has a greater detrimental effect on solution viscosity than Mg^{2+}.

Smith et al. [20] investigated the possibility of using in-depth CDG to improve recovery from the Daqing oil field in China. The experimental work included screening tests to find the best polymer type and formulation, followed by core flooding to monitor the recovery performance. The results showed that CDGs had the same injectivity as non cross-linked polymers in synthetic cores with permeabilities of 1 to 3 Darcy, for flow rates ranging from 0.05 to 4 ml/min. Injection of CDG recovered 9.6% OOIP more oil than non cross-linked polymer in the core floods. The adsorption of polymer from the CDG floods where found to be higher than those of the non cross-linked polymers. They also observed that aluminium retention occurred, verifying that the aluminium stays inside the core with the adsorbed CDG. They experienced no plugging of the cores. The final conclusion was that in-depth CDG was a viable technology for enhanced recovery at the Daqing oil field.

Spildo et al.[7] conducted LPS flooding on cores from a North Sea oil field. The cores was saturated with oil before water flooded down to residual oil saturation, and finally flooded with LPS. All experiments showed a significant reduction of residual oil saturation, ranging from a 19 to 61% reduction. The trend was that cores with the highest permeability showed highest improvement. They suggest that the increased recovery is mainly caused by increased microscopic diversion as LPS particles block pores and pore throats, the so called Log-Jamming effect, as shown in Figure 4.4.1. Since LPS has a higher viscosity than the initial water flood, they do not preclude that the more favourable mobility ratio may be partly responsible for the increased recovery. However, based on the relative pressure build-up during LPS injection versus reduction in residual oil saturation for each core, pressure build-up caused by the viscous contribution did not seem to be a necessary condition for additional recovery.

Spildo et al.[21] investigated the retention and propagation of polymer and aluminium during flooding of Berea sandstone cores. LPS systems at a 20:1 polymer to aluminium ration were injected, as well as pure polymer- and aluminium solutions. The results showed that LPS propagated through the cores with no chromatographic separation between polymer and aluminium. The effluent had a notably higher polymer to aluminium ratio than the injected LPS, which indicated an excess of aluminium at the injected ratio, 1:20. The retention of HPAM was found to be slightly lower in LPS compared to that of a pure polymer solution.

During recent years, reports from field applications of LPS have been published. Chang et al. [2] reported from a CDG pilot project at the Daqing Oil Field conducted in 1999. The authors found that CDG systems can be applied before, after or during a conventional polymer flood, thereby controlling water production and maintaining high oil rates. Chemical cost was lower compared to conventional polymer flooding, and the produced water was cheaper to dispose due to lower polymer concentrations. The authors stated that CDG systems have a wide application in heterogeneous reservoirs to improve water flooding efficiency and oil recovery.

Diaz et al.[22] reported preliminary results from a CDG pilot at the mature Loma Alta Sur oil field in Argentina. Due to the heterogeneity in the reservoir, conventional polymer flooding was not an option. The aim was to reduce water channelling in the high permeability zones, and as a secondary benefit increase the mobility ratio. The results from the first CDG injection phase indicated a clear oil response and a lowered water-oil ratio (WOR). No significant operational problems where encountered during the fourteen months of injection, and the projected improved oil recovery after the second injection phase was 2.9% OOIP.

Skauge et al.[23] compared oil mobilisation properties in water wet Berea cores by injection of several fluids. They compared nano-sized silica particles, nano-sized silica particles dispersed in a polymer solution, polymer solutions, and nano-sized LPS particles, which provided data to evaluate the importance of viscoelastic properties with respect to increased recovery. The results showed that silica particles propagated through the porous media, but did not mobilize oil. When dispersed in a polymer solution, silica particles mobilized oil equal to about 20% reduction in S_{or}. Pre-generated nano sized LPS particles mobilized oil in cores where polymer and silica particles failed.

Nordli[24] investigated the properties of LPS systems in synthetic seawater (SSW) compared those in 0.5%wt NaCl. The author found that polymer solutions in SSW showed little difference regarding viscosity and pressure build-up over a filter when AlCit cross-linker was added at a 30:1 PtC ratio. This indicated that divalent ions in SSW will cross-link polymers by themselves. Particle size measurements by DLS indicated that the size of aggregates in the LPS systems was constant, regardless of polymer concentration.

Skauge et al.[6] estimated the feasibility of LPS flooding at an offshore North sea oil field, based on a compilation of previous papers and recent experimental work. Both the science regarding LPS systems as well as the operational topside challenges were discussed. The

authors concluded that LPS systems can be handled offshore, and that the cross-linker concentration may be reduced for brines with high concentrations of divalent ions.

2.3 Polymer rheology

2.3.1 Non-Newtonian behaviour

Viscosity is a measure for a fluids resistance to deform when under influence of an external force. It is not a fixed value, and depends on the fluids nature, temperature and the amount of force applied. The viscosity is defined as:

$$\mu = \frac{\tau}{\gamma} \qquad \textbf{(2.3)}$$

Where μ is the viscosity, τ is the shear stress, and γ is the shear rate.

Fluids can be divided into several classes based on their behaviour compared to the shear rate applied. A flow chart is a plot of shear rate versus shear stress, and can be used to determine which class a certain fluid belongs to. For Newtonian fluids, the viscosity is independent of the shear rate, i.e. $\frac{\tau}{\gamma}$ are constant. Typical examples of Newtonian fluids are water, mineral oils and very thin suspensions[25], but the vast majority of fluids are non-Newtonian. HPAM solutions are known to exhibit non-Newtonian behaviour during shear flow, which means that the viscosity is dependent upon the shear rate[11]. Figure 2.3.1 shows a typical flow curve for a dilute polymer solution, with 4 distinct regions;

1) The Newtonian region: The viscosity is constant, i.e. independent of the shear rate. This behaviour can be interpreted as that the shear forces are not high enough to break the equilibrium structure of polymer molecules in the solution, caused mainly by inter-molecular association.
2) The shear thinning region: The viscosity is decreasing for increasing shear rates. Above a certain shear rate, the shear forces start to break up the equilibrium structure and un-coils the molecules, resulting in reduced number of associations between the polymer molecules[26]. This results in a decreased viscosity as more and more the particles are un-coiled and aligned with the flow direction.
3) Bottom point of the shear thinning region: The viscosity is at its lowest as the polymer molecules are at their most aligned conformation.

4) The shear thickening or dilatant region: The viscosity is increasing with the shear rate. This behaviour can be interpreted as elastic stretching and the following relaxation of the already aligned LPS/polymer particles. This phenomenon is also known as the viscoelastic effect.

For sufficiently high shear rates during flow in porous media, another shear thinning region can occur due to mechanical degradation by rupture of the polymer molecules. This region is not discussed for this thesis because this kind of degradation is not significantly occurring within the experimental ranges as discussed in section *4.3 LPS-Characterization by high shear rheology*.

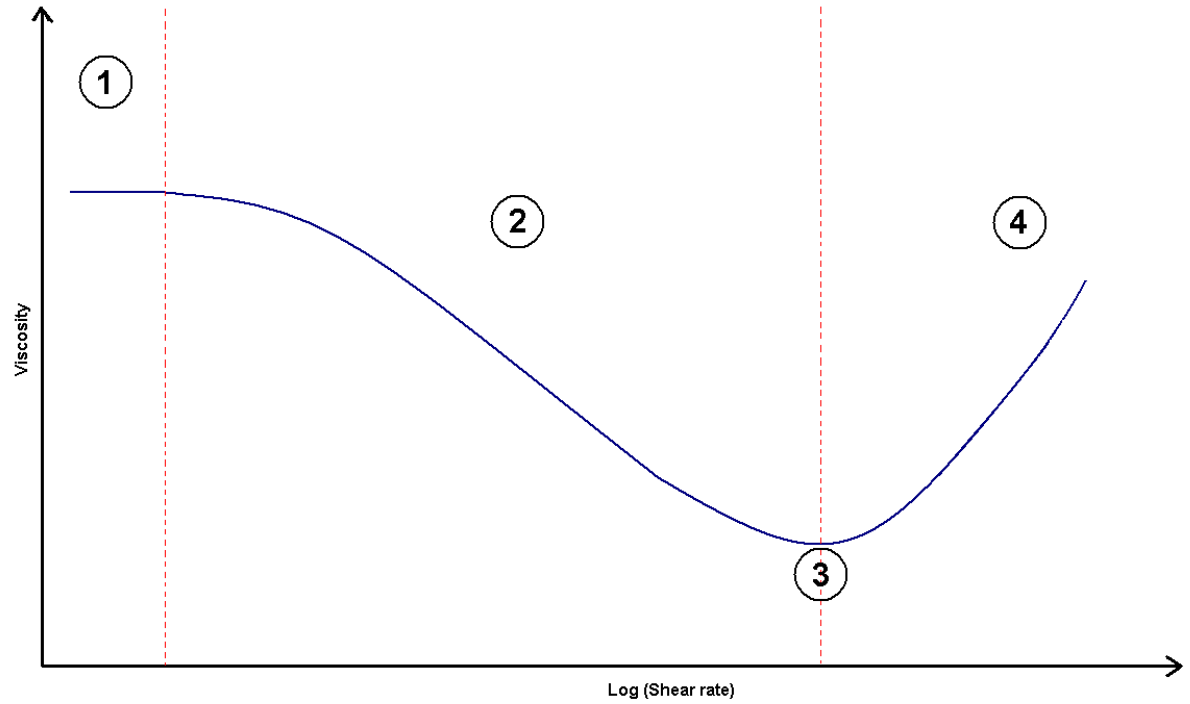

Figure 2.3.1: *Schematic viscosity curve of a polymer solution as a function of shear rate, each number represents a specific region.*

For an EOR application involving injection of LPS/polymer, the ideal scenario would be shear rates around region 3 in the near-injector area, and shear rates in the left part of region 2 during transport through the reservoir, as the flow rates decline away from the injector. This would result in the ultimate injectivity, as well as the highest possible viscosity during oil displacement inside the reservoir.

2.3.2 Models for shear flow

Various mathematic models have been proposed to describe the shear rate dependence of non-Newtonian fluids. The most commonly encountered model is the Power Law Model (PLM), which describes the shear thinning region of shear flow[11]. The PLM is given by the expression:

$$\mu(\gamma) = K'\gamma^{n-1} \qquad \textbf{(2.4)}$$

Where μ is the shear dependent viscosity, γ is the shear rate, and *K'* and *n* are empirical constants. The constant *n* is also known as the Power Law index. For a Newtonian fluid, *K'* is the constant viscosity, and *n* is unity. For a non-Newtonian fluid in the shear thinning region, $n < 1.0$. The PLM is not applicable outside the shear thinning region and can hence not be used for sufficiently low or high shear rates.

A more satisfactory model for wider shear rate ranges is the Carreau-Bird-Yasuda model (CBY), given as:

$$\mu(\gamma) = \mu_\infty + (\mu_0 - \mu_\infty)[1 + (\gamma\lambda)^2]^{\frac{n-1}{2}} \qquad \textbf{(2.5)}$$

Where $\mu(\gamma)$ is the shear dependent viscosity, μ_∞ is the infinite shear viscosity, $\mu_0$is the zero-shear viscosity, γ is the shear rate, λ is a time constant, and *n* is the Power Law index. λ can be estimated by the approximation $\gamma_c = 1/\lambda$, where γ_c is the critical shear rate for the transition between the Newtonian- and the shear thinning regime as shown on Figure 2.3.1 Even though it has been reported to give a better fit to empiric data, the CBY requires four parameters compared to the PLM's two. The CBY model neglects the shear thickening region and has a negative slope until μ_∞.

Extended models have been proposed to also include the shear thickening region. However, these models involves more parameters, and therefore demands precise input data over a wide range of shear rates to give accurate output.

2.3.3 Intrinsic viscosity and Huggins constant

The most import quantity regarding the viscosity in dilute solutions is the intrinsic viscosity$|\eta|$. It is a measure for the solute's contribution to the solutions viscosity, and is defined as[11]:

$$|\eta| = lim_{c\to 0}\frac{\eta-\eta_s}{\eta_s \cdot c} = lim_{c\to 0}\frac{\eta_{sp}}{c} \qquad \textbf{(2.6)}$$

Where η is the solution viscosity, $\eta_s$is the solvent viscosity, c is the polymer concentration, and η_{sp} is the specific viscosity.

M.L Huggins suggested today's most widely used method for extrapolation of $|\eta|$ from viscosity measurements in 1942:

$$\eta_{sp} = |\eta|c + k_H|\eta|^2c^2 \qquad \textbf{(2.7)}$$

Where η_{sp} is the specific viscosity, $|\eta|$ is the intrinsic viscosity, k_H is Huggins constant, and c is the polymer concentration.

The Huggins constant characterizes the hydrodynamic interactions between dispersed particles during shear flow. If the interactions are neither attractive nor repulsive at short distances, the Huggins constant depends only on the particle conformation in solution. For polymer solved in neutral solvents, k_H≈ 0.5. For polymers in good solvents, k_H≈0.3, while it is known to decrease down to about 0.1 - 0.2 for fractal objects as microgels in good solvents. "Good" solvents means in this perspective that the particles are repulsive at very short distances[27].

Several models for estimation of the critical overlap concentration, C*, directly from the intrinsic viscosity has been suggested. Sorbie[11] suggested that the critical overlap concentration could be estimated by the expression $C^* = \frac{1}{|\eta|}$, while Chauveteau[28] suggested that the relationship was $C^* = \frac{0.7}{|\eta|}$.

2.4 Particle size measurements by Dynamic Light Scattering (DLS)

Particles suspended in a solution undergo constant random movement caused by collisions with the solvent molecules surrounding them. Given the same solvent, small particles will have a more rapid movement than large particles, since collisions with solvent molecules will have larger impact the smaller the suspended particles are. The movement is called Brownian motion as shown in Figure 2.4.1, and makes the basis for particle size measurements by dynamic light scattering (DLS).

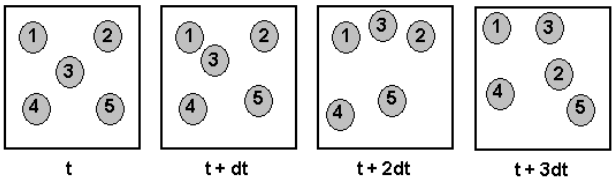

Figure 2.4.1: *Brownian motion of suspended particles (*redrawn from Nordli[24])

The velocity of the Brownian motion is defined by the translational diffusion coefficient D, and the particle size is calculated using the Stokes-Einstein equation:

$$d(H) = \frac{kT}{3\pi\mu D} \qquad (\mathbf{2.8})$$

Where *d(H)* is the hydrodynamic diameter, *D* is the translational diffusion coefficient, *k* is Boltzmann's constant, *T* is the absolute temperature, and μ is the viscosity.

It is important to note that the diameter given by the Stokes-Einstein equation is the *hydrodynamic* diameter, which refers to a value for how a particle diffuses within a fluid. The diameter obtained in a DLS measurement corresponds to the diameter of a sphere with the same translational diffusion coefficient as the particle in the solution. The diffusion is also dependent on the surface structure, concentration and the type of ions present. Presence of ions in the solution will determine the thickness of the electric double layer, or Debye length, surrounding the particles. A low conductivity medium will give a thicker layer, which will result in a reduced diffusion speed, and a larger apparent hydrodynamic diameter will be measured. Vice versa, a high conductivity media will result in a smaller apparent hydrodynamic diameter. The Rayleigh approximation, $I \propto d^6$, states that the intensity *I* of the reflected light is proportional with the particle diameter *d* in the sixth power. In other words, a 10nm particle will scatter one million times more light than a 1nm particle. This means that

the scattered light from larger particles in a polydisperse solution may wipe out the scatter from smaller particles due to the extreme difference in intensity.
Particle measurement by DLS works by comparing the “image” of the scattered light over time. If there is no change in the “image” over a certain time interval *dt* as shown in Figure 2.4.1, no Brownian motion is observed and perfect correlation is achieved. Since large particles moves slower than small particles, the correlation over time will be higher for larger particles. Based on the correlation over time, the Zetasizer’s corresponding software calculates the hydrodynamic diameters of the particles.

A prerequisite for valid particle size measurements using DLS is constant temperature to avoid convection currents that will cause irregular particle motion. The viscosity of the dispersant has to be known, and are also temperature dependent. DLS measurements on polymers and Linked Polymer Solutions can be challenging due to their high polydispersity.

3 Experimental

3.1 Chemicals

3.1.1Salts

For preparation of saline LPS solutions, polymer solutions and the corresponding brine solutions, sodium chloride and calcium chloride salts were applied. The cross-linker solutions were prepared with aluminium citrate salt. Properties of all the applied salts are shown in Table 3.1.1.

Table 3.1.1: *Properties of salt used for experimental solutions.*

Type	Manufacturer	Purity [%]
Calcium Chloride dihydrate	Riedel-de Haën, Germany	≥99
Sodium Chloride	Sigma-Aldrich, Switzerland	≥99,5
Aluminium Citrate	Dr. Paul Lohmann, Germany	Chemical pure

The aluminium content of the applied Aluminium Citrate salt is measured to 8.8% by weight by ICP-AES (Inductively Coupled Plasma – Atomic Emission Spectroscopy)[24]. This corresponds to approximately a 1:1.5 molar relationship between Al^{3+} and Cit^{2-}.

3.1.2 Polymers

The polymers used for all LPS solutions and polymer solutions were the Flopaam partial hydrolyzed polyacrylamide (HPAM) manufactured by SNF Floerger, France. Both polymers were assumed to have a 10% water content, i.e. a purity of 90%. Table 3.1.2 shows the properties of the two Flopaam types used.

Table 3.1.2: *Properties of applied HPAM polymers.*

FLOPAAM HPAM Polymers		
Product name	**Appr. Molecular weight [MDa]**	**Hydrolysis degree [mole %]**
3430S	12	25-30
3630S	20	25-30

3.1.3 Reference fluid for viscosity measurements

For reference viscosity measurements on the Rheometer, a polydimethylsiloxane solution manufactured by Sigma-Aldrich has been applied. Note that the viscosity provided by the manufacturer as shown in Table 3.1.3 is the kinematic viscosity.

Table 3.1.3: *Properties of the reference fluid for viscosity measurements.*

Reference fluid for viscosity measurements		
Type	Manufacturer	Viscosity [cSt]
PDMS200	Sigma-Aldrich, Switzerland	5 (25°C)

All applied chemicals were used as received.

3.2 Experimental fluids

3.2.1 Solvents – Brines

Table 3.2.1 presents the composition and ionic strength of the brines used as solvents for the applied LPS/polymer systems. Ionic strengths are presented in moles ions/kg solution as this is more expedient and does not require precise density measurements of the solutions.

Note that the 5% brine, and both the calcium enriched brines (CeB) have an equal ionic strength.

Table 3.2.1: *Compositions and ionic strengths of applied brines*

Nomenclature	**Content [% by weight]**		**Ionic strength [mol/kg solution]**
	NaCl	**$CaCl_2$**	
0.5 %	0.50	0.00	0.086
5 %	5.00	0.00	0.856
CeB 0.5/4.21	4.21	0.50	0.856
CeB 1.0/3.42	3.42	1.00	0.856

.

Stock solutions of 2 to 10 times the final concentrations was prepared by weighing in the required amounts of salt and dilute to the desired concentration with distilled water. The solution were left for heavy stirring over night, and then filtered through a 0.45µm membrane filter using a vacuum pump. During this step, particulate impurities that could affect the filter performance were removed, and any undissolved salt was revealed visually. Stock solutions were then diluted with distilled water until desired concentration, and left over night for mixing. The diluted brines were made in batches of 2 to 10 kg and stored in 10 L plastic cans at room temperature.

3.2.2 Polymer solutions

Stock solutions of HPAM were prepared by mixing dry polymer granulate with a 0.5% NaCl solution. To ensure sufficient stirring, a Heidolph rack-mounted overhead mixer was used instead of a magnetic stirrer. The mixer propeller was custom made by the polymer manufacturer, with rounded blades to avoid unwanted shear. The standard concentration for a stock solution was 5000 ppm, and stock solutions were prepared by the following procedure:

1) HPAM granulate and the 0.5% NaCl solution was weighed in separately, onto a weighing tray and a 800 ml beaker respectively.
2) The beaker was placed on jack plate and placed under the Heidolph mixer. The propeller should be centred in the beaker, approximately 2.5 cm above the bottom. The mixer was set to 600 rpm, and a vortex without stagnant air bubbles should appear.
3) HPAM granulate was poured slowly into the vortex without contacting the propeller shaft. A rate of approximately 0.5 g granulate per minute proved to be adequate.
4) The mixer ran for 12 to 24 hours mixing at 600 rpm, before the solution was transferred to a Duran flask. Stock solutions were stored without stirring, but a Parafilm seal on the flask was applied.

Note that all HPAM stock solutions was prepared using a 0.5% NaCl solution as solvent, even though they were intended for diluted polymer/LPS solutions with different salinities and/or salt compositions. This was done because higher salinities may result in

precipitation of polymer molecules due to saturation of the anionic sites[11], and the presence of divalent ions could lead to cross-linking and gel formation in the stock solutions.

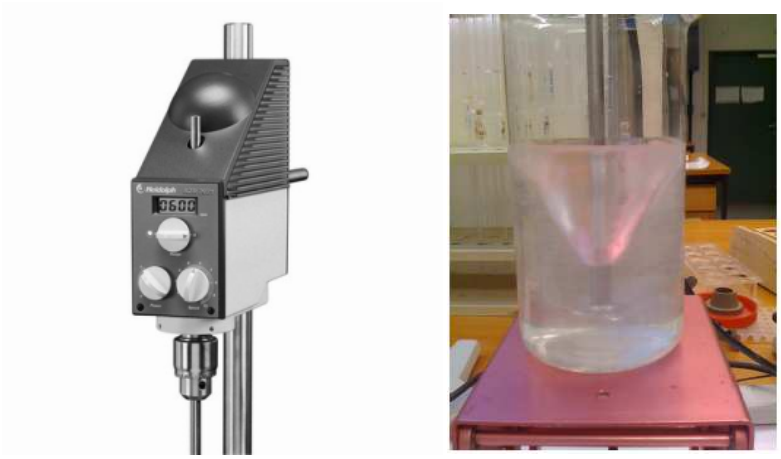

Figure 3.2.1: *Right: Heidolph mixer, Left: Mixing of HPAM stock solution.*

The preparation and handling of diluted polymer solutions differed slightly based on their solvent composition. For polymer solutions in 0.5% NaCl, HPAM stock solutions were diluted with 0.5% NaCl and stirred for two hours. The solution was then left for at least 24 hours before use. For polymer solutions in 5% NaCl and calcium enriched brines, the mixing procedure became more complex since the HPAM stock solution was solved in 0.5% NaCl. The amounts of the required salts were calculated using an Excel spreadsheet, and the different salt solutions were added to the HPAM stock solution in a sequence that prevented the salt concentrations in the pre-mix to exceed those of the final concentration. Due to greater risk of precipitation in high salinity brines, the final mixtures were gravity filtered through a 25µm filter before stirred sufficiently for two hours. Polymer solutions solved in CeB may experience cross-linking because of the divalent Ca^{2+} ions. Thus these solutions were left for at least three days to ensure complete cross-linking before use.

All polymer solutions were stored at room temperature in Duran flasks with Parafilm seals and continuously stirred gently. The solutions were considered usable for seven days after mixing. Prior to an experiment, the solutions were gravity filtered through a 40µm filter to remove precipitations and/or microgels.

3.2.4 Aluminium Citrate solutions

The standard for aluminium citrate stock solutions was 5000 ppm, solved in 0.5% NaCl. At this concentration the mixture is a suspension, and particles will settle when not stirred. The solution was therefore always stirred properly before used to prepare LPS solutions. As with the HPAM stock solutions, all AlCit solutions were prepared with 0.5% NaCl as solvent regardless of the salinity and salt composition in the LPS system they were intended for. By using the same solvent in both kinds of stock solutions, calculations of salt quantities when preparing 5% NaCl and calcium enriched polymer/LPS solutions were simplified.

3.2.5 Linked Polymer Solutions

Two methods were proposed for preparation of the linked polymer solutions;

A) HPAM stock solution is diluted to desired concentration without AlCit. AlCit is then added drop wise into the HPAM solution under heavy stirring until desired concentration is achieved. The solution is heavy stirred for two hours after mixing, and then gentle stirred for approximately three days before use.

B) HPAM and AlCit stock solutions are diluted separately to twice their respective desired concentration. The two diluted solutions are then mixed 1:1 which results in a final concentration equal to one half of the initial. The solution is sufficiently stirred for two hours, and then gentle stirred for approximately three days before use.

As with the polymer solutions, LPS solutions in 5% NaCl and calcium enriched brines were gravity filtered through a 25µm filter before the cross-linker was added to remove precipitates.

Viscosity measurements by the MCR-300 Rheometer, particle size measurements by DLS, and filter-floods would provide experimental data for a total review.

Two 600/20/0.5 LPS solutions where prepared with method A and B respectively. Dynamic Light Scattering measurements where done after two hours, and after one, two and three days to monitor the development of inter- and intra-molecular cross-linking, i.e. coils and aggregates present in the solutions at the given times. The viscosities were measured after

three days, and both solutions were filter-flooded. Prior to each measurement, the solutions were gravity filtered through a 40µm filter.

Regarding Concentrations
All presented concentrations are in mass-to-mass, parts per million (ppm) or percent (%). These units are used rather than molar concentrations for two reasons; i) easier comparison with previous reports, and ii) the long-term goal of an offshore LPS-application, where mass-to-mass concentrations are preferred by the operators. Ionic strengths are presented in moles ions/kg solution as this is more expedient and does not require precise density measurements of the solutions.

3.3 Filter-flooding

Core flooding is time-consuming and demands careful preparations of each core before the experiment can be performed. To simulate flow at the entrance of a porous material and evaluate the differential pressure behaviour, filter-flooding is a quicker and more expedient method.

Previous filter-flooding experiments [7, 21, 23, 24] have been carried out on a setup with the filter holder hanging on two pegs in horizontal position, and with all valves, tubings and fittings hanging freely. The applied filter circuit had close to no back pressure, i.e. less than 100 mbar. For this thesis, a new setup was to be made with the following improvements:

- The filter mounted vertically in a rigid filter holder rack.
- Valves fastened onto a rigid plate.
- An increased back pressure.

By mounting the filter vertically instead of horizontally, the chance that fluids could bypass the filter would be reduced. Fastened valves, filter holder and accordingly tubings, would minimize the risk of irregular pressure behaviour caused by bent or squeezed tubings during experiments. With an applied back pressure in the magnitude of about 6 to 7 bar, the influence of any air bubbles present in the circuit would be greatly reduced. A sketch of the new filter setup is shown in Figure 3.3.1.

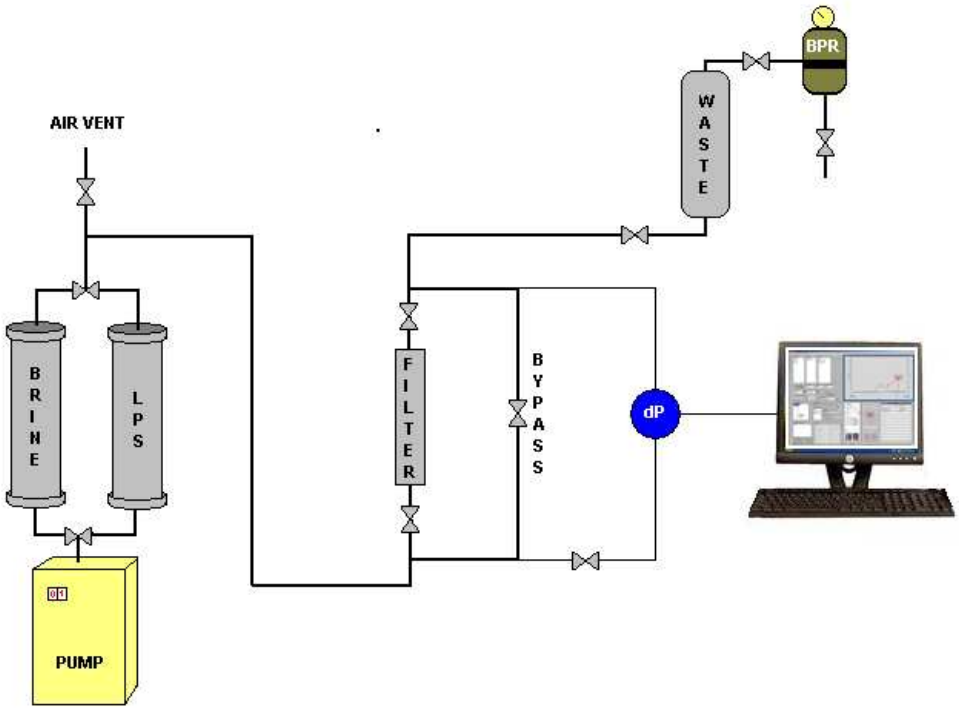

Figure 3.3.1: *Sketch of filter-flooding setup.*

During a filter-flood, it is important to follow a standard procedure for each run to obtain comparable data. Before an experimental session begins, all air must be removed from the system to get valid data. It is also important to flush the system properly after an experiment to avoid that LPS/Polymer left in the tubing will affect the differential pressure in the subsequent experiment. The following procedure is used for all filter-flooding experiments, presented visually in Figure 3.3.2:

- Piston cylinders for brine and LPS/polymer solutions were cleaned and filled with their respective fluids. The LPS/polymer solutions were gravity filtered through a 40µm filter before use, to remove any gels or precipitations could cause plugging of the filter.
- The piston cylinders were connected to the pump at their inlet and to the setup at their outlet. Valves were opened and any present inside the cylinders air was bled out through the air vent. This procedure was done first with the LPS/polymer cylinder, then the brine cylinder, to avoid any polymer residues in the tubing before test start.
- All tubings were checked for air bubbles. If present, they were bled out through the nearest exit or vent.
- The filter was installed in the filter holder, which then was connected to the tubing and clipped onto the filter holder rig.

- Brine was injected over the filter with the desired pump rate to displace air in the filter. A few pressure pulses were built up and released by the filter outlet valve to release any stubborn air bubbles inside the filter holder. Back pressure was applied, and piston cylinders were pumped up to a pressure exceeding the back pressure. The differential pressure of the brine injection over the filter was recorded and compared to previous data. If deviation, tubings was re-checked for air, DPT pressure chambers were bled, or in worst case the filter was discarded.
- Bypass line was opened and differential pressure over bypass line was checked and recorded.
- Bypass line was closed and the differential pressure over the filter should remain the same as before.
- The injection fluid was changed from brine to a LPS/polymer solution. Injection lasted until differential pressure was stable or steadily, but for at least 11 minutes, depending on the injection rate.
- The injection fluid was changed back to brine. Injection lasted until a stable differential pressure was achieved.
- After the test was done, the filter and piston cylinders were disconnected and the system was flushed for two to three minutes with 10ml/min brine or spring water.
- Piston cylinders and filter holder were dismantled and cleaned. All valves on the setup were left closed when the experiment was over.

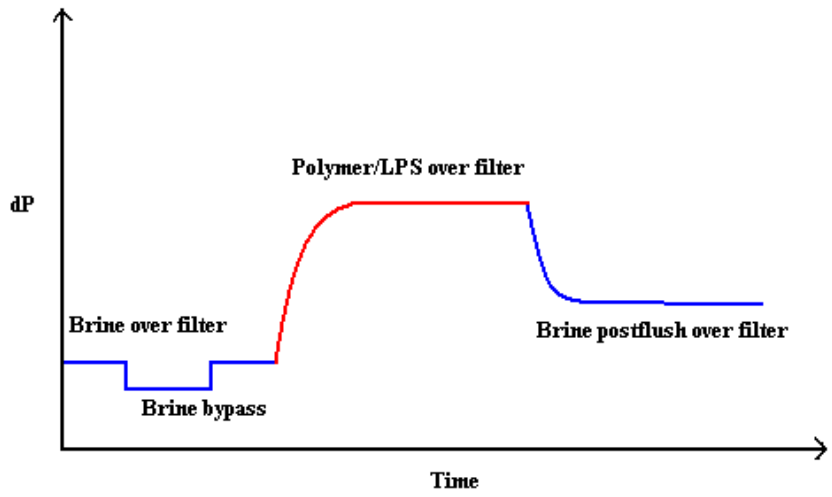

Figure 3.3.2: *Idealized differential pressure profile for a constant rate polymer/LPS filter-flood.*

3.4 Components and equipment

3.4.1 QUIZIX QX-500 Pump

For all experiments involving a pump, the QX-500 by QUIZIX is used. The QX-500 can deliver either constant rate or constant pressure. It features two 151ml cylinders working together and assuring continuous flow, i.e. cylinder A is retracting while cylinder B is expanding. Maximum pressure is 34 bars, and the pump can deliver rates of up to 500 ml/min (30.000 ml/h). Each cylinder is operated by a sprocket and a timing belt. One step on the belt displaces a volume of 0.000025 ml (25 nanoliters). This gives the outgoing rate an excellent resolution and makes the QX-500 suitable for filter-flooding under constant rate. The pump operation is controlled by a computer program and saves recordings of cumulative volume injected. However, rate and outlet pressure are only displayed in real time.

Figure 3.4.1: *Left: Quizix QX-500 pump, Right: FUJI FCX series differential pressure transmitter.*

3.4.2 FUJI FCX-Series differential pressure transmitter

Measurements of the differential pressure over the filters have been carried out by FUJI FCX-Series differential pressure transmitters (DPTs). The DPTs gives an output current of 4.0 to 20.0 mA depending on the flex of the diaphragm between the high- and low pressure chamber, i.e. the differential pressure. Differential pressures can be measured in the range of ± 5000 mbar depending on the model, and the instruments are capable of absolute pressures of several hundred bars. The uncertainty is stated by the manufacturer to be ±0.04% of the measured value.

The DPT was set to a measuring in the range from -100 mbar to 4900 mbar. It was then calibrated with a Druck DPI 610 pressure calibrator to assure accurate pressures**.**

3.4.3 Valves, fittings and tubing

The tubing setup is constructed of Swagelok 1/8” stainless steel valves, fittings and filter holder, and perfluoroalkoxy (PFA) tubing. To avoid any oxidizing iron ions in the system, all components should ideally been non-steel. However, this is a question of availability and practicality, and the total flow length trough steel is minimal compared to that of through PFA. The PFA tubing is also very convenient when removing air from the system, since its transparency reveals air bubbles easily.

3.4.4 Filters

The filter holder is an in-line straight type, containing a Swagelok stainless steel filter as shown in Figure 3.4.2. For this type of filter holder, 0.5, 2, 7, and 15 µm filters are available. The filters are made up by a layered stainless steel mesh with a given nominal pore size. The pore size distribution has not been possible to determine in-house because of the shape of the filter, the small volume of the filter, and the lack of proper instruments to perform such measurements. The manufacturer has stated the pore size ranges shown in Table 4.1.1, but the relative distributions were not known. The filters are for single-use only, and are discarded after a test is done.

Figure: 3.4.2: *Left: Filter mounted in holder, Right: stainless steel filters.*

Table 3.4.1: *Pore size ranges for Swagelok stainless steel filters.*

Nominal pore size [µm]	**Pore size range [µm]**
0.5	0.5 - 2
2	1 - 4
7	5 - 10

To be able to compare pressure data for filters of different pore sizes, it was necessary to determine their respective permeabilities. Differential pressures for a 0.5 % NaCl solution where recorded for all filter sizes for the rates 1, 5 and 10 ml/min, for at least three different filters of each size. The pressures were recorded manually directly from the pressure transducer to avoid uncertainties by the data acquisition program.

3.4.5 Piston cylinders

Piston cylinders were mounted in the circuit between the pump and the filter. Two chambers are separated by a piston in a stainless steel cylinder, with valves at the in- and outlet as shown in Figure 3.4.3. The piston ensures no contact between the fluids as well as a output rate equal to the pump rate. By using piston cylinders, the injection fluid can easily be switched between brine or LPS/polymer, without having to clean the cylinders inside the pump

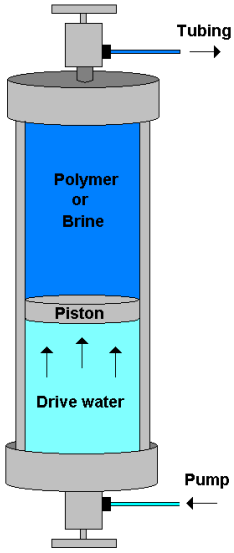

For the filter-floods, two 1000 ml piston cylinders are used, one for LPS/polymer and one for brine. This provides enough volume for multiple experiments, depending on the rate. The cylinders must be cleaned and dried as soon as possible after use to avoid oxidation.

Figure 3.4.3: *Piston cylinder*

3.4.6 Backpressure regulator

To reduce the influence of possible air-bubbles present in the tubing or filter, a backpressure is applied before a filter-flooding starts. The backpressure regulator (BPR) is basically a valve, which opens only if the pressure P at the inlet is larger than the pressure in the regulator chamber, $P_{r.}$ Two-phase flow inside the regulator will worsen the pressure-sensitivity, so a waste flask is installed before the BPR. The BPR used for the filter-floods had a range of 0 to 10 bars. The concept is shown in Figure 3.4.4.

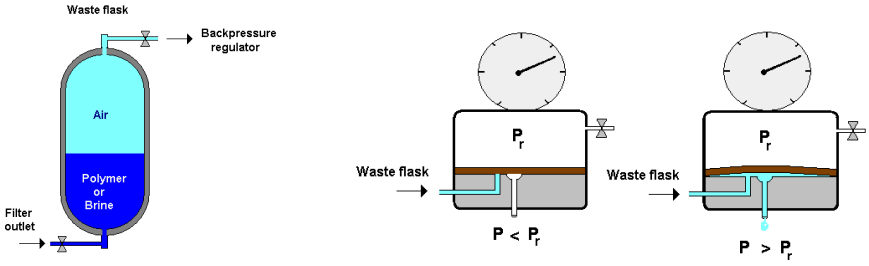

Figure 3.4.4: *Left: Waste flask setup, Right: Principles of the back pressure regulator*

3.4.7 Data acquisition and logging

The voltage of the output from the differential pressure transmitter is measured by a National Instruments USB-6008 voltmeter. The voltage is then converted to a corresponding differential pressure by an in-house made LabVIEW program on the computer. If the measuring range of the DPT is changed, the program has to be calibrated to the new settings. The circuit is shown in Figure 3.4.5. The LabVIEW program is also communicating with the pump, and shows differential pressure, cumulative volume injected, pump outlet pressure and rate, all as a function of time.

Figure 3.4.5: *Chart of data acquisition circuit; Differential pressure transmitter – Voltmeter – LabVIEW program.*

All data are viewed in real time and written to a datasheet every 10 seconds. There is some sinusoidal noise in the voltmeter that results in a certain fluctuation of measured differential pressures, even when the differential pressure is constant or zero. The noise is constant in terms of voltage fluctuation, and will hence give larger uncertainties the wider the range of the transducer. If possible, filter-floods expecting low differential pressures should be performed with a narrower range in the differential pressure transducers, thus lowering the relative uncertainties. The LabVIEW program can be unstable, so a restart of the computer after each experiment is recommended to avoid crashes and lost data.

3.5 Particle size measurements - Malvern Zetasizer Nano ZS

Particle size measurements using dynamic light scattering has been performed using the Zetasizer nano ZS manufactured by Malvern. The concept of particle size measurements by DLS are presented in section *2.4 Particle size measurement by Dynamic Light Scattering (DLS).* The Zetasizer can measure particle sizes ranging from 1nm up to 3µm. For all experiments, the sample was placed in a disposable plastic cuvette and equilibrated for two minutes. The experimental procedure consisted of three runs with 12 measurements per run. The solution viscosity was set to 0.9540 mPa·s and the refractive index (RI) to 1.33. Prior to measurements, the sample fluid was gravity filtered through a 40µm filter. All measurements were performed at 22±0.1°C.

Figure 3.5.1.: *Left: Physica MCR300 Rheometer, Right: Malvern Zetasizer nano ZS.*

3.6 Physica MCR300 Rheometer

3.6.1 Viscosity measurements

The viscosity measurements were performed with a modular compact rheometer, the Physica MCR300 by Anton Paar. The MCR300 features two measurement-geometries. The cone plate geometry (CP-75) is for samples with a presumed viscosity higher than 10 mPas (e.g. stock solutions and concentrated solutions) and consists of a sample plate stator and a slightly coned plate rotor. The stator has diameter of 74.987 mm and a 0.994^0 angle. For samples with a presumed viscosity below 10 mPa·s (e.g. diluted solutions and brines) the double gap geometry (DG-26.7) was used. As the name implies, this geometry has two sets of measuring surfaces, and consists of a concentric cylinder stator and an open-end cylinder rotor. This provides a larger area and a better sensitivity compared to the cone plate geometry. The rotor has a 23.83mm internal and a 27.59mm external radius. Both geometries are shown in Figure 3.6.1.

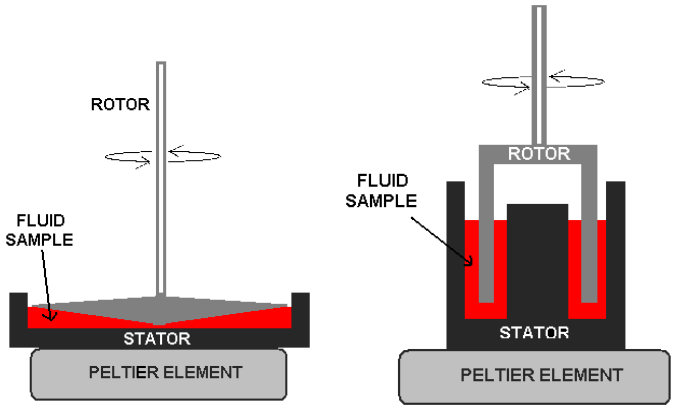

Figure 3.6.1: *Measuring geometries for the MCR300 rheometer by Anton Paar. Left: Cone plate geometry, Right: double gap geometry.*

The rheometer measures the rotor's speed, and can by multiplying with a known constant C_1 calculate the shear rate. Similarly, the shear stress is given by the torque multiplied with a constant C_2. The viscosity is then calculated as the shear stress divided by the shear rate. C_1 and C_2 constrains are unique for each measuring system.

For temperature control, both stators are mounted on a Peltier apparatus with water cooling and electric heating. The apparatus has a resolution of $\pm 0.1^0$C, and all experiments are carried out at 22 ± 0.1^0C.

Periodically and if the geometry is changed, the rheometer has to be checked for erratic behaviour. This is done by measuring the viscosity of the Newtonian fluid PDMS200.

Before each measurement, all parts that are in contact with the sample fluid were thoroughly cleaned and dried. First with soap and water, then rinsed 3 to 5 times with distilled water and finally dried with clean pressurized air. Before any measurements can be done, the Rheometer and corresponding software must be turned on an initialized. The sample cup or plate is placed in the holder and fastened, and then levelled with a tubular spirit level. The fluid sample is then carefully dispensed with a pipette onto the plate or cup. The volume required is 4.1 ml for the DG and 3.0 ml for the CP. After the Peltier apparatus has been set to the desired temperature, one should wait a few minutes with the rotor placed in measuring position to let the heat distribute thorough the sample. During measurements a Plexiglas cover is put over the Rheometer to protect the sample from debris and air fluctuations.

For both geometries, the measurement procedure starts with five minutes of temperature equilibration, thereafter the software starts the measurements automatically when the temperature has been constant at 22±0.1°C for ten seconds. The measurement starts with six measuring points with logarithmic increase in the shear rate range of 10 to 100 1/s. Finally, the same points are measured again with decreasing shear rate. The measuring time for each point varies logarithmically from 10 s for the highest shear rate, and up to 30 s for the lowest.

Because polymer solutions and LPS systems are non-Newtonian fluids, their bulk viscosities can only be compared for a constant shear rate. The reference shear rate for all viscosities stated in this thesis is 100 (1/s). This shear rate ensures torques large enough to get precise viscosities, and enables comparison of previously reported viscosities[24].

3.6.2 High shear viscosity measurements

The high shear experiments were performed with the CP-geometry to obtain highest possible shear rates. Each fluid was measured for four different maximum shear rates of 5500, 3000, 1000 and 100 1/s, respectively. For each run, a fresh sample of the fluid was used. The viscosities where compared at a reference shear rate of 100 1/s. All experimental fluids were gravity filtered through a 40µm filter prior to measurements.

3.7 Weighing scales

Three different weighing scales have been used during the sample preparations and dilutions. They are all manufactured by Mettler Toledo and have fine, medium and coarse resolutions. The different types and their technical specifications are presented in Table 3.8.1.

Table 3.8.1: *Different types of Weighing scales used for sample preparations*

Maufacturer	Mettler Toledo		
Type	AB 204-J	PB 3002S	SG 16001g
Resolution	*Fine*	*Medium*	*Coarse*
Min wt	0.01 g	0.5 g	-
Max wt	220 g	3 100 g	16 100 g
Deviation	0.0001 g	0.01 g	0.1 g

The deviations in the weights are minor compared to the uncertainties in the sample preparation and filter permeabilities as discussed in section *4.4.2. Reproducibility and uncertainties,* and are therefore neglected.

4 Results and discussion

4.1 Fluid preparation

4.1.1 Linked Polymer Solutions

If AlCit is added to a HPAM solution with concentration above the critical overlap concentration *C**, cross-linking may mainly be inter-molecular and gels will form[9]. The higher over C* the solution is, the more likely gels are to be formed. This gives a challenge when mixing the linked polymer solutions, since the desired concentrations may be close to, or above the critical overlap concentration. To overcome this problem, two separate mixing methods for preparation on linked polymer solutions, method A and B, were known from previous authors[7, 24].

A) HPAM stock solution is diluted to desired concentration without AlCit, and AlCit is then added drop wise into the HPAM solution under heavy stirring until the desired concentration is achieved. The solution then is sufficiently stirred for two hours after mixing, and then gently stirred for approximately three days prior to use.

B) HPAM and AlCit stock solutions are diluted separately to twice their respective desired concentration. The two diluted solutions are then mixed in a ratio 1:1 resulting in a final concentration equal to one half of the initial. The mixed solution is sufficiently stirred for two hours, and then gentle stirred for approximately three days before use.

Both procedures has been used in previous work[7, 24], but there has not been done any particular comparison between them. To compare the rheological properties, particle size distribution (PSD) and flow performance for solutions prepared by the two methods, two 600/20/0.5 LPS solutions of HPAM 3630S where prepared with the proposed methods A and B respectively. Dynamic light scattering (DLS) were used to determine particle size distribution at two hours and at 1,2 and 3 days after mixing. Viscosity measurements were done after 3 days, and eventually both solutions were filter-flooded.

Prior to the comparison, method A could be considered best regarding the critical overlap concentration, since the HPAM solution was the most diluted. However, a problem occurred when AlCit was to be added to the mixture: Both solutions should be stirred, HPAM to assure

god mixing, and AlCit to maintain the suspension and a uniform concentration. It is not possible to stir while on a weighing scale, thus AlCit had to be weighed into a temporary container before drop wise added to the polymer solution. Even though the temporary container was weighed before and after to account for residual AlCit, some of the AlCit will precipitate when no stirring was applied, giving a greater uncertainty regarding the concentration of the residual AlCit.

Method B was expected to provide better experimental conditions for an accurate AlCit-concentration since the stock solutions could be stirred constantly while pipetting into a beaker on the weighing scale. Nevertheless, the concentration of the HPAM solution was twice that of method A, and accordingly further over C*. On the other hand, the AlCit solution was far more diluted before mixed with the polymer solution for this method.

Bjørsvik et al.[16] found the hydrodynamic diameter for x-coils to range between 50-100 nm for HPAM LPS solutions solved in brines containing 0.2 – 5% NaCl. Li et al. [10] estimated the hydrodynamic diameter of x-coils to be in the range of 200-400 nm for HPAM LPS solutions solved in 2% NaCl. Aaraa et al.[17] estimated the mean diameters of x-coils in similar systems to be approximately one tenth of these, but compared the Z-average values from DLS measurements. Comparison of Z-average values is only valid for solutions that have spherical particles, a narrow size distribution, and are mono-modal, i.e. have only one peak on their PSD charts. This is not the case for the solutions investigated for the present thesis.

For interpretation of the PSD-charts, it is assumed that peaks between 30 and 200 nm are x-coils, and peaks between 250 and 2000 nm are x-aggregates as shown in Figure 4.1.1.

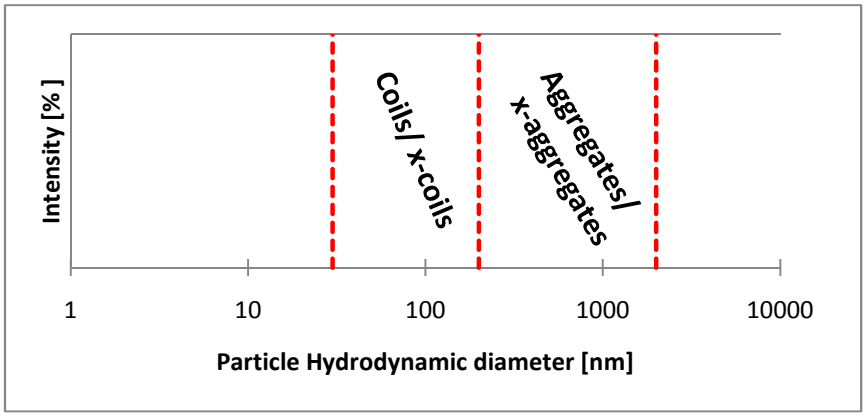

Figure 4.1.1: *Limits in hydrodynamic diameters for interpretations of coils and aggregates in polymer solutions, and in LPS solutions (x-coils and x-aggregates).*

Figure 4.1.2 shows the particle size distribution (PSD), two hours after mixing. At this time, the PSD of the LPS solutions had a small deviation compared to that of the normal polymer solution. The cross-linking that may had occurred by this time was probably mainly intra-molecular as both LPS A and B appears to have developed slightly smaller particles than the polymer solution.

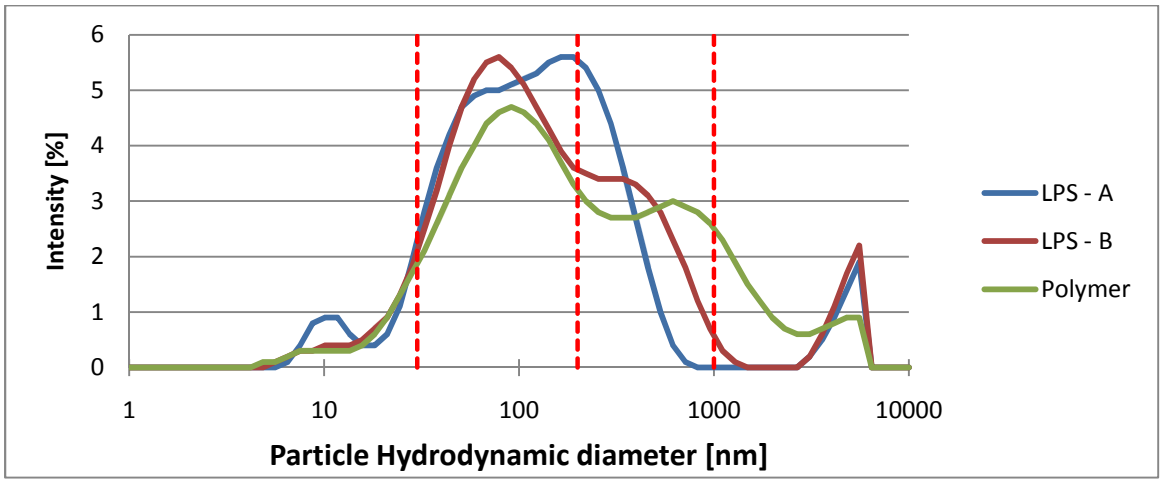

Figure 4.1.2: *PSD-charts for HPAM 3630S 600/20/0.5 LPS solutions prepared by method A and B as after two hours. The PSD for the corresponding polymer solution is shown for comparison. Horizontal dotted lines sets limits for interpretation of coils/x-coils and aggregates/x-aggregates.*

Three days after mixing, two distinct peaks could be observed as seen in Figure 4.1.3, assumed to be cross-linked polymer coils and aggregates, as suggested by Nordli[24]. Compared to the polymer solution, it seemed like polymer molecules in the LPS solutions were cross-linked into x-coils and x-aggregates. It should be noted that even though the aggregate peak has a higher intensity than the coil peak, it does not imply that the

concentration of x-aggregates are higher than the concentration of x-coils in the solution. The measured intensity is dependent on the amount of light scattered for a particle of a given hydrodynamic diameter, and by the Rayleigh approximation, $I \alpha d^6$, larger particles will scatter significantly more light than smaller particles. PSD-charts for the solutions at all measured time steps can be found in appendix section A.1.

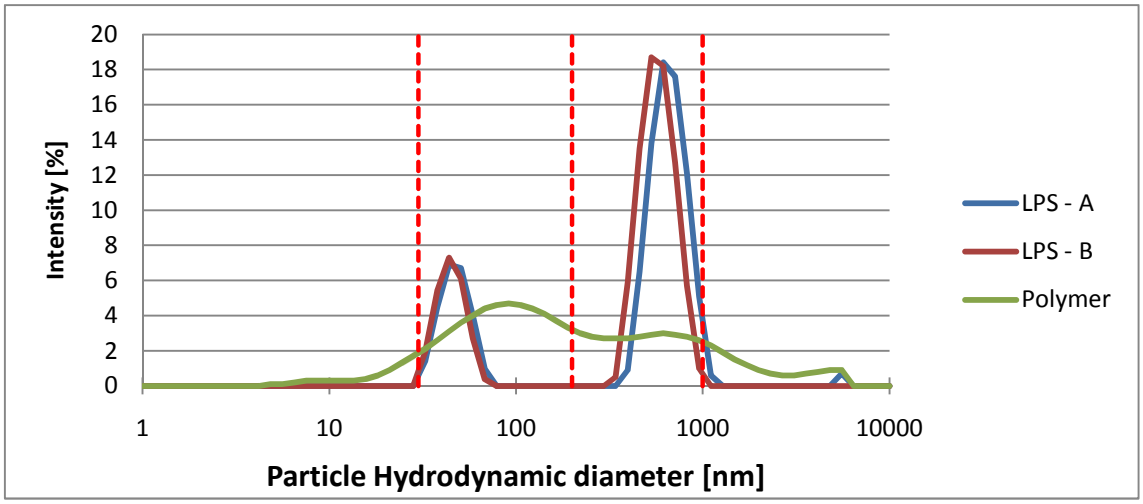

Figure 4.1.3: *PSD-charts for HPAM 3630S 600/20/0.5 LPS solutions prepared by method A and B after three days. The PSD for the corresponding polymer solution is shown for comparison. Horizontal dotted lines sets limits for interpretation of coils/x-coils and aggregates/x-aggregates*

The hydrodynamic diameters obtained for each peak and time, and the viscosities for solution A and B is presented in Table 4.1.2.

Table 4.1.2: *Hydrodynamic diameters of x-coils and x-aggregates obtained for method A and B as a function of time. Viscosities are given at a shear rate of 100 1/s and 22±0.1°C. The corresponding uncertainties are given in percent.*

Solution	**One day**		**Two days**		**Three days**		
	x-coil	**x-aggregates**	**x-coil**	**x-aggregates**	**x-coil**	**x-aggregates**	**Viscosity @ 100 1/s**
	[nm] ± 11%		[nm] ± 11%		[nm] ± 11%		[mPa·s] ± 1%
A	45	330	49	585	46	667	4.53
B	43	306	46	556	47	584	4.49

As seen in Table 4.1.2, the variation in both hydrodynamic diameters and viscosities are within the uncertainties. Both solutions were filter-flooded after three days, but no pressure profiles were obtained as both solutions plugged the 2µm filter. The critical overlap

concentration for LPS solutions of HPAM 3630S solved in 0.5% NaCl is estimated to range between approximately 140-200 ppm as presented in Table 4.5.4. This indicates that the tested LPS solutions were in the int*er*-molecular cross-linking regime, favouring formation of x-aggregates. The x-aggregates are estimated to be in the size range of approximately 600-700 nm by DLS, which appear to be too large to pass through a 2µm filter without resulting in aggregation and plugging of the filter.

Conclusion

Sorbie [11] states that the method applied for mixing a polymer before testing, can strongly influence the rheological properties of the solution in question. The author claims that many problems related to interpretation of results from polymer- and core flooding experiments are caused by irregular handling and treatment of the polymer solutions

Data acquired by the established methods available for LPS characterization in-house, did not reveal any notable differences in properties between LPS solutions prepared with the two proposed methods. Most of the previous LPS-related experimental work at Uni CIPR has been carried out using method A [7, 23], and it was therefore decided to continue experiments using this method. For further experiments, it was determined to use polymer concentrations of 300 ppm instead of 600 ppm to avoid plugging of filters.

4.1.2 Aluminium Citrate solutions

The stock solutions of Aluminium Citrate (AlCit) were prepared to have a concentration of approximately 5000 ppm, solved in 0.5% NaCl. At this concentration, the solutions were suspensions. When freshly made, the solutions were slightly grey but transparent, with no visible larger particles when under stirring. However, after three to four weeks the solutions tended to precipitate and/or turn milky white. Figure 4.1.4 shows the transition for a 5000 ppm AlCit solution in 0.5% NaCl after two and 30 days, respectively. Various attempts to identify the determining factor for the phenomenon have been performed. The following possible factors checked were: a) AlCit concentration, b) solvent salinity, c) storing with or without stirring, and d) addition of small amounts of polymer to simulate contamination. Additionally, a dedicated spatula was used for weighing in the AlCit powder, and all flasks were cleaned by hand and rinsed with distilled water to avoid any external contamination. All attempts resulted in precipitation/white solutions, thus the reason for the phenomenon is still unknown. To overcome this problem, solutions were discarded as they turned white, and fresh

solutions were prepared regularly. The solutions were stored under very gentle stirring, but stirred heavily for at least five minutes to obtain a uniform concentration in the suspension before they were applied.

The pH of the solutions ranged from 2.5 up to 3.0, both for transparent and white solutions. This may indicate formation of $Al(OH)_3$ which will result in excess H^+, hence the lowered pH. The white slurry observed in the flasks could be precipitation of $Al(OH)_3$, as the water solubility of this compound is low (≈ 0.001 g/L at 20°C). To obtain stable concentrated solutions of AlCit, Smith[8] patented a comprehensive method, involving dilution of aluminium chlorohydrate and citric acid with distilled water, before raising the pH of the solution by addition of ammonium hydroxide. The pH was initially about 1.3, and was raised to approximately 7. During this shift the AlCit solution was reported to turn from cloudy slurry to completely clear. The patent involves very strict preconditions and guidelines for the preparation, underpinning its complexity. Attempts to prepare AlCit by the patented method has not been performed for the present thesis due to time limitations.

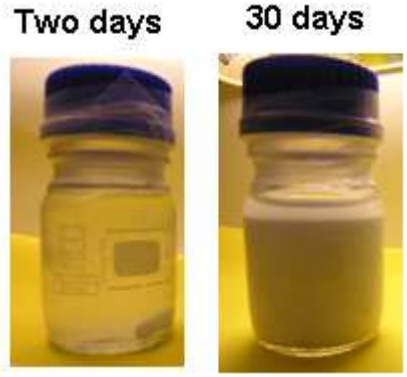

Figure 4.1.4: *Polymerization of AlCit solution after 30 days. Note the transformation from a transparent, to a non-transparent milky white solution.*

4.2 Filter setup

During the present thesis, a new and improved filter-flooding setup was to be made as described in section *3.3 Filter-flooding*.

In order to observe the flow behaviour properties of pre-filtered solutions, an extra filter was initially mounted in series after the first filter. However, this strategy had to be discarded due to constraints in the experimental equipment. The final setup was mounted as previously described in Figure 3.3.1.

4.2.1 Filter permeabilities

To be able to relate data from filter-floods to other porous media, and to be able to calculate the shear rates during filter flow, the permeabilities of the applied filters had to be estimated. The determination of permeability was challenging due to the shape of the filters. As seen in Figure 4.2.1 the filters were shaped like a thimble, and the flow is moving through two main areas; i) flow through the bottom of the filter , and ii) radial flow through the filter walls into the void space inside the filter. There are probably minor amounts of fluid passing through the lower "corners" of the filter (hatched area on Figure 4.2.1), since the flow length will be shorter through either the walls or bottom**.** The area of the outer cylinder walls was about 20 times larger than that of the bottom, depending on the inner diameter, which varies slightly for each filter size. It can thus be assumed that the majority of the flow is radial through the filter walls, which makes up the base for the proposed model for permeability estimation.

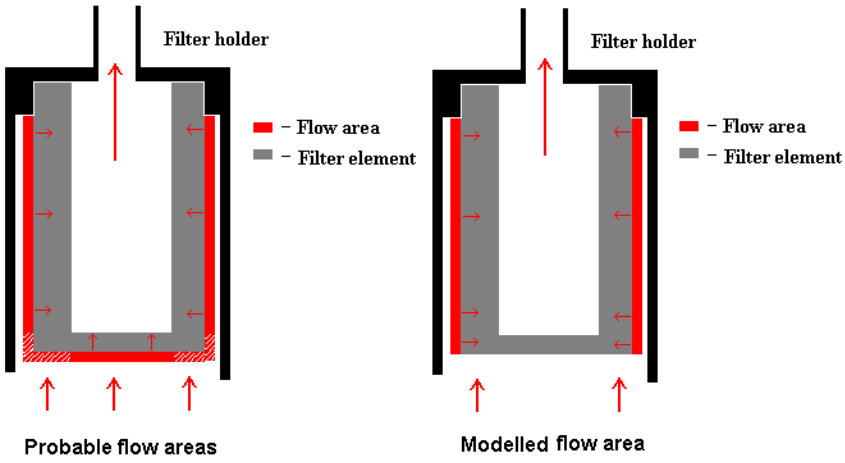

Figure 4.2.1: *Cross section of the filter confined by the filter holder, showing the flow areas through the stainless steel filters. Left: probable occurring flow areas, Right: modelled flow area. The hatched area on the left Figure represents the lower "corners" of the filter.*

To estimate the permeability, flow through the bottom was neglected, and all flow through the filter was assumed radial through the filter walls. The flow height was assumed to be the total filter height minus the upper part that is confined by the filter holder. Thus, the "corners" were assumed to be a part of the flow area, partly reducing the impact of neglecting the flow area through the bottom. The probable and the modelled areas are compared in Figure 4.2.1.
For radial flow in a cylinder shaped porous medium, the flow rate is given as[29];

$$Q = \frac{KA}{\mu}\frac{dP}{dr} = \frac{2\pi hK}{\mu}\frac{p_B - p_A}{ln\frac{R}{a}} \qquad \textbf{(4.1)}$$

Where Q is the flow rate, h is the height of the medium, K is the permeability, μ is the viscosity of the fluid, p_B and p_A is the pressures on the outside and inside of the medium respectively, and R and a is the inner and outer radii of the medium.

Pressure data from 0.5 % NaCl solution where recorded for all filter sizes for the rates 1, 5 and 10 ml/min, for at least three different filters of each size. The brine viscosity was assumed equal to water viscosity. Differential pressures were recorded manually directly from the display on the pressure transducer to avoid uncertainties by the data acquisition program. The permeabilities where calculated by solving Formula 4.1 for K. Table 4.2.1 presents the obtained data and calculated permeabilities for 0.5µm filters. Differential pressure as a function of flow rate is shown in Figure 4.2.2.

Table 4.2.1: *Obtained differential pressure data and estimated permeabilities for 0.5% NaCl injected over three different 0.5µm filters. Each colour represents one filter. Note that the differential pressures are given relative to the zero in the measurement range on the differential pressure transmitter, equal to minus 100 mbar.*

0.5µm filter				
Q[ml/min]	**dP_{Total} [mbar]**	**dP_{Bypass}[mbar]**	**dP_{Filter}**	**K [mD]**
1	110.0	100.0	10.0	129.4
	108.5	100.0	8.5	158.4
	109.0	100.0	9.0	149.6
5	159.0	107.5	51.5	125.6
	151.0	107.5	43.5	154.8
	154.0	107.5	46.5	144.8
10	223.5	116.5	107.0	120.9
	204.0	117.0	87.0	154.8
	205.5	117.0	88.5	152.2
Average			**143.4 mD**	

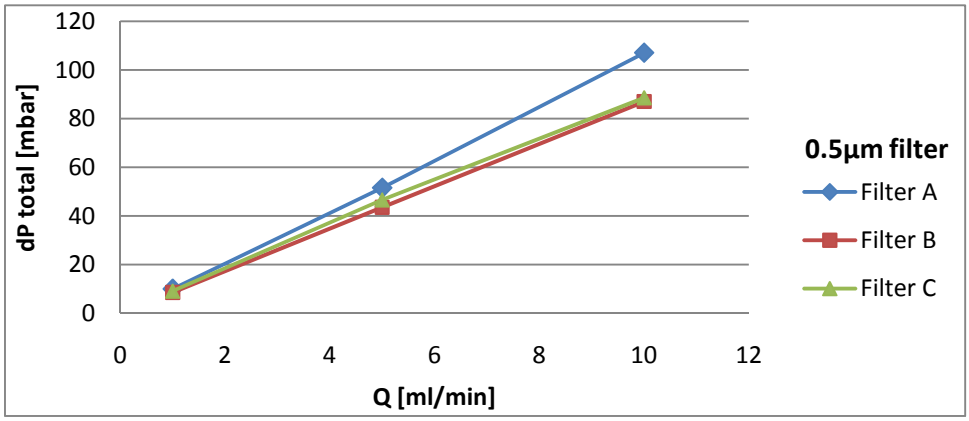

Figure 4.2.2: *Differential pressure of 0.5% NaCl brine injected over 0.5µm filter as a function of flow rate, for three separate filters.*

As seen in Table 4.2.1, three parallels were performed for each rate. Different filters were applied for each parallel. The differential pressures show a certain variation for each filter, but the pressure drops over the bypass line are virtually constant within each rate. This implies that the differential pressure transmitter provides reproducible and consistent measurements,

and that the 0.5µm filters does not have equal permeabilities. Permeabilities for all filters and sizes are shown graphically in Figure 4.2.3.

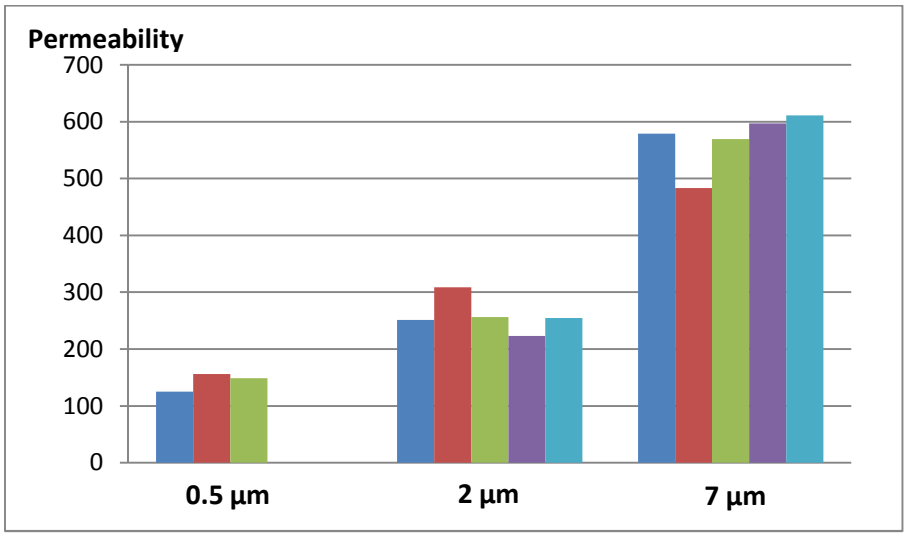

Figure 4.2.3; *Measured permeabilities for the applied filter sizes. Each column represents the average permeability from three different rates for one filter of the given size.*

As seen in Figure 4.2.3, there is a certain permeability variation within each filter size, also for 2 and 7µm filters. The average permeabilities and corresponding standard deviations for each filter are shown in Table 4.2.2.

Table 4.2.2: *Average permeabilities and standard deviations for each filter size*

Filter size [µm]	**Average K [mD]**	**Standard deviation**	
		±[mD]	**% of average**
0.5	140	14	10 %
2	260	40	15 %
7	570	70	12 %

The impact of the permeability deviation in the filters will be discussed later in section *4.2.2 Reproducibility and uncertainties.* Obtained data and estimated permeabilities for all filters and sizes can be found in appendix section A.3.

4.2.2 Reproducibility and uncertainties

The filter permeability measurements showed that the differential pressure transmitter provided reproducible and consistent differential pressures when recorded manually from its display. To ensure reproducible data from the LPS filter-floods, multiple experiments were performed with the same rate, fluid type and concentration, but for different fluid batches. The benchmarks were determined to be a 3430S 300/10/0.5 LPS solution, injected with a flow rate of 3.0 ml/min over a 2µm filter. The results from these experiments can be seen in Figure 4.2.4.

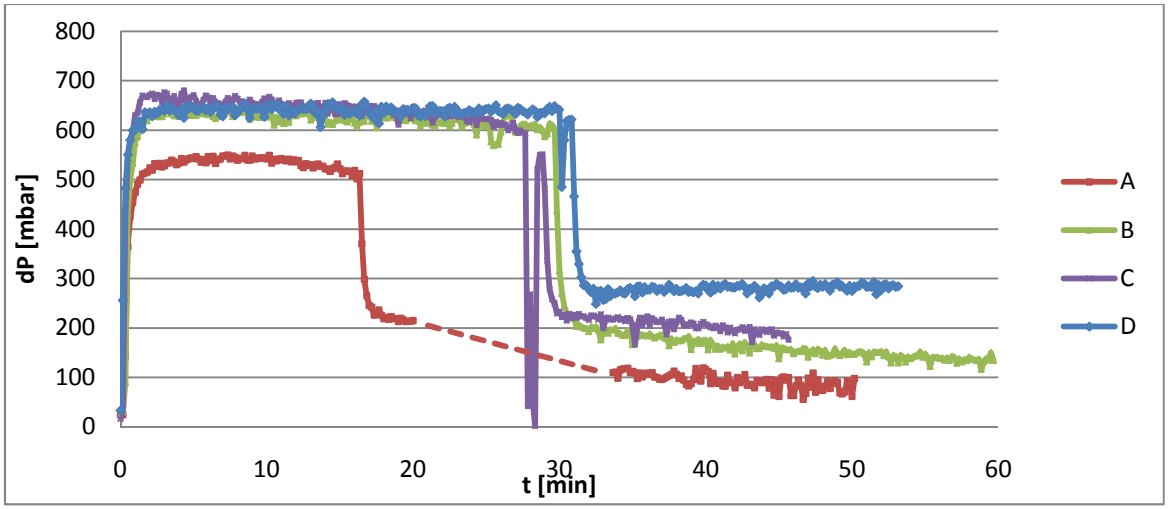

Figure 4.2.4: *Differential pressure profiles for four parallels 3430S 300/10/0.5 LPS solutions injected over a 2µm filter at Q=3.0 ml/min. Each parallel is from separate batches. The sudden drops in the pressures are caused by the injection fluid being switched from LPS to brine. Dotted line is an estimate of lost data points due to acquisition failure.*

The zero time on Figure 4.2.4 represents the moment when the respective LPS solutions reaches the filter. The aim for the experiments was approximately 30 minutes of LPS injection, but experiment A was ended sooner due to shortage of LPS solution.
The deviation in differential pressures for the four LPS solutions could be caused by the data acquisition circuit, the filter permeabilities, the properties of the LPS solutions, or a combination of these.

Differential pressure profiles as those shown in Figure 4.2.4 are based on data points logged automatically every ten seconds by the data acquisition circuit, as described in section *3.4.8 Data acquisition and logging*. There seems to be some noise in the data acquisition circuit, fluctuating in a seemly sinusoidal pattern. Figure 4.2.5 shows a series of data points as

obtained from the data acquisition circuit for a period without any flow over the filter, i.e. zero differential pressure, compared to a sine curve and the average value of the data points. The average amplitude of this fluctuation is interpreted as the uncertainty of the data acquisition circuit, estimated to ±6 mbar.

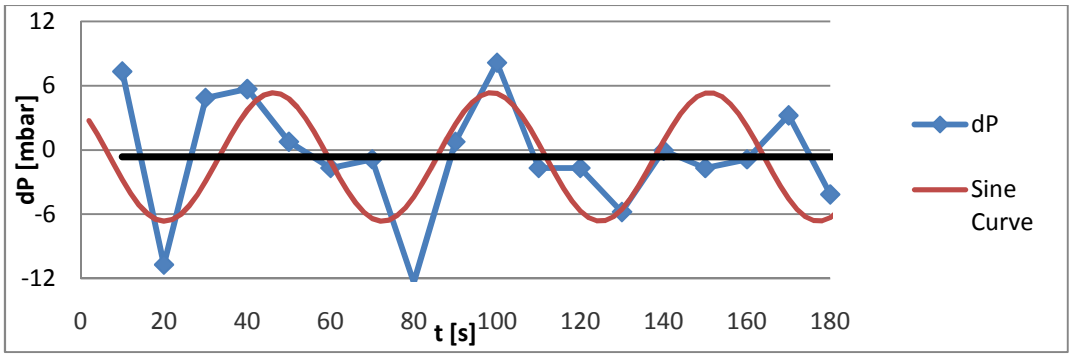

Figure 4.2.5: *Section of data points obtained from the data acquisition circuit, compared to a sine curve and the average data point value*

The deviation between the differential pressures during LPS injection for the four parallels shown in Figure 4.2.4 could also be caused by the variation in viscosity between each batch, since higher solution viscosities may increase the pressure build-up caused by the viscous contribution as shown in Formula 4.1.

Table 4.2.3: *Viscosities and standard deviation for the four reference LPS solutions. All viscosities are given at a shear rate of 100 1/s and 22±0.1°C.*

Solution	**Viscosity [mPa·s]**	**Average [mPa·s]**	**Standard deviation**	
			±[mPa·s]	**% of average**
A	2.60	2.41	0.16	7 %
B	2.46			
C	2.37			
D	2.21			

The uncertainty in the Rheometer with the double-gap geometry is presented in Table 4.2.6, and is estimated to be 1% of the measured viscosity. The standard deviation within the four reference LPS solutions as presented in Table 4.2.3 is 7%, and thus significantly higher. It can be concluded that the viscosity variation within the measured reference solutions may have an impact on the reproducibility.

To rule out the LPS viscosity factor, the concept of the relative differential pressure, dP* is introduced. The dP* is given as:

$$dP_i^* = \frac{dP_i}{\mu_i} \qquad \textbf{(4.2)}$$

Where dP^*_i is the relative differential pressure, dP_i is the differential pressure and μ_i is the viscosity, all for the fluid *i*. The relative differential pressure (dP*) has the unit [10^{-5}/s], but will hereafter be referred to as [mbar/mPa·s] to avoid confusion with shear rate, [1/s]. By applying dP* instead of dP, the differential pressure profiles becomes independent of the variation in solution bulk viscosities. Hence, the dP* will reflect the solution pressure build-up properties caused by the preparation method. The dP* profiles of solutions A-D are shown in Figure 4.2.6.

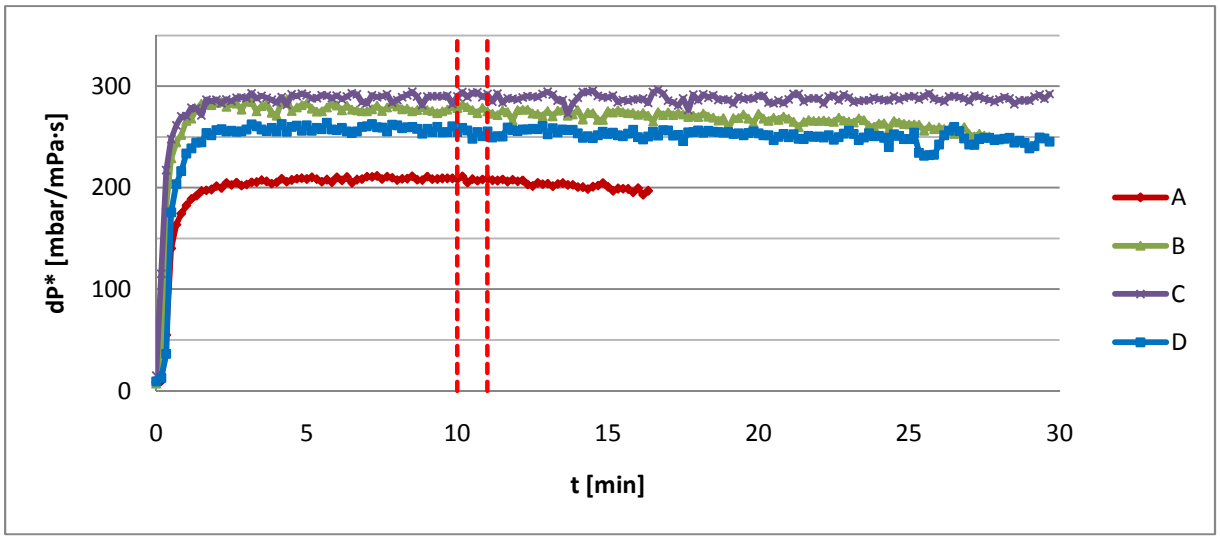

Figure 4.2.6: *Relative differential pressure profiles for four parallels 3430S 300/10/0.5 LPS solutions injected over a 2µm filter at Q=3 ml/min. Each parallel is from separate batches. Horizontal dotted lines sets the time interval for average dP*.*

A benchmark of the average dP* from 10-11 minutes of LPS injection is chosen for comparison of the dP* values, seen in Figure 4.2.6 as horizontal dotted lines.

Table 4.2.4: *Values of dP* for solutions A-D with its corresponding standard deviations.*

Solution	dP* [mbar/mPa·s]	Average dP* [mbar/mPa·s]	Standard deviation	
			[mbar/mPa·s]	% of average
A	208.1	260	40	15 %
B	254.1			
C	277.6			
D	291.7			

As seen in Table 4.2.4, the LPS solutions A-D has an average dP* = 260 ±40 mbar/mPa·s, giving a standard deviation equal to 15% of the average. This concurs with the permeability deviation within the 2µm filters as presented in Table 4.2.2, which equalled 15% of the average permeability. It also suggests that the variation in solution viscosity can be seen as a measure for the magnitude of the uncertainties caused by the LPS preparation method.

Table 4.2.5: *Values for endpoint dP* for post LPS brine injection with its corresponding standard deviations.*

Solution	dP [mbar]	Average dP [mbar]	Standard deviation	
			[mbar]	% of average
A	82.2	200	±100	50 %
B	185.9			
C	284.4			
D	288.2			

The endpoint dP* for the post-LPS brine injections spreads from about 80 up to approximately 300 mbar as shown in Figure 4.2.4. Table 4.2.5 shows that the average dP*= 200±100 mbar/mPa·s, a standard deviation equal to 50% of the average. This indicates poor reproducibility, and are consistent with the results obtained from similar filter-flooding experiments performed by Nordli[24]. The author compared brine permeabilities in the filters before and after LPS-injection to estimate the residual resistance factor (RRF) as a function of time after adding cross-linker to polymer solutions. The RRF is defined as:

$$RRF = \frac{K_{b,LPS}}{K_{b,i}} = \frac{dP_{b,LPS}}{dP_{b,i}} \qquad \textbf{(4.3)}$$

Where $K_{b,i}$ and $K_{b,LPS}$ are the brine permeabilities before and after LPS injection, respectively. The permeabilities are directly proportional to the differential pressures of brine

before and after LPS injection, $dP_{b,i}$ and $dP_{b,LPS}$. Nordli[24] found RRF variations of up to 300% for fixed LPS systems injected over Swagelok 2µm filters, and the RRF did not show any reproducible trend. Smith[30] found that the RRF for injection of HPAM solutions in Berea cores varied from 1 up to about 10, depending on the polymer molecular weight, flow rate and core permeability. A reason for the variation in RRF for LPS injection over the Swagelok filters could be deviation in the pore size distributions within the filters, as a larger amount of smaller pores would enhance pore blocking during LPS injection. As discussed in section *3.4.5 Filters*, the pore size distributions could not be determined for the applied filters.

To ensure producible and accurate viscosity measurements, periodical measurements on a reference fluid were performed. An off-the shelf Polydimethylsiloxane (PDMS) solution was chosen as the reference fluid. This was mainly because of the Newtonian flow behaviour and adequate viscosity possessed by this fluid. Properties of the PDMS can be found in Table 3.1.3. The deviation in the measured viscosities of the PDMS solutions were used to estimate the uncertainties in viscosity measurements as seen in Table 4.2.6.

Table 4.2.6: *Measured viscosities for the reference fluid PDMS200 with corresponding standard deviations. Each letter A-E represents a measurement.*

Reference measurements PDMS200								
Shear rate [1/s]	**Viscosity [mPa·s]**					**Average**	**Standard deviation**	
	A	B	C	D	E	**[mPa·s]**	**[mPa·s]**	**% of average**
10.0	5.34	5.26	5.25	5.20	5.25	5.26	0.05	1 %
15.8	5.30	5.25	5.23	5.16	5.25	5.24	0.05	1 %
25.1	5.31	5.24	5.21	5.21	5.25	5.24	0.04	1 %
39.8	5.33	5.25	5.24	5.20	5.25	5.25	0.05	1 %
63.1	5.33	5.25	5.24	5.19	5.25	5.25	0.05	1 %
100.0	5.33	5.25	5.24	5.20	5.25	5.25	0.05	1 %
100.0	5.32	5.26	5.24	5.20	5.25	5.25	0.04	1 %
63.1	5.32	5.25	5.23	5.19	5.24	5.25	0.05	1 %
39.8	5.34	5.25	5.24	5.19	5.24	5.25	0.05	1 %
25.1	5.33	5.25	5.25	5.18	5.25	5.25	0.05	1 %
15.8	5.30	5.23	5.19	5.19	5.24	5.23	0.05	1 %
10.0	5.33	5.26	5.24	5.20	5.24	5.25	0.05	1 %

As seen in Table 4.2.6, the uncertainty in the rheometer is estimated to 1% of measured viscosity.

Conclusion

The primary sources of uncertainty in filter-flooding is attributed the permeability deviance in the filters, followed by the viscosity variation for different LPS batches, which is probably caused by the preparation method. The cumulative standard deviation for dP* of injection of LPS solutions is estimated to ± 15%.

The filter setup and LPS solutions provides consistent and reproducible differential pressure profiles within reasonable uncertainties when the following precautions are taken:

- Viscosity is a major source of variation in dP. dP is therefore substituted with dP* to reduce the influence of viscosity variation within batches of the same LPS system.
- All applied values of dP* used for comparison must be averages over at least one minute/six data points to reduce the impact of fluctuation of dP* in the data acquisition circuit.

dP* for post LPS brine injection has proven poor reproducibility and conclusions cannot be made based on these data.

The aim for the present thesis was to study effects on solution pressure build-up properties by filter-flooding under variation of various parameters. The experimental procedures and equipment discussed in this section seems adequate for this purpose.

4.3 LPS-characterization by high shear rheology

LPS solutions may contain both x-coils and x-aggregates, depending on a number of factors as presented in section *2.1 Linked Polymer Solutions (LPS)*. Our hypothesis was that based on the difference in size between the species, x-coil and x-aggregates would respond differently when applied to the same amount of shear during viscosity measurements on a rheometer.

Larger particles would typically demand more energy to maintain their size during shear flow. For most colloidal systems, smaller particle sizes are energetically favourable. Li et al.[10] found that x-coils are spherical, which means that for a fixed salinity/polymer concentration, the size cannot be reduce further without simultaneously reducing the length of their polymer backbone. On the other hand, x-aggregates may reduce their size by disintegrating into smaller x-aggregates and/or x-coils, which may be likely to occur during shear flow. If the viscosity deviation caused by the rupture of x-aggregates was significant, it could be used to quantify the x-coil/x-aggregate ratio in LPS solutions. An idealized model of the proposed transformation is shown in Figure 4.3.1.

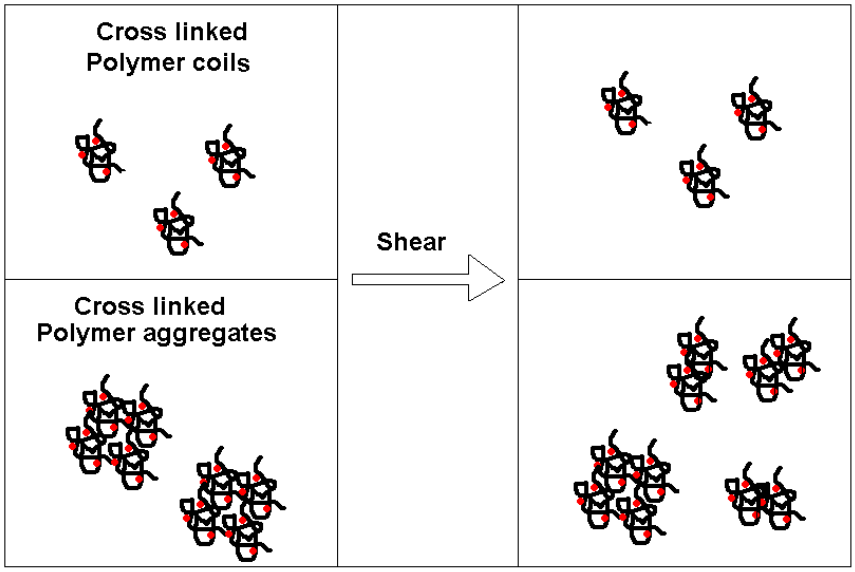

Figure 4.3.1: *Idealized model of cross-linked polymer coils and aggregates and their proposed respective response when applied to the same amount of shear.*

The disintegration of x-aggregates into smaller x-aggregates results in a lower average particle size, thus a reduced viscosity of solution, while the x-coils remains the same size and maintains their solution's viscosity. For a non-cross-linked polymer solution, the concept would be analogous, but as the aggregation in non-cross-linked are dominated by van der

Waals- and hydrogen bonds instead of ionic bonds, the shear necessary to disintegrate a polymer aggregate should be lower than for an x-aggregate. The proposed model would hence give a hysteresis in measured viscosity for increasing and decreasing shear rate, when compared at a reference shear rate. The difference in viscosity taken at a reference shear rate for increasing and decreasing shear rate ,would according to the present hypothesis, depend on the x-coil/x-aggregate ratio in the measured solutions as illustrated in Figure 4.3.2.

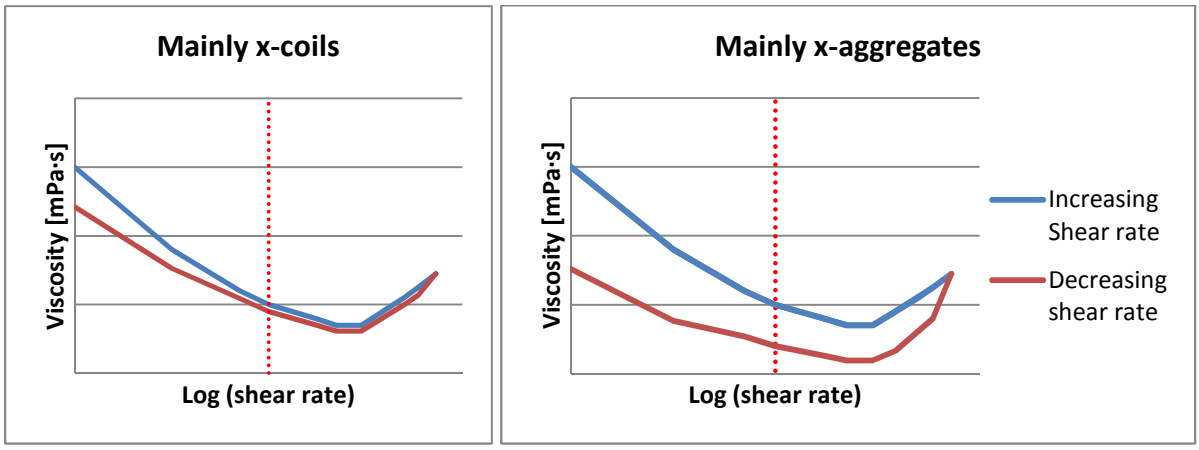

Figure 4.3.2: *Expected flow curves and deviation between viscosities for increasing/decreasing shear rates for solutions containing mainly x-coils (left) or mainly x-aggregates (right). Horizontal dotted line denotes the reference shear rate.*

Figure 4.3.2 shows the expected flow curves for solutions containing mainly x-coils or x-aggregates. The flow curves behaves both shear thinning and shear thickening for increasing shear rate, this type of behaviour is discussed in section *2.3.1 Non-Newtonian behaviour*. As seen, the solution containing mainly x-aggregates has an expected larger deviation in viscosity, caused by disintegration of the aggregates. Polymer and LPS solutions of two compositions/concentrations were chosen to represent each fringe of the model, presented in Table 4.3.1.

Table 4.3.1: *Properties, features and expected cross-linking regimes for the experimental fluids.*

Polymer	Concentration/ composition	Features	Expected cross-linking regime
3430S	*300/10/5 LPS* *300/0/5 Polymer*	*Low molecular weight*	Intra-molecular, x-coils
		Low HPAM concentration	
		High salinity solvent	
3630S	*600/20/0.5 LPS* *600/0/0.5 Polymer*	*Higher molecular weight*	Inter-molecular, x-aggregates
		Higher HPAM concentration	
		Low salinity solvent	

The expected cross-linking regimes in Table 4.3.1 is deduced from on the previously reported factors discussed in section *2.1 Linked Polymer Solutions (LPS).* Even though the expected cross-linking regime promotes either x-coils or x-aggregates, it must be stressed that both species will be present in the solution, but at different equilibriums. The four solutions presented in Table 4.3.1 were measured with the cone plate geometry on the rheometer, for shear rates ranging from 10 to 5300 1/s, which is the highest shear possible for this geometry. For each solution, four separate measurements were performed with shear rates ranging from; 10-100 1/s, 10-1000 1/s, 10-3000 1/s and finally 10-5300 1/s. To obtain data for the relative degradation from bulk viscosity to sheared viscosity for each shear rate interval, fresh samples of the solution was applied for each measurement. The reference viscosities are given as the viscosities from the measurement point closest to 100 1/s, which varies slightly for each interval due to the logarithmic increase in shear rates. The difference in measured viscosity at a reference shear rate for increasing and decreasing shear rate can be expressed by the relative viscosities, $\mu_{decreasing/}\ \mu_{increasing,}$. Relative viscosities for all solutions are showed in Figure 4.3.3:

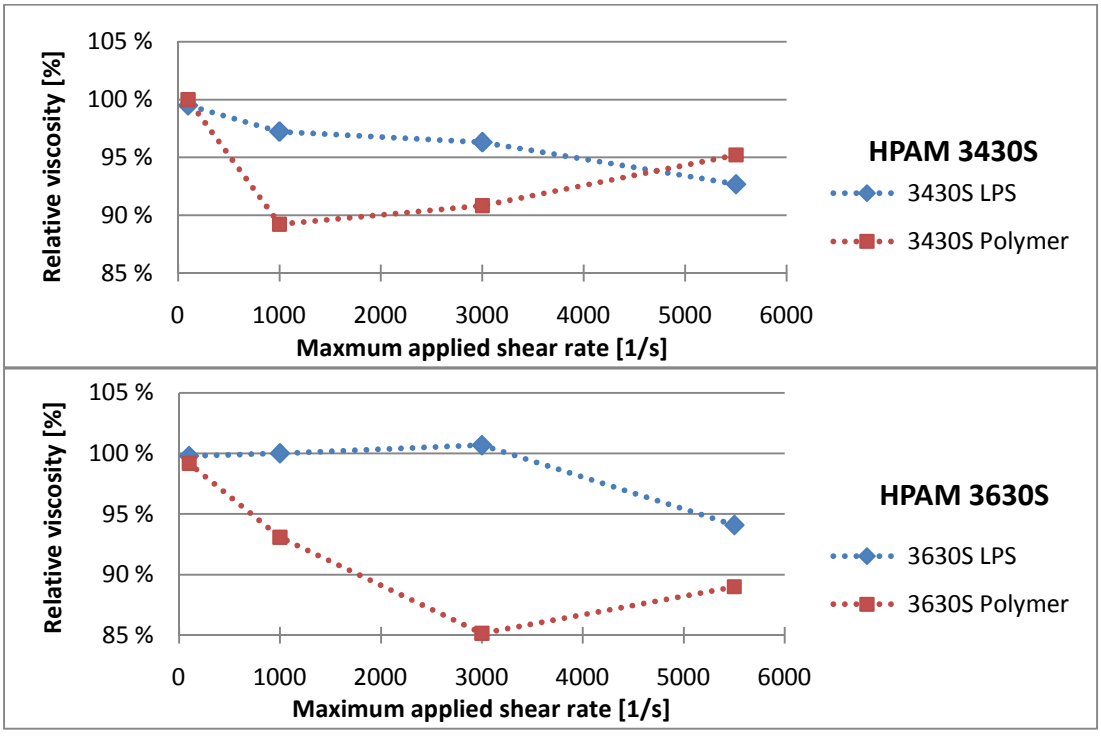

Figure 4.3.3: *Relative viscosities ($\mu_{decreasing/}\ \mu_{increasing}$) for increasing/decreasing shear rate for LPS and polymer solutions of HPAM 3430S and 3630S.*

As seen in Figure 4.3.3, the relative viscosity for the LPS solutions is decreasing with increasing shear for 3430S, but is stable for 3630S until the final shear rate range. The polymer solutions of both types had a decreasing relative viscosity for increasing shear rates up to 1000 and 3000 1/s, but had thereafter an increased relative viscosity. The shear curves did not turn out in accordance with the proposed hypothesis. Neither of the measured solutions lost more than 15% of their original viscosity, and there is no trend for monotonically viscosity loss with increasing shear rate.

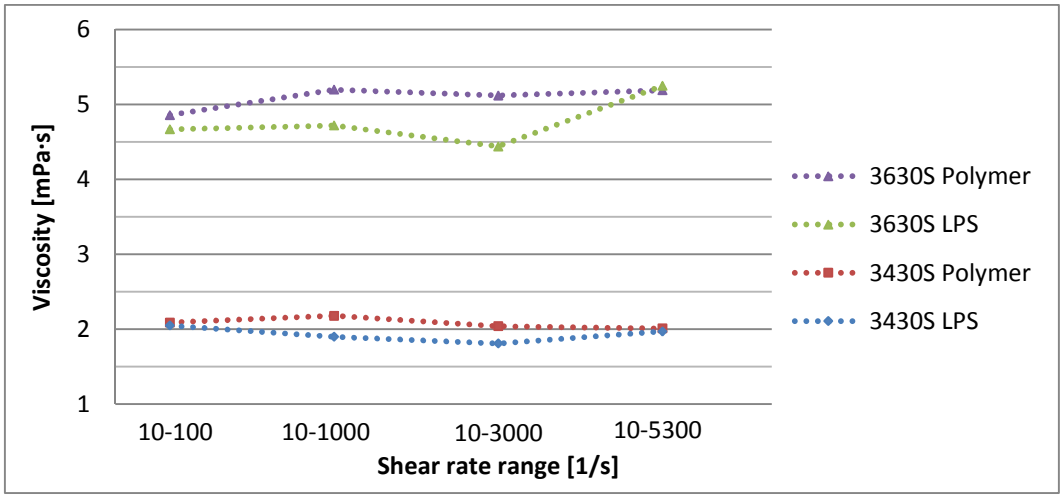

Figure 4.3.4: *Increasing shear viscosities at 100 1/s for the measured solutions at each shear rate range.*

The spread in increasing shear viscosities for the different shear rate ranges at the reference shear rate of 100 1/s are shown in Figure 4.3.4 , and the corresponding standard deviations are presented in Table 4.3.2. The standard deviations are ranging from 3 to 7%, which implies that the variations in relative viscosities shown in Figure 4.3.3 are mainly within the standard deviations. The cone plate geometry was chosen for these experiments due its capability of high shear rheology, but the magnitudes of the standard deviation suggests that the cone plate is not suited for rheology measurements for viscosities within these ranges. The double gap geometry has a better accuracy for viscosity measurements on low-viscous solutions, but has proven unfit for measurements above shear rates of approximately 1000 1/s due to turbulence in the sample cup.

Table 4.3.2: *Average viscosities and standard deviations for all solutions and shear rate ranges.*

Solution		Average μ [mPa·s]	Standard deviation	
			[mPa·s]	% of average
3430S	LPS	2.05	0.10	5 %
	Polymer	2.09	0.06	3 %
3630S	LPS	4.77	0.34	7 %
	Polymer	5.09	0.16	3 %

Conclusion

The difference between $\mu_{decreasing}/\mu_{increasing}$ was not large enough to distinguish between LPS solutions thought to contain mainly x-coils and mainly x-aggregates. Disintegration of x-aggregates into smaller x-aggregates and/or x-coils does not seem to have occurred in significant degree for the applied shear rates. The cone plate geometry seems to be too inaccurate for measurements within these shear rate- and viscosity-ranges.

Based on the presented experimental data and discussion, it is suggested that LPS characterization by high shear rheology is not achievable within the experimental viscosity range and for the available rheometer geometries.

4.4 LPS-characterization by the critical rate - Qc

Spildo et al.[7] suggested that one of the major oil mobilizing mechanisms during LPS injection in porous mediums is the so called Log-Jamming effect as described in section *2.2 LPS for enhanced oil recovery (EOR)*. Fallah et al.[31] developed a network model for pore scale modelling of LPS flooding. The authors found that the Log-Jamming effect was mainly dependent upon the particle concentration and effective hydrodynamic radius, the pore size distribution in the porous medium, and the flow rate. A visualization of the Log-Jamming mechanism is shown in Figure 4.4.1.

The phenomenon of non-LPS particles accumulating in porous media or capillaries has been reported by other authors. RezaeiDoust et al.[32] suggested that clay fragments, so-called fines, that were released from the reservoir rock during low-salinity water injection, could block pores, thereby divert flow and mobilize oil from previously unswept pores. Rahmann et al.[33] studied the transport of clay suspensions through a capillary. Based on their findings, the authors stated that "*...particle deposition is a threshold type process, and there exists a critical condition for the every system (reservoir) which below the pressure drop across a porous medium is insignificant and above which particles deposit randomly at the pore surface resulting in an a rapid increase in pressure drop*".

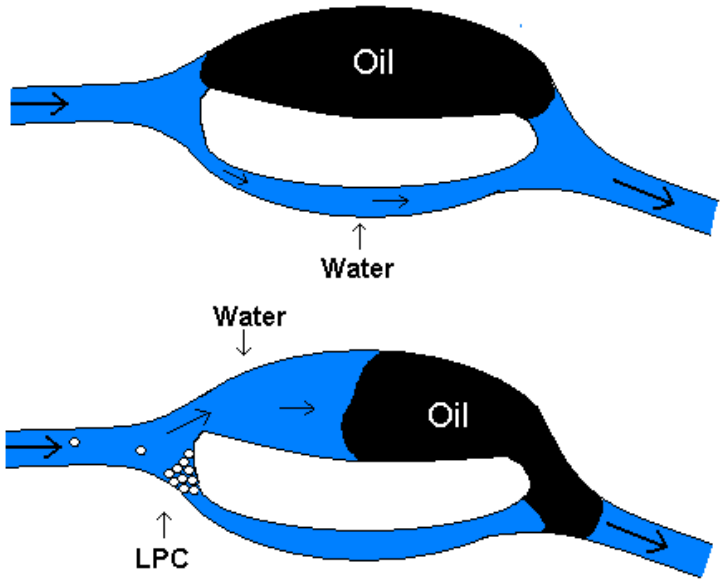

Figure 4.4.1: *The Log-Jamming effect; accumulation of linked polymer coils (LPC) at pore throats, diverting flow. Redrawn from Spildo*[7].

4.4.1 Method development

To further study the concept of the Log-Jamming effect, initial experiments were performed to determine whether there could be estimated limits for the effect to occur during filter-flooding of LPS solutions. The applied filters have a narrow pore-size range as presented in Table 3.4.1 and would therefore be adequate to determine whether the Log-Jamming effect is a threshold-type effect, featuring a critical rate. The corresponding polymer solution was also included in the experimental matrix for comparison. The polymer chosen for these experiments was HPAM 3430S at a 300/10/0.5 LPS system. By using this relatively low-molecular weight polymer at the chosen concentration, there should be a reduced risk that the LPS system would plug the filters, as have occurred in previous trials with 600/20/0.5 LPS systems of HPAM 3630S. Based on the factors discussed in section *2.1 Linked Polymer Solutions (LPS)*, the low molecular weight should also promote the formation of x-coils rather than x-aggregates. The viscosity of the 3430S 300/10/0.5 solution was also sufficiently low to ensure a satisfactory high flow rates without exceeding the range of the differential pressure transmitter, 4900mbar. The complete series of initial experiments, Matrix B, is described in Table 4.4.1.

Table 4.4.1*; Initial experimental matrix for filter-flooding. Each dot represents an experiment.*

MATRIX B - Initial experiments							
HPAM 3430S /0.5% NaCl/ 2µm filter							
Q [ml/min]	0.5	1.0	1.5	3.0	5.0	7.0	10.0
Polymer 300/0/0.5	•	•	•	•	•	•	•
LPS 300/10/0.5	•	•	•	•	•	•	•

As suggested in chapter *4.2.2 Reproducibility and uncertainties*, the differential pressure dP should be substituted with the relative differential pressure dP* when comparing dP for multiple solutions. One matrix may contain experiments done with several LPS/polymer batches, thus dP* reduces the impact of viscosity variation within batches. Furthermore, this enables a comparison of different fluid systems with respect to the pressure build up properties isolated, since the viscous contributions are accounted for. The relative differential pressures reported for a solution at a certain flow rate is given as the average of dP* from 10 - 11 minutes of injection of the applied fluid.

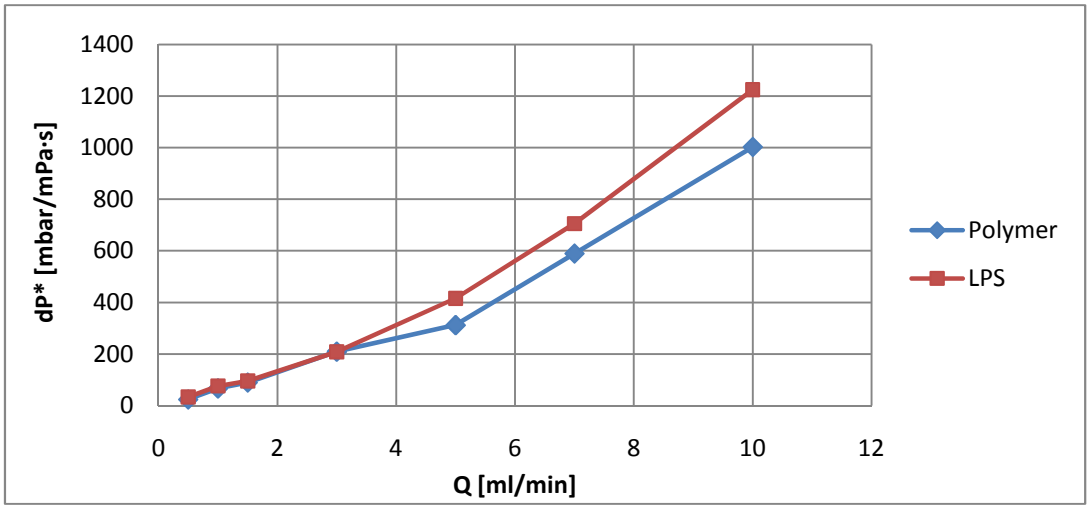

Figure 4.4.2; *Relative differential pressures for a HPAM 3430S 300/10/0.5 LPS and the corresponding polymer solution 300/0/0.5 injected over a 2µm filter.*

As seen in Figure 4.4.2, the LPS and polymer solution provides virtually equal dP* over the filter up to a flow rate of about 3 ml/min. For higher rates, transition to what seems like a new flow regime appears, with rising slopes in dP*/Q for both the LPS and polymer solution. However, the LPS solution has steeper slope than the polymer solution. For the both solution, it is possible to quantify the rate that separates the two regimes by intersection of linear extrapolations as shown in Figure 4.4.3.

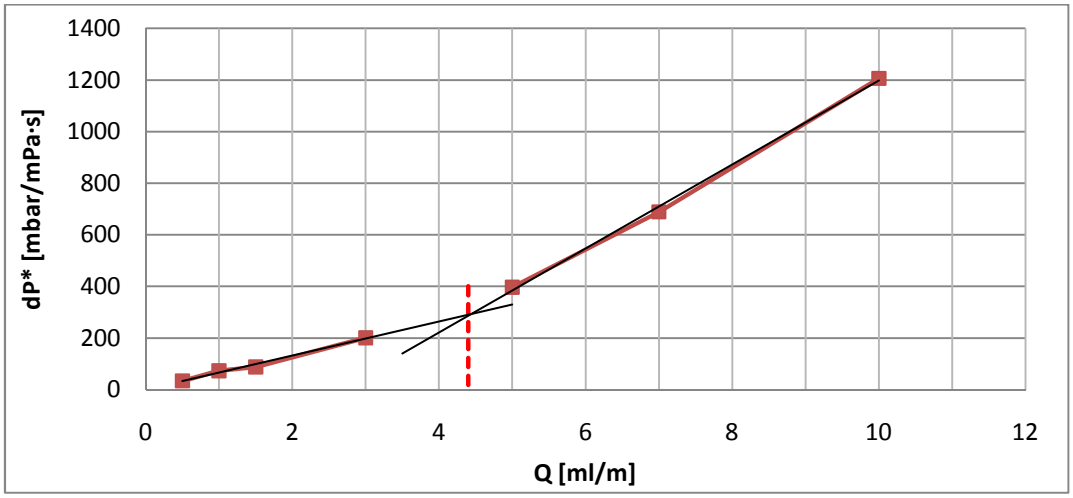

Figure 4.4.3; *Estimation of Q_c for a 3430S 300/10/0.5 LPS solution by intersection of linear extrapolation for the to apparent flow regimes in the measured region. The dotted red line denotes the Qc.*

The results from Matrix A as presented in Table 4.4.1, indicated that it was possible to determine a critical rate, Qc, for the shift between the two apparent flow regimes. However, there several likely mechanisms suggested responsible for the increasing pressure;

i) The Log-Jamming effect, where polymer coils or x-coils accumulates and aggregates at pore throats, causing local permeability decreases and diverts flow[7]. This implies that the pressure build up is rate-dependent, i.e. depends on how many particles that passes through the pore throat per time before jamming occurs.

ii) Plugging of pore throats by already existing larger aggregates or gel phases of a size significantly larger than the coils and x-coils, constricting the flow area and thus leading to increased differential pressure. If the particles are able to plug a pore throat alone, the pressure increase is independent of the rate, but volume-dependent.

iii) Shear thickening behaviour of the LPS/polymer solutions, resulting in higher differential pressure due to increased shear viscosity in accordance with Formula 4.1.

The increased dP*(Q) for $Q > Q_c$ was until further investigation consistent with mechanism i) and ii), since a higher rate implies a higher number of x-coils per time, but also an equivalent increase in volume passing the filter per time. The impact of shear thickening behaviour during shear flow will be further discussed in section *4.5.7 Shear dependent viscosity*.

To determine whether the pressure build ups were rate- or volume- dependent, filter-floods were performed with a rate of 1ml/min, but for approximately 200 minutes, replicating the volume for a 10ml/min filter-flood that lasted for 20 minutes.

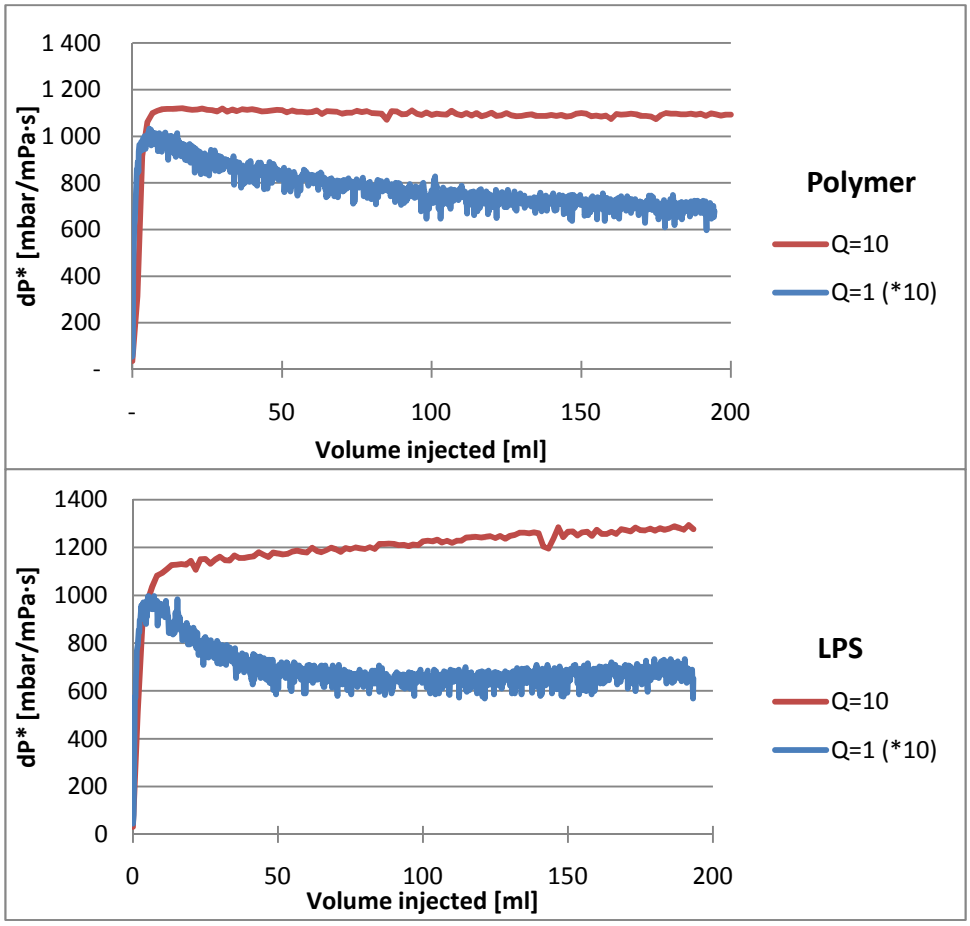

***Figure 4.4.4**; dP* as a function of injected volume of a 3430S 300/10/.5 LPS and the corresponding polymer solution 300/0/0.5, over a 2µm filter. For comparison, the differential pressures for Q=1 are multiplied by 10.*

As seen from Figure 4.4.4, the pressure profile for Q=1 reaches a maximum, then decreases for both solutions. For the LPS solution, a slight increase is observed from about 100 up to 200 ml injected. Hence, the test does not fully exclude the mechanism of aggregates blocking throats for the LPS, but the magnitude of the pressure increase is far less than that for Q=10. This indicates that the increase in pressure is mostly rate-dependent. For the Q=10 experiments, the LPS exhibits a steady increase in dP* during the injection, whereas the polymer solutions is close to stable. This suggests that the affinity between the x-coils that are aggregated at pore throats during Log-Jamming is stronger than the affinity between the polymer coils in the same situation.

The data from the experiments presented in Figure 4.4.4 indicates that the observed increase in dP* are caused by a rate-dependent mechanism, and the increased volumes implicated by

higher flow rates has minor impacts on dP*. This concurs with the findings of Fallah et al.[31], which found that for a fixed particle concentration, porous medium, and particle size (i.e. fluid system), the Log-Jamming effect is governed by the flow rate. Attractive or repulsive forces between LPS particles may also influence the Log-Jamming ability of the solution. Therefore, the magnitude of Qc may be seen as a measure for both the particle size and the affinity between particles in LPS solutions.

Conclusions

The relative differential pressure as a function of flow rate, dP*(Q), shifts into a new flow regime with steeper slope for rates over a certain rate defined as the critical rate, Qc. Qc can be quantified by intersection of the linear extrapolations made from the obtained data points for dP*(Q) from the flow regimes below and above Qc.

The increased dP*(Q) seems to be predominantly rate-dependent, and to a lesser extent dependent on the cumulative volume that passes through the filter. The shift into a new flow regime for Q>Qc is presumably caused by the Log-Jamming effect.

The increased dP*(Q) for Q>Qc is observed both for LPS and polymer solutions, but based on the slope it is indicated that the affinity between the aggregated x-coils are stronger than within the polymer coils.

The magnitude of Qc may reflect the Log-Jamming ability of LPS solutions, which is thougth to be dependent on the particle size and the affinity between the particles.

Variables that influences the critical rate

The initial experiments suggested that there is a critical rate (Qc) for Log Jamming, which could be quantified, and could be a measure of the average particle size and the affinity between the particles in a LPS solution.

To further investigate the critical rate Q_c as a function of various factors, new experiments for filters with different pore sizes where conducted. Finding Qc was an iterative process by measuring dP* for several rates, but as it was quantified for several LPS systems/permeabilities, one would have a certain sense of the expected magnitude of Qc for

other LPS systems/permeabilities. Filter-flooding are relatively time-consuming, so to reduce the number of experiments necessary to determine the Qc for each system, the following criteria was set for each system:

- At least two runs for rates below $Q_{c,}$ and two runs for rates above Q_c should be conducted. This would provide enough data points to estimate the intersection between the linear extrapolations.
- A polymer solution with corresponding concentration is filter-flooded for at least two rates per filter size, to compare the dP* with those of the LPS solution.

***Table 4.4.2**; Variables varied for investigation of Qc.*

Factor	**Types**	**Features**	
Polymer molecular weight	HPAM 3430S	Low molecular weight	
	HPAM 3630S	High molecular weight	
Brine salinity and composition	0.5 % NaCl	Low ionic strength	Monovalent ions
	5% NaCl	High ionic strength	Monovalent ions
	CeB 0.5/4.21		Di- and monovalent ions
Filter pore size	0.5µm	Low permeability	
	2µm	Medium permeability	
	7µm	High permeability	

The Qc was investigated by variation of the factors as presented in Table 4.4.2: Two polymer molecular weights, three different brines, and three different filter sizes. Note that the two high salinity brines, 5% NaCl and CeB 0.5/4.21 have equal ionic strength, isolating the difference to only their respective ionic composition. Properties of all the applied chemicals and filters are described in detail in section *3.1 Chemicals*.

Table 4.4.3: *Experimental matrixes conducted for investigation of Qc. Each Letter represents one matrix, containing at least 4 LPS experiments and two polymer experiments. Dashes (-) indicates excluded but possible matrixes.*

Filter size	**300 ppm Polymer concentration, 30:1 PtC-ratio**					
	0.5% NaCl		**5% NaCl**		**CeB 0.5/4.21**	
	3430S	**3630S**	**3430S**	**3630S**	**3430S**	**3630S**
0.5 µm	*A*	-	*F*	*H*	*J*	*L*
2 µm	*B*	*D*	*G*	*I*	*K*	*M*
7 µm	*C*	*E*	-	-	-	-

As seen in Table 4.4.3, only 13 of the 18 possible matrixes for the variation of the factors presented in Table 4.4.2 has been conducted. HPAM 3630S solved in 0.5% NaCl are known to plug the 0.5µm filters for certain concentrations, and has been excluded. The missing matrixes for 7µm filters are excluded because no Qc was found within the range of the differential pressure transmitter for the 2µm filters, or the Qc was at the fringe of the measurable range. Hence, Qc was not possible to determine for a filter with larger average pore size, and correspondingly higher flow rates and dP*.

Raw data from all experiments for both LPS and polymer solutions for all matrixes can be found in appendix A.5. The proposed method for quantification of Qc by intersection of the linear regressions did not apply to LPS solutions of Matrix K and L. Qc for these matrixes have therefore been estimated to the mean rate between the two apparent flow regimes

4.4.2 Variation of polymer molecular weight

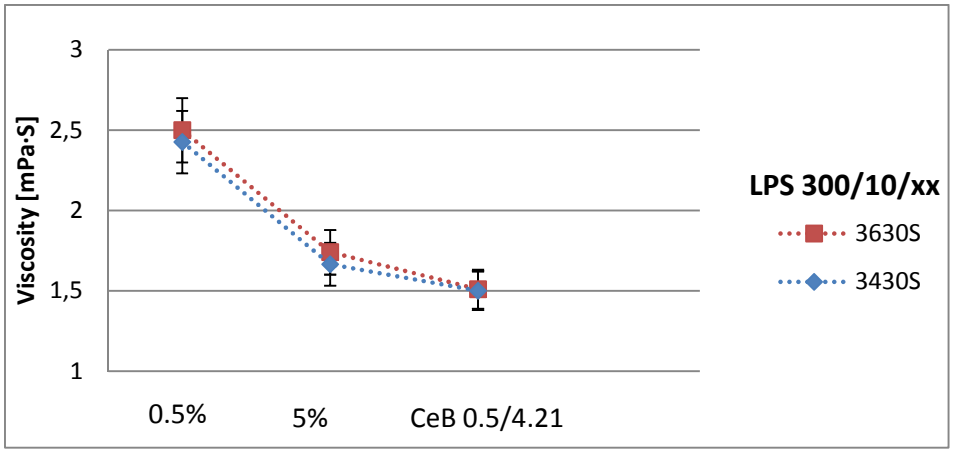

Figure 4.4.5: *Viscosities of HPAM 3430S and 3630S LPS 300/10 systems solved in different brines as denoted along the x-axis. The error bars denotes the total uncertainties in both measurement and preparation.*

As seen in Figure 4.4.5, the viscosities of the two polymer types are equal within the uncertainties for all solvents for LPS systems with 300ppm polymer. The viscosity variation caused by molecular weight is more notable for higher concentrations as shown in Figure 4.4.6:

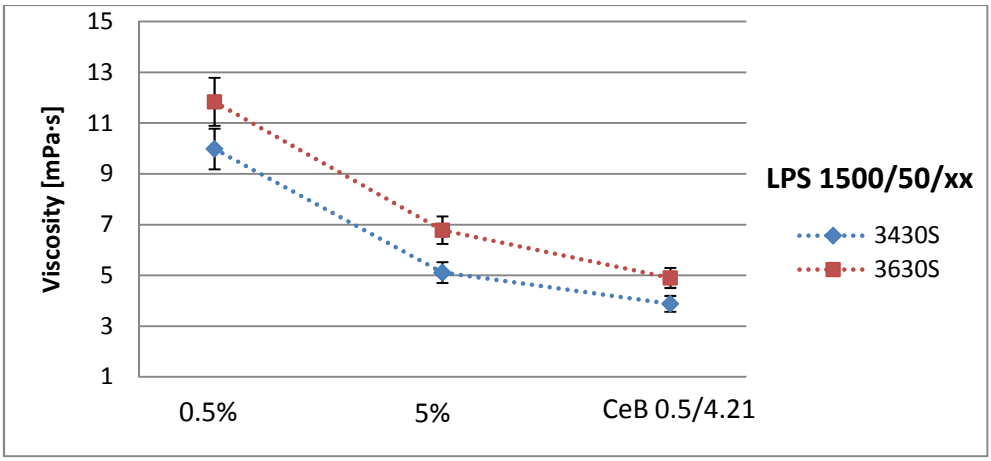

Figure 4.4.6: *Viscosities of HPAM 3430S and 3630S LPS 1500/50 systems solved in different brines as denoted along the x-axis. The error bars denotes the total uncertainties in both measurement and preparation.*

As seen in Figure 4.4.6, the LPS systems of the high molecular weight polymer 3630S has higher viscosity than those of the low molecular weight polymer 3430S, for all solvents.

Higher polymer molecular weights implies a longer polymer backbone for a linear polymers like HPAM, and are generally associated with higher solution viscosity[11] and higher particle sizes, both for cross-linked and non cross-linked coil and aggregates. Li et al.[10] found that the size of x-coils increased with polymer molecular weight as long as the concentration was

below the critical overlap concentration. Aarra et al. [17] reported that in a 600/30 LPS system, high molecular weight polymers had a significantly higher average particle size than low molecular weight polymers, both when solved in distilled water and in SSW.

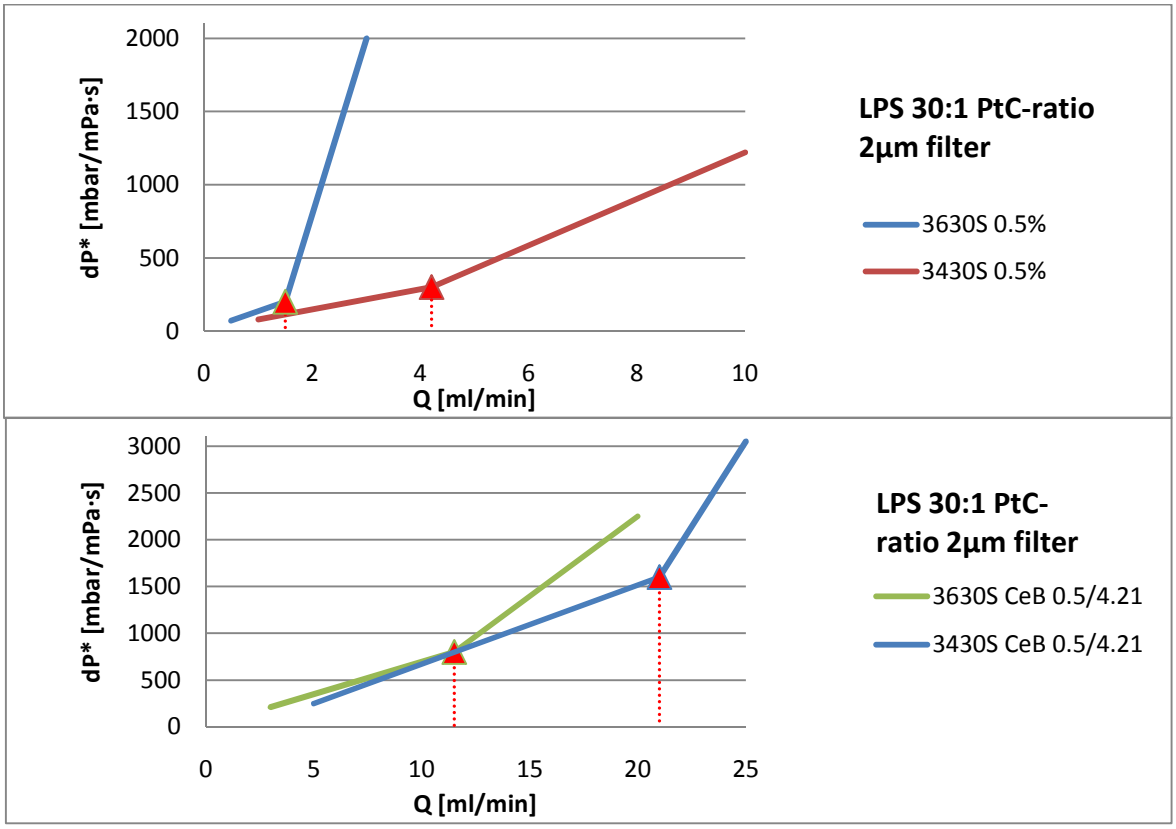

Figure 4.4.7: *Curves for dP*(Q) for 300/10 LPS systems of the two applied polymers solved 0.5% NaCl and CeB 0.5/4.21, injected over a 2µm filter. The red triangle and dotted line represents Qc, the shift between the two apparent flow regimes. The presented lines for dP* above and below Qc are linear regressions of the obtained data points.*

According to the Log Jamming hypothesis[7, 31], larger particle size in a solution should result in lower critical rate, Qc, as well as higher relative differential pressures, dP*, for rates below the critical. As seen in Figure 4.4.7, the LPS solutions of 3630S exhibits higher dP* for Q>Qc than those of 3430S. The critical rates, denoted by red triangles and a dotted red line in Figure 4.4.7, are also lower for 3630S than 3430S, both for LPS systems solved in 0.5% NaCl and CeB 0.5/4.21.

Table 4.4.4: *Estimated values of Qc for all polymer types, solvents, and filter sizes. (N/A) denotes that the particular system has not been filter-flooded, while (>) denotes that Qc was above the measured range. Each colour represents comparable critical rates with respect to polymer weight.*

Qc [ml/min] ±15%				
Filter size	**Polymer type**	**Solvent**		
		0.5 % NaCl	**5% NaCl**	**CeB 0.5/4.21**
0.5 µm filter	3430S	0.6	5.6	2.1
	3630S	N/A	2.3	0.8
2 µm filter	3430S	4.2	>25	21.0
	3630S	1.5	>20	11.5
7 µm filter	3430S	>25	N/A	N/A
	3630S	3.8	N/A	N/A

Table 4.4.4 presents the critical rates, Qc, for all applied filters and solvents, and for both polymer types. Each colour represents comparable Qc (3430S versus 3630S) for each filter size and solvent. The overall trend for comparable sets is a decrease in Qc for increased molecular weight. The trend is reproducible for all applied filter sizes and solvents where the critical rate has been found. The differences in Qc are significantly larger than the estimated uncertainty of ± 15%. Note that Qc was not investigated for all filter sizes of some brines (N/A), in accordance with the discussion following Table 4.4.3. For all applied systems, LPS solutions of 3630S gave higher dP*(Q) for rates below Qc than 3430S.

Conclusion

The experimental results presented in this section showed that increased molecular weight of the polymer applied in the LPS solutions results in higher bulk viscosity, lower Qc, and higher dP* for Q>Qc. The trends are reproducible for several filter sizes, i.e. different permeabilities, and solvents. This suggests that particle size in the solutions increases with polymer molecular weight for the measured concentration and experimental range.

4.4.3 Variation of ionic strength of solvent

HPAM is a polyelectrolyte and has a flexible chain structure, making its molecular conformation dependent on interactions with ions present in the solution. Compared to other polymers like Xanthan, HPAM has no permanent secondary structure, making it particularly sensitive with respect to molecular conformation in high ionic strength solutions[11].

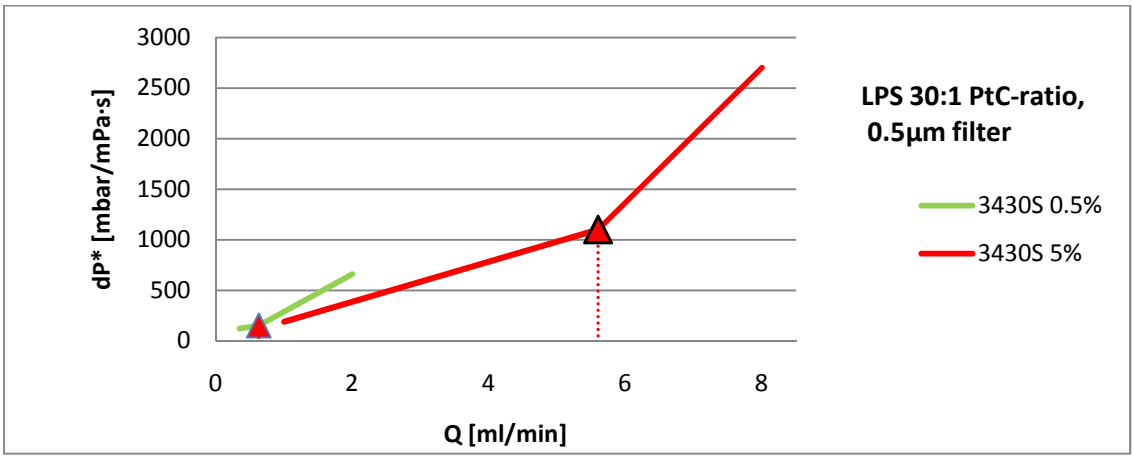

Figure 4.4.8: *Curves for dP* for 3430S 300/10 LPS systems solved in 0.5 and 5% NaCl brines, injected over a 0.5µm filter. The red triangle and dotted line represents Qc, the shift between the two apparent flow regimes. The presented lines for dP* over and below Qc are linear regressions of the obtained data points.*

As seen in Figure 4.4.8, the LPS solution solved in 5% NaCl exhibits lower dP* than that solved in 0.5% NaCl. Qc appears to occur at lower rates for 0.5% than 5% for 3430S. Table 4.4.5 presents comparable systems with respect to ionic strength. Qc is lower for LPS solved in 0.5% NaCl than those solved in 5% NaCl for all comparable systems. The trend applies both to 0.5 and 2µm filters. This means either that the x-coils in LPS systems solved in 5% NaCl are smaller than those solved in 0.5% NaCl, or that the affinity between the particles are higher when solved in 0.5% NaCl.

Table 4.4.5: *Estimated values of Qc for 300/10/xx LPS systems of different polymer types, solvents, and filter sizes. (N/A) denotes that the particular system has not been filter-flooded, while (>) denotes that Qc was above the measured range. Each colour represents comparable critical rates with respect to ionic strength.*

Qc [ml/min] ±15%			
Filter size	**Polymer type**	**Solvent**	
		0.5 % NaCl	**5% NaCl**
0.5 µm filter	3430S	0.6	5.6
	3630S	N/A	2.3
2 µm filter	3430S	4.2	>25
	3630S	1.5	>20
7 µm filter	3430S	> 25	N/A
	3630S	3.8	N/A

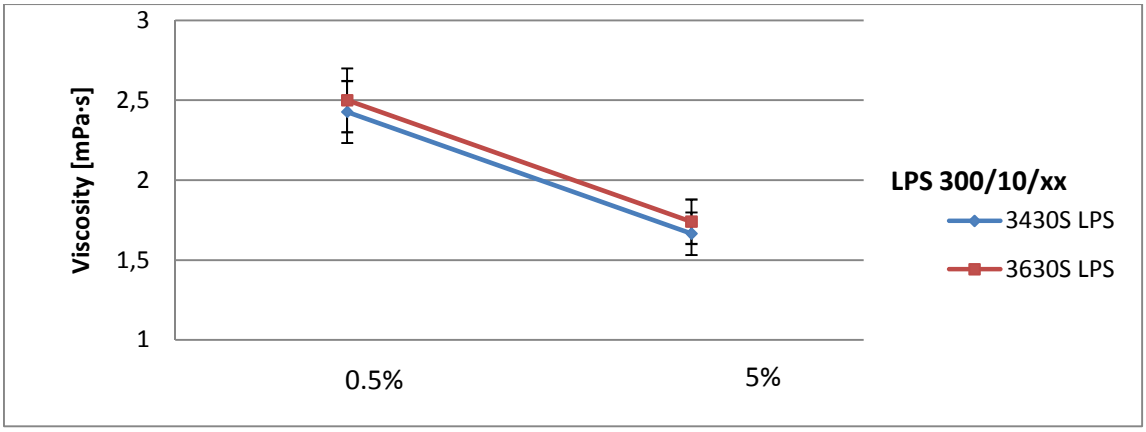

Figure 4.4.9: *Viscosities of 3430S and 3630S 300/10 LPS systems, solved in 0.5% and 5% NaCl. The error bars denotes the total uncertainties in both measurement and preparation.*

As seen in Figure 4.4.9, the viscosities for LPS systems of both polymer types has a viscosity loss for higher ionic strength of the solvent. Both solvents are sodium chloride brines, which cannot cross-link polymer molecules. Martin and Sherwood[34] claims that the viscosity of a solution is dependent on the degree of coiling of the polymer molecules. The more coiled, the lower the viscosity.

Conclusion

Based on the experimental results and the discussion in this section, it is suggested that increased ionic strength of the solvent in LPS solutions results in lower viscosities, lower dP* and higher critical rates. Higher ionic strength in the solution is reported to result in smaller average particle sizes, as the repulsive forces between the negatively charged carboxylate groups along the polymer backbone and the ions in the solution causes the polymer to coil up[11]. This indicates that the LPS particles have a smaller sizes for higher ionic strength, and that high ionic strength favours the formation of x-coils rather than x-aggregates in accordance with the findings of Wang and Lu[13]. The lower critical rates for LPS solved in 0.5% NaCl may also be due to higher affinity between the particles for this solvent compared to the affinity between the particles for LPS solved in 5% NaCl. These findings suggest that the Log-Jamming ability of LPS solutions are reduced for higher ionic strength of the solvent.

4.4.4 Variation of solvent composition

Unlike Na^+, polyvalent ions have greater impact on the ionic strength of solutions, and are capable of cross-linking without addition of a dedicated cross-linker. In the literature, several authors have reported that addition of divalent ions results in lower viscosities for HPAM solutions, but without considering the cross-linking aspect[19, 34]. The viscosity reduction caused by ions in solutions have been seen as a limiting factor for conventional polymer EOR-applications[35], and salt-resistant non-polyelectrolyte polymers like Xanthan have been applied instead of HPAM for particular saline reservoirs[36]. Mack and Smith[1] reported that CDG applications for water shut-off was not successful for reservoirs containing more than 30,000 ppm total dissolved solids (TDS).

Spildo et al.[7] reported lowered S_{or} after post-water LPS floods in reservoir cores. The experimental data indicated that the increased recovery was caused by the Log Jamming mechanism as presented in section *2.2. LPS for Enhanced Oil Recovery (EOR)*, resulting in microscopic flow diversions that mobilized oil previously bypassed by the brine flood. This interpretation means that the viscosity degradation of HPAM for increased solvent salinity is not a limiting factor for LPS applications in saline reservoirs, since the major recovery mechanism is governed mainly by the particulate properties, not the viscous properties, of the injected solution

Wang et al.[18] reported that for 700 mg/L HPAM solution solved in distilled water, addition of ≥ 216 mg/L Ca^{2+} provided the optimum concentrations for formation of x-coils. The experimental data also showed that Ca^{2+} was more likely to enhance formation of intra-molecular cross-linking than Mg^{2+} in a LPS system.

To investigate the effect of Ca^{2+}-addition, polymer and LPS solutions of both polymer types were filter-flooded solved in a calcium enriched brine, CeB 0.5/4.21, containing 0.5% by weight $CaCl_2$ and 4.21 percent by weight NaCl. CeB 0.5/4.21 has an ionic strength equivalent to a 5% NaCl brine as seen in Table 3.2.1. This should keep the effect of ionic strength on the polymer molecular conformation constant, any changes in conformation should therefore be attributed the Ca^{2+} ions.

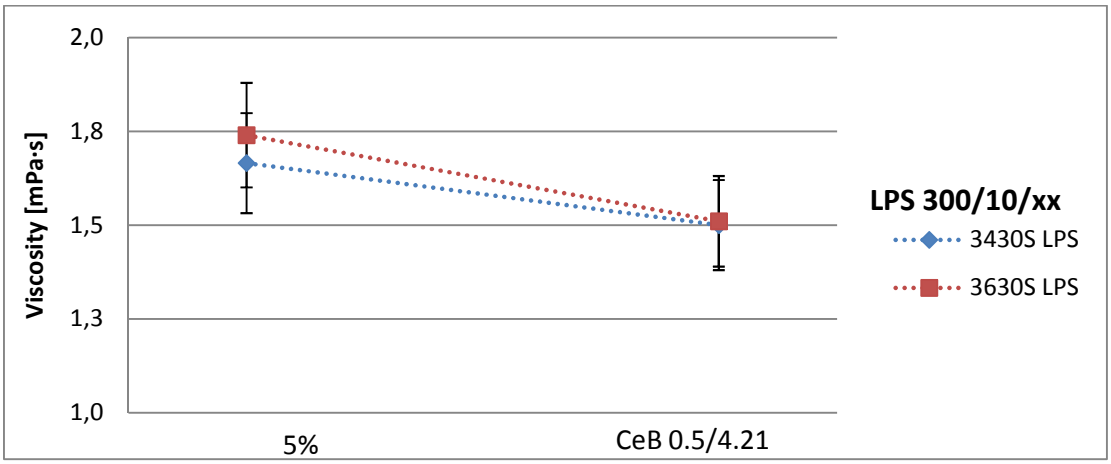

Figure 4.4.10: *Viscosities of 3430S and 3630S 300/10 LPS systems, solved in 5% NaCl and CeB 0.5/4.21. The error bars denotes the total uncertainties in both measurement and preparation.*

As seen in Figure 4.4.10, the viscosity loss when Ca^{2+} ions are added to the solution is within the uncertainties. However, there is a trend for decreasing viscosity for both polymer types, indicating smaller particles for the solutions containing Ca^{2+} than of those containing only NaCl.

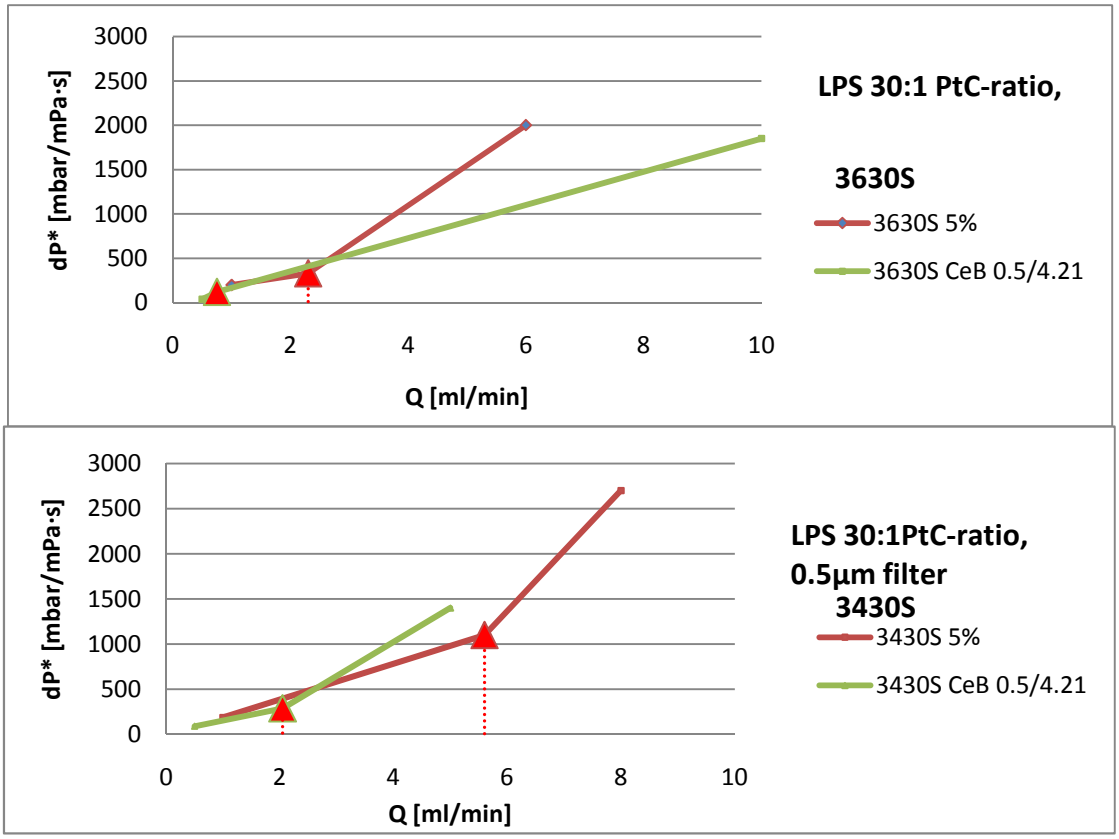

Figure 4.4.11: *Curves for dP* for 300/10 LPS systems of the two applied polymer types solved in 5% NaCl and CeB 0.5/4.21 brines, injected over a 0.5µm filter. The red triangles and dotted lines represents Qc, the shift between the two apparent flow regimes. The presented lines for dP* over and below Qc are linear regressions of the obtained data points.*

As seen in Figure 4.4.11, both LPS systems solved in CeB 0.5/4.21 exhibits lower dP* than the corresponding LPS solved in 5% NaCl, for rates below Qc. However, Qc for the CeB 0.5/4.21 systems are lower than those solved in 5% NaCl for both polymer types. The trends applies also to the filter-floods performed over the 2µm filters as shown in Table 4.4.6, and shows good reproducibility.

Table 4.4.6: *Estimated values of Qc for 300/10 LPS systems of different polymer types, solvents, and filter sizes. (>) denotes that Qc was above the measured range. Each colour represents comparable critical rates with respect to particle size versus solvent composition.*

Qc [ml/min] ± 15%			
Filter size	**Polymer type**	**Solvent**	
		5% NaCl	**CeB 0.5/4.21**
0.5 µm filter	3430S	5.6	2.1
	3630S	2.3	0.8
2 µm filter	3430S	>25	21.0
	3630S	>20	11.5

The LPS systems solved in calcium enriched brine has lower Qc than those solved in 5% NaCl for all comparable sets. Following the previous argumentation, this would suggest an increase in particle size when Ca^{2+} is added to the solution, i.e. Ca^{2+} enhances the formation of x-aggregates. However, both the reduced dP* for rates below Qc, and the fact that the viscosity of the solutions does not increase predicts the opposite; Ca^{2+} promotes the formation of x-coils. Regarding the influence of molecular weight and ionic strength, both dP*, Qc and µ concurred that the particle size either in- or decreased. Since both dP* and the viscosities points in the direction of enhanced formation of x-coils for this case, alternative interpretations of the difference in Qc is proposed:

i) Calcium ions promotes formation of x-coils, but does also increase the absolute number of x-coils in the solution, resulting in reduced average particle size but a larger particle volume per fluid volume, hence Log-Jamming will occur at lower flow rates.

ii) Calcium ions promotes formation of x-coils with a higher density than x-coils cross-linked by Al^{3+}. Hence, these particles will accumulate more efficiently at the pore throats, causing Log-Jamming at lower flow rates.

iii) The x-coils cross-linked by calcium have a higher affinity between each other, improving their ability to aggregate, resulting in Log-Jamming for lower flow rates.

Interpretation i) is supported by the fact that when Ca^{2+} is introduced into the solution, the concentration of potential cross-linkers (Ca^{2+} and Al^{3+}) are greatly increased as shown in Table 4.4.7:

Table 4.4.7: *Stoichiometric relationships between the charges hydrolyzed polymer monomers (negatively charged) and charge of Al^{3+}/Ca^{2+} ions, for the applied polymer types and brine compositions.*

Brine	Polymer type	Av. Mw	$C_{polymer}$	C_{Al3+}	C_{CaCl2}	Hydrolyzed monomers	Charge of Al^{3+}/Ca^{2+}	Charge ratio
		[Mda]	[ppm]	[ppm]	[ppm]	[H.monomers/ kg solution]	[Σcharge/kg solution]	[Σcharge/ H.monomers]
5% NaCl	3430S	12	300	10	0	7.0E+20	6.7E+20	1
	3630S	20	300	10	0	7.0E+20	6.7E+20	1
CeB 0.5/4.21	3430S	12	300	10	5000	7.0E+20	5.5E+22	78
	3630S	20	300	10	5000	7.0E+20	5.5E+22	78

The numbers presented in Table 4.4.7 are calculated assuming 27.5% average degree of hydrolysis, and an average monomer molecular weight of 70.34 g/mol derived from this hydrolysis degree. Σ_{charge} is calculated by weighting the polyvalent ions for their valence. As suggested in section *2.1 Linked Polymer Solutions (LPS)*, the equilibrium between HPAM, cross-linker, and LPS particles may be given as:

$$\text{Cross-linker} + \text{HPAM} \leftrightarrow \text{LPS} \qquad \textbf{(2.1)}$$

Because both Ca^{2+} and Al^{3+} ions are capable of cross-linking, the equilibrium should shift towards the formation of more LPS particles with addition of Ca^{2+} in the solution. As seen in Table 4.4.7, charge of potential cross-linkers are increased by a factor 78 for CeB 0.5/4.21 compared to that of 5% NaCl.

Interpretation ii) can be supported by the experimental work by Rahmann et al.[33]. The authors injected clay suspensions through a thin capillary tube and studied the critical conditions for particle deposition in the tube, leading to increased differential pressure and plugging. The threshold number for particles per time entering the capillary before deposition occurred was found to be inverse proportional to the density of the particles, i.e. a higher density resulted in a lower threshold number. These findings cannot be directly related to the experiments done for this thesis, but since many of the concepts and questions are similar, the effect of density on Qc cannot be totally disregarded. Fallah et al.[31] suggested that the

accumulation of the particles that causes Log-Jamming where related to the density difference between the particles and the solvent. As a LPS solution flows through a pore throat, the density difference will cause the water to flow faster than the particles, resulting in a net accumulation of particles. The mean density of spherical microgels can be evaluated by the Einstein relation[4], given as:

$$V_{sp} = 2.5|\eta|_o \quad \textbf{(4.4)}$$

Where V_{sp} is the mean volume of the microgel particles, and $|\eta|_o$is the zero-shear intrinsic viscosity. Tables 4.5.3 and 4.5.4 presents intrinsic viscosities,$|\eta|_{100}$, obtained from reduced viscosities at a reference shear of 100 1/s. There is observed a trend for decreasing $|\eta|_{100}$ for addition of calcium under constant ionic strength. X-coils are known to be spherical[10], and assuming that $|\eta|_{100}$ is proportional to $|\eta|_0$it is thus suggested that addition of Ca^{2+} results in lower intrinsic viscosities, thereby smaller mean particle volumes, i.e. higher density of the cross-linked particles.

Interpretation iii) is based on the findings of Chauveteau et al.[4], which related Huggins constant, K_H, to the hydrodynamic interactions between dispersed colloids during shear flow. The authors suggested that K_H rises sharply when attractive interactions between the colloids are involved. As seen in Tables 4.5.3 and 4.5.4, K_H is mainly increasing for addition of Ca^{2+} under constant ionic strength for all solutions. This may indicate that addition of Ca^{2+} increases the affinity between the x-coils in the solution, improving their ability to aggregate, and causing Log-Jamming for lower rates.

Conclusion

Based on the presented experimental data and discussion, it seems that addition of Ca^{2+} to the solvent under constant ionic strength results in constant solution viscosities, lower dP* for rates Q<Qc, but also lower critical rates. The lowered critical rates suggest an increase in either the number of x-coils, x-coil density, or affinity between the x-coils.

4.4.5 Aluminium substituted by calcium

As suggested from experiments in this thesis and previous reports, Ca^{2+} ions in the solvent are capable of cross-linking polymer molecules without addition of a dedicated cross-linker. Considering an offshore LPS-application, it would be convenient to inject a LPS system cross-linked solely with Ca^{2+}, because Ca^{2+} is one of the major ionic components in seawater which is widely injected for pressure maintenance in existing offshore oilfields. It would also simplify the preparation of LPS solutions, as the challenging preparation of AlCit stock solutions as described in section *4.1.2 Aluminium Citrate solutions* would not be necessary. By excluding AlCit as cross-linker, one would also avoid the alien substance Citrate inside the reservoir, which may adsorb onto the reservoir rock. Injecting a LPS system solved in calcium enriched seawater in an already seawater-flooded reservoir would hence give a reduced risk of precipitation, adsorption of ions onto reservoir rock, or other unwanted effects, compared to a corresponding LPS system cross-linked by AlCit.

AlCit is known to ensure a relatively slow rate of cross-linking[8]. In contrast, $CaCl_2$ are completely disassociated when in the concentrations used for the experiments. This could lead to an increased rate of cross-linking, which may result in precipitations or gel formation. To monitor the behaviour of LPS solved in brines containing increasing concentrations of Ca^{2+}, and estimate equivalent concentration of Ca^{2+} to 10ppm Al^{3+} for 300 ppm polymer/LPS solutions, dP*, Qc and viscosity have been compared for the solutions presented in Table 4.4.8.

Table 4.4.8: *Solutions compared to estimate the Ca^{2+} equivalence of Al^{3+} in a LPS system.*

Polymer type	**Solution**	**C_{Al3+} [ppm]**	**C_{NaCl} [ppm]**	**C_{CaCl2} [ppm]**	**Ionic strength**
3430S	LPS 300/10/5%	10	50000	-	0.856 mol/ kg solution
	Polymer 300/0/5%	-	50000	-	
	Polymer 300/0/CeB 0.5/4.21	-	42100	5000	
	Polymer 300/0/CeB 1.0/3.42	-	34200	10000	

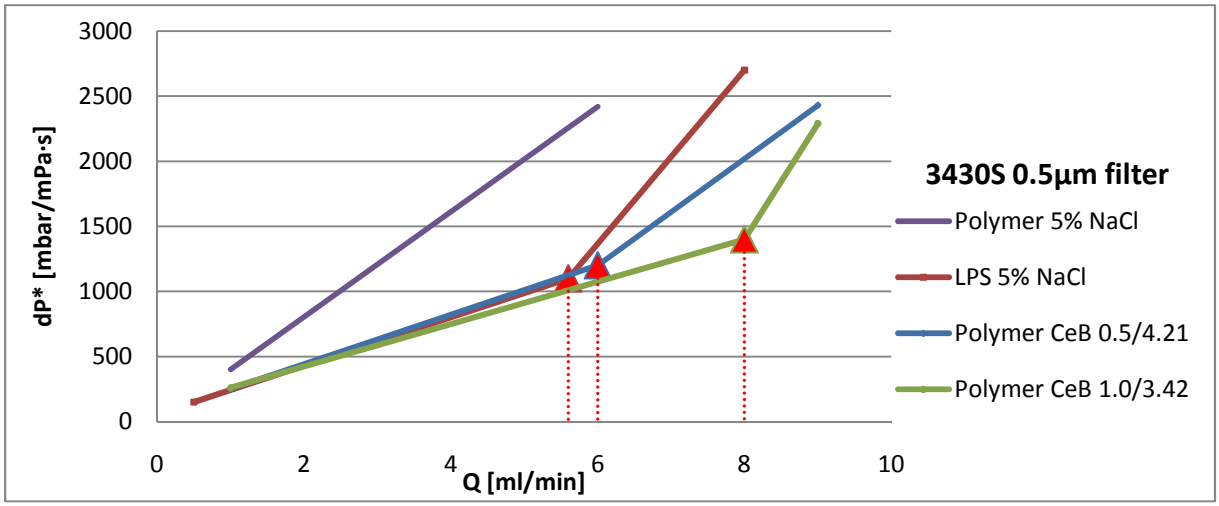

Figure 4.4.12: *Curves for dP* for 300/10/5 LPS and polymer solutions of different brines as described in the legend, injected over a 0.5µm filter. Qc was not observed for the polymer system solved in 5% NaCl.*

As seen in Figure 4.4.12, Qc was not observed within the experimental range for the 5% NaCl polymer solution. The two polymer solutions solved in calcium enriched brines have virtually equal dP* to the LPS system solved in 5% NaCl, for rates below their critical rate. As seen in Table 4.4.9, the Qc of 300/0/CeB 0.5/4.21 is equal to that of 300/10/5 within the uncertainties.

Table 4.4.9: *Estimated critical rates for the fluid systems shown in Figure 4.5.8.*

Filter size	Polymer type	Solvent	Fluid system	Qc [ml/min] ± 15%
0.5 µm filter	3430S	5% NaCl	300/0/5	>6
		5% NaCl	300/10/5	5.6
		CeB 0.5/4.21	300/0/CeB 0.5/4.21	6.0
		CeB 1.0/3.42	300/0/CeB 1.0/4.21	8.0

The discussion in section *4.4.4 Variation of solvent composition,* suggested that addition of Ca^{2+} to a LPS solution could result in higher affinity between the x-coils, therefore Qc occurred for lower rates than LPS solutions solved in 5% NaCl. However, the data shown in Table 4.4.8 indicates that increased Ca^{2+} concentrations to above 0.5% results in a higher Qc, while the dP* for rates below the critical are approximately unchanged. This could mean that the particles solved in the two calcium enriched brines have about the same particle sizes, but a different affinity between each other. An explanation for this could be that in a LPS system solved in CeB 1.0/3.42, the negative sites along the polymer molecule could be over-

saturated, resulting in Ca^{2+} that are not cross-linking, but rather bonding to just one carboxylate group. This would cause repulsion between the particles, since these Ca^{2+} ions still would have a net positive charge, resulting in reduced Log-Jamming abilities, and hence a higher Qc. This proposal is supported by the fact that the concentrations of divalent ions are twice as high in CeB 1.0/3.42 as in CeB 0.5/4.21.

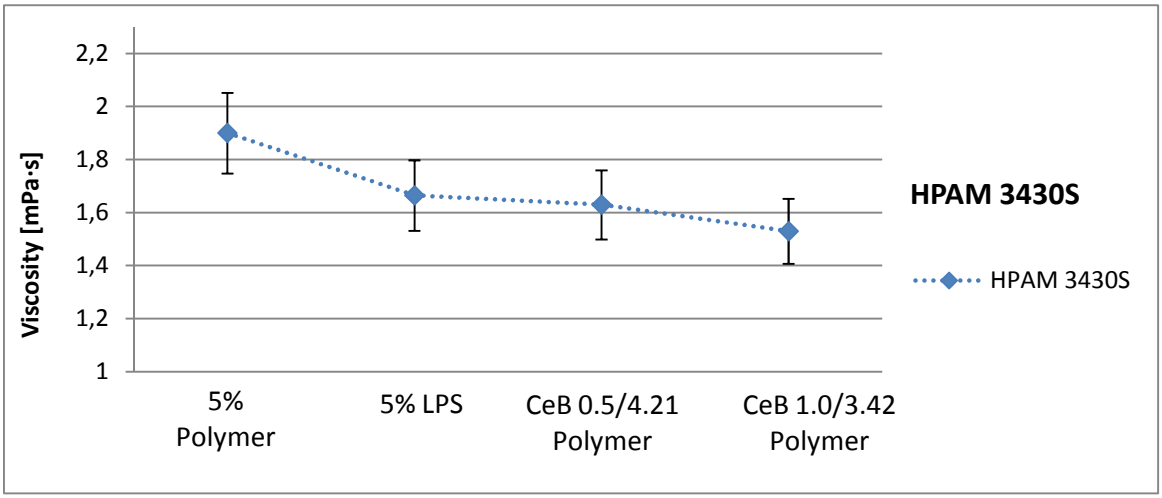

***Figure 4.4.13**: Measured viscosities of the solutions presented in Table 4.4.9. Error bars represent the uncertainty in both preparation and measurement.*

As seen in Figure 4.4.13, the non cross-linked polymer solution in the monovalent brine 5% NaCl has the highest viscosity, followed by a decrease in viscosity with addition of Al^{3+} or Ca^{2+} to the solutions. The reduction in viscosities is within the uncertainties for each step, but there is a trend for decreasing viscosity with higher concentration of polyvalent ions (Al^{3+} and Ca^{2+}).

Conclusions

None of the applied solutions solved in brines containing Ca^{2+} resulted in precipitations or plugging of the filters.

Addition of 0.5% $CaCl_2$ to a polymer solution under constant ionic strength seems to give equivalent dP*, μ, and Qc as the corresponding LPS solution solved in 5% NaCl cross-linked by 10 ppm Al^{3+}. This suggests that the two solutions have the same Log-Jamming ability when flooded through a porous medium.

Addition of 1.0% $CaCl_2$ to a polymer solution under constant ionic strength seems to give equivalent dP* and μ, but a higher critical rate than both the corresponding LPS solution solved in 5% NaCl, and the corresponding polymer solutions solved in CeB 0.5/4.21. A proposed reason for this is repulsion between the particles in CeB 1.0/3.42, caused by oversaturation of the negative sites along the polymer backbone.

4.4.6 Differential pressure of non-cross-linked polymer solutions

To minimize the number of experiments needed for each experimental matrix, the corresponding polymer solutions of the applied LPS solutions have only been filter-flooded for two rates per experimental matrix, except for matrixes B, F and J, where the polymer solutions have been filter-flooded for all the same rates as the LPS solutions. This means that the data sets for the relative differential pressure properties of polymer compared to LPS solutions are not complete, but some trends have appeared. The relative differential pressures for all LPS/polymer solutions of all matrixes can be found in appendix A.5.

When solved 0.5% NaCl, polymer solutions exhibited approximately the same dP* as the corresponding LPS solution for rates below Qc. This trend applied to both LPS/polymer systems of HPAM 3430S and 3630S. Based on the data obtained from the experiments in Matrix B, there occurs a critical rate also for polymer solutions within the experimental range, but the slope of dP*(Q) for rates above Qc are lower than that of the LPS solution.

When solved 5% NaCl, polymer solutions exhibited higher dP* than the corresponding LPS solutions for rates below Qc. The trend was reproducible for all filter sizes and both polymer types, with an average of approximately 90% higher dP* than the corresponding LPS solutions. Based on the data obtained from the experiments of Matrix F, the Qc was not observed for the polymer solution within the experimental limits.

When solved in CeB 0.5/4.21, polymer solutions exhibited higher dP* than the LPS solutions for rates below Qc. The trend was reproducible for all filter sizes and both polymer types, with an average of approximately 60% higher dP* than the corresponding LPS solutions. Based on the data obtained from the experiments of Matrix J, Qc of the polymer solution occurs for higher rates than the corresponding LPS solution.

The main trend found from the comparison between polymer/LPS is that the polymer solutions exhibit higher dP* than the LPS solutions, when solved in high salinity brines. A reason for this observation may be the model for polymer flow through a capillary presented by Zaitoun[37] as seen in Figure 4.4.14.

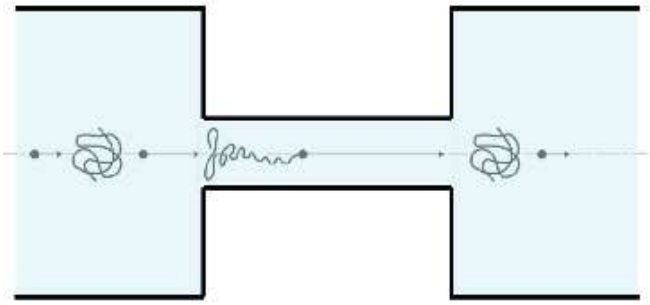

Figure 4.4.14*: Model for the conformation-transition of a polymer molecule during shear flow through a capillary (Zaitoun[37])*

As seen in Figure 4.4.14, the polymer molecule is coiled before entering the capillary, stretches during flow inside the capillary, before it re-coils after leaving the capillary. The energy needed to stretch the molecule is thought to be dependent on the degree of coiling in the polymer molecule, which in turn is dependent on the solvent ionic strength. This approach suggests that since polymer molecules solved in the high salinity brines 5% NaCl or CeB 0.5/4.21 are more coiled than polymer molecules solved in 0.5% NaCl, it is more energy demanding for high salinity brine polymer solutions to flow through the filters, which results in higher dP*. LPS particles are reported to be more rigid than non-cross-linked polymers[10], and are thus believed to be less stretched during flow in the capillary when solved in high salinity brines, resulting in lower dP* than the polymer solutions.

When solved in 0.5% NaCl, both LPS and polymer solutions exhibit approximately the same dP*. This may be due to that both cross-linked and non-cross-linked polymer molecules are less coiled for this solvent compared to the high ionic strength solvents, resulting in similar resistance to stretching for both species.

Based on the available experimental data, these suggestions are only valid when comparing dP* of LPS/polymer solution for rates below the critical. This is because the dP* of the LPS

solutions for rates above Qc is governed also by the Log-Jamming effect, not only the conformation-transition model as shown on Figure 4.4.14.

Conclusion

The proposed mechanisms and experimental observations suggests that when solved in 0.5% NaCl, the energy needed to flow non-cross-linked polymer molecules trough porous media is equivalent to the energy needed to flow LPS particles through porous media. However, when solved in 5% NaCl or CeB 0.5/4.21, non-cross-linked polymer molecules are more energy demanding to flow through porous media than LPS particles, probably due to the increased degree of coiling implied by higher ionic strength of solvent. Based on the available experimental data, these suggestions are only valid for rates below Qc.

4.4.7 Shear dependent viscosity

The dP*(Q) charts that formed the basis for estimation of Qc were made under the assumption of a constant viscosity for all flow rates, i.e. shear rates, in the filters. The viscosity used for substitution of dP with dP* were the bulk viscosities, stated for a reference shear rate of 100 1/s by convention as discussed in section *3.6.1 Viscosity measurements*. This approach would be appropriate for a Newtonian fluid, which has a constant viscosity regardless of the shear rate, but polymer solutions are known to exhibit non-Newtonian behaviour, which implies that their viscosities are dependent on the shear rate, as discussed in section *2.3.1 Non-Newtonian behaviour*.

The shear thickening behaviour of polymer solutions means that for shear rates above a certain magnitude, the apparent viscosity during shear flow is increasing. The increased apparent viscosity could have resulted in higher differential pressures during filter-floods. To investigate if the shear thickening behaviour of could explain the observed increase in dP* for rates above Qc, the following model was applied:

Shear rates in the filter were estimated by an approximation commonly used for shear estimation in porous media[38] as shown in Formula 4.5:

$$\gamma_{pm} = \frac{(1+3n)}{4n}\frac{4u}{\sqrt{8k\emptyset}} = \alpha\frac{4u}{\sqrt{8k\emptyset}} \qquad \textbf{(4.5)}$$

Where γ_{pm} is the shear rate in the porous media, u is the Darcy velocity, K is the permeability, $\emptyset$ is the porosity, and n is the power law exponent which governs the "shift

factor" α. The power law exponent *n* is usually ranging from 0.6 up to1.0, but is assumed unity for this model, giving α =1. The Darcy velocity *u* is defined as *Q/A*.

Viscosity measurements for shear rates ranging from 10 up to 5300 1/s were conducted with the rheometer using the cone plate geometry. Shear curves for LPS/polymer solutions of HPAM 3430S solved in all applied brines were obtained. The shear rates for each rate over a given filter where matched with the corresponding viscosities from the obtained shear curves. These viscosities were thereafter used to calculate the shear-dependent relative differential pressure, given by formula 4.6:

$$dP_i^{*\gamma} = \frac{dP_i}{\mu^{\gamma}{}_i} \qquad \textbf{(4.6)}$$

Where $dP_i^{*\gamma}$ is the shear-dependent relative differential pressure, dP_i is the differential pressure, and $\mu^{\gamma}{}_i$ is the shear-dependent viscosity, all for solution *i*. The shear dependent relative differential pressure enables interpretation of dP as function of flow rate with the shear thickening behaviour of the LPS/polymer solution accounted for.

Figure 4.4.15 shows the shear rates for the applied filters, estimated by Formula 4.5. The corresponding shear rates for a 1.5" 600 mD core plug with Ø = 0.35 is included for comparison.

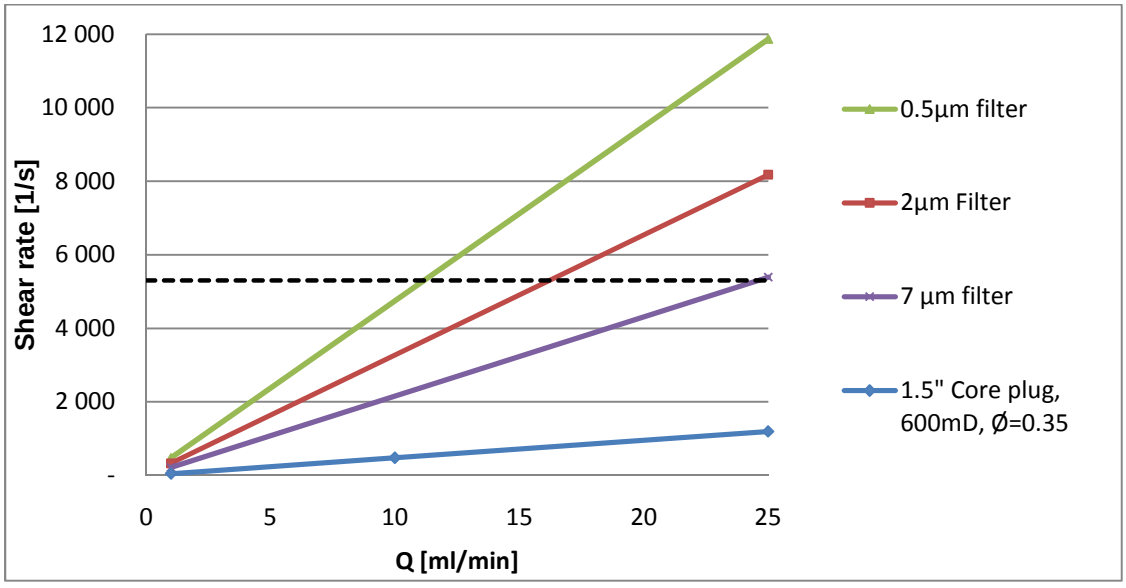

Figure 4.4.15: *Estimated shear rates for the applied filter and a core plug for comparison, all as a function of flow rate. The horizontal dotted line represents the upper shear rate limit for the shear curves obtained from the Rheometer.*

As seen in Figure 4.4.15, all the filters gives significantly higher shear rates than a typical 1.5” 600 mD core plug with a porosity of 0.35, due to the lower flow areas and permeabilities in the filters. The horizontal dotted line on Figure 4.4.15 represents the upper shear rate limit for the shear curves obtained from the Rheometer as seen in Figure 4.4.16. This means that $dP^{*\gamma}$ cannot be estimated for flow rates above this limit, 5300 1/s.

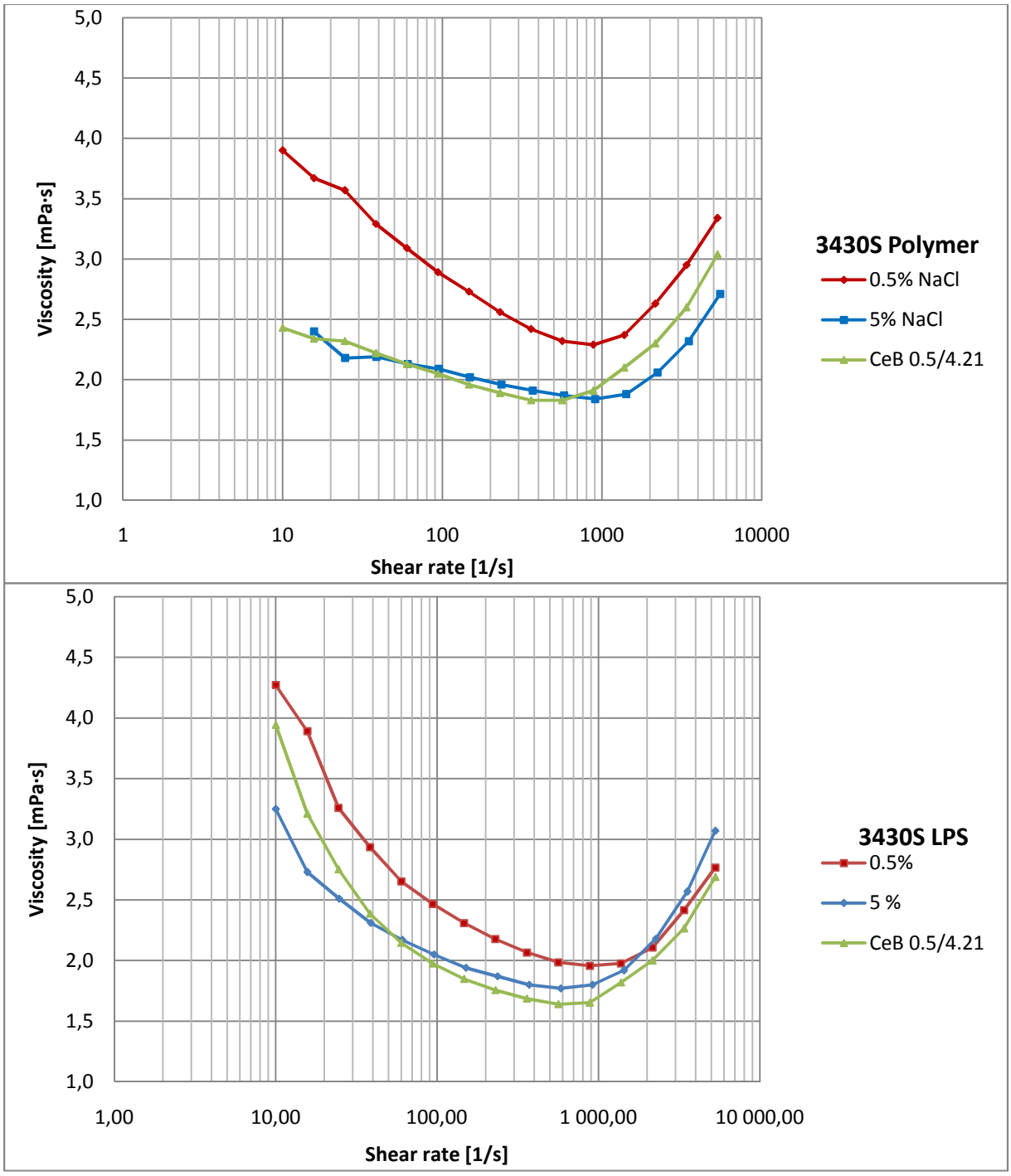

Figure 4.4.16: *Shear curves for LPS/polymer solutions of HPAM 3430S solved in the applied brines, obtained from the Rheometer.*

Figure 4.4.16 shows that the different solutions exhibit shear thinning behaviour up to a shear rate of about 600 to 1000 1/s before becoming shear thickening. None of the solutions has been measured for shear rates below 10 1/s or above 5300 1/s due to limitations in the Rheometer.

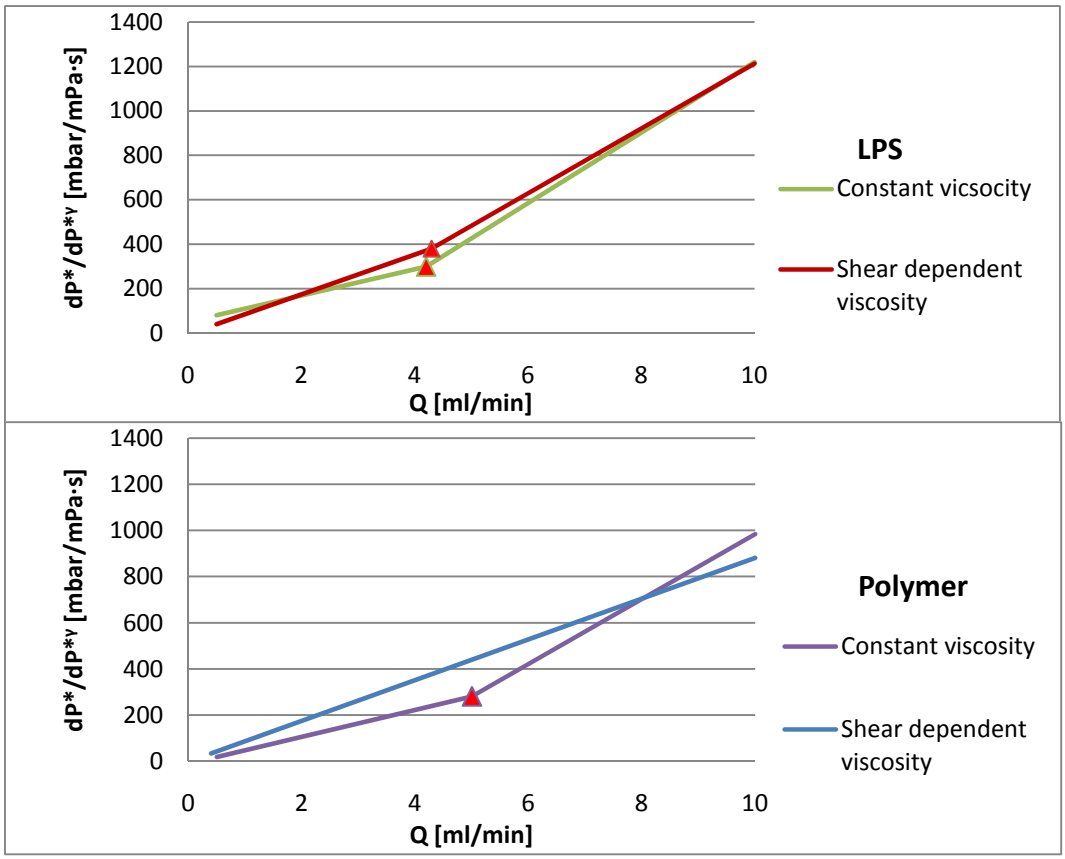

Figure 4.4.17: *Curves for the relative differential pressure calculated by constant viscosity (dP*), and shear dependent viscosity ($dP^{*\gamma}$) for a 3430S 300/10/0.5 LPS and the corresponding polymer solution, injected over a 2µm filter.*

Figure 4.4.17 shows the results from the initial experiments, Matrix B as presented in Table 4.4.1, for constant viscosity and shear dependent viscosity. To estimate the shear dependent viscosity, the shear rate for the filter and rate in question was found from Figure 4.4.15, and the corresponding viscosity for the particular fluid/rate was obtained from Figure 4.4.16. As seen in Figure 4.4.17, the vertex in dP*(Q) for LPS is reduced, but the critical rate is still possible to locate by intersection of the linear extrapolations from each flow regime. However, the vertex disappears for the polymer solution when the shear dependent viscosity is applied instead of the constant viscosity, and no critical rate is observed. These trends is observed for all experimental matrixes where the model for shear dependent viscosity has been applied (Matrixes A, B, F and J).

The observations indicates that the increased dP*(Q) observed for polymer solutions is due to the shear thickening behaviour, whereas the pressure build up seen for LPS solutions exceed that of the shear thickening contribution. This supports the hypothesis that the increased dP* for LPS solutions above the critical rate is caused by the Log-Jamming effect, not the viscoelastic effect.

Figures for all LPS systems where $dP^{*\gamma}$ has been applied can be found in appendix A.7.

As shown in Figure 4.4.17 there is a certain deviation in the magnitude of Qc for the LPS solution based on which viscosity approach that is applied. Table 4.4.10 shows the values of Qc for both approaches, as well as the standard deviations. As seen, the average deviation between the two approaches is within the estimated uncertainty for the critical rate.

Table 4.4.10: *Values of Qc calculated by constant and shear dependent viscosity, for 3430S 300ppm LPS solutions solved in different brines, flooded over a 0.5µm filter.*

Brine	**Qc [ml/min] ± 15%**		**Standard deviation**	
	Constant viscosity	**Shear dep. viscosity**	**[% of $Qc_{Const.\ Visosity}$]**	**Average**
5 %	5.60	5.90	4 %	9 %
0.5%	0.63	0.70	8 %	
Ceb 0.5/4.21	2.05	1.60	16 %	

Conclusion

The effective shear rates in the filters where estimated to be significantly higher than those encountered during flow in typical core flooding materials or reservoirs. Rheological data obtained from high shear rheology measurements suggested that the LPS/polymer solutions could exhibit shear thickening behaviour for the flow rates encountered during filter-flooding.

The estimated shear rates were matched with corresponding shear dependent viscosities obtained from rheometer measurements for the respective flow rates and LPS/polymer solutions. The shear dependent viscosities were thereafter used to estimate the shear dependent relative differential pressures, $dP^{*\gamma}$.

The application of $dP^{*\gamma}$ suggested that the increased dP* seen for polymer solutions above Qc was caused by the shear thickening effect. However, the increased dP* of LPS solutions above Qc could not be explained solely by the shear thickening effect. These findings support

the hypothesis that Log-Jamming is the major mechanism for increased dP* of LPS solutions at rates above Qc .

Figure 4.4.18 presents a schematic model of the proposed mechanisms responsible for pressure build up for various fluids and increasing flow rates. Brines have linear curve for dP(Q) within the experimental ranges. Polymer solutions behave like brine, but with higher dP, until the flow rates results in shear rates that causes shear thickening behaviour. LPS solutions behave like polymer solutions, but will also have an additional pressure build up when the Log-Jamming effect occurs for rates above Qc.

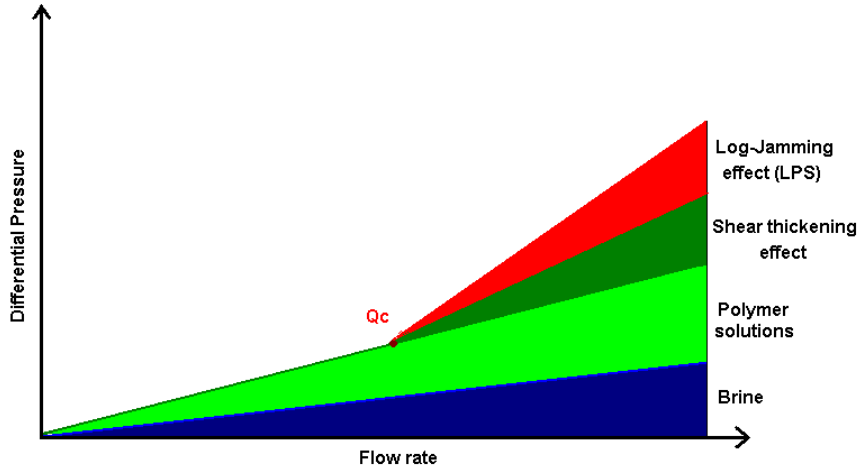

Figure 4.4.18: *Schematic model of the proposed mechanism for pressure build up during flow of various fluid types in porous media.*

The variation in Qc for LPS solutions were within or close to the uncertainty (±15%) for the two approaches (dP* and $dP^{*\gamma}$). The shear dependent relative differential pressure $dP^{*\gamma}$ was therefore not applied to more experimental matrixes for determination of Qc.

4.5. Polymer properties

4.5.1 Models for shear flow

Section *2.3.2 Models for shear flow* presented two mathematical models to describe the non-Newtonian flow of polymer, the Power law model and the Carreau-Bird-Yasuda model, as given by Formula 2.4 and 2.5 respectively.

$$\mu(\gamma) = K'\gamma^{n-1} \qquad \textbf{(2.4)}$$

$$\mu(\gamma) = \mu_\infty + (\mu_0 - \mu_\infty)[1 + (\gamma\lambda)^2]^{\frac{n-1}{2}} \qquad \textbf{(2.5)}$$

Parameters and the limitations for both models are given in section *2.3.2 Models for shear flow.*

The Power Law indexes (*n)* has been calculated for LPS and polymer solutions of HPAM 3430S solved in the applied brines, with both the PLM and the CBY model. The indexes have been calculated by fitting the measured viscosities to the Formulas 2.4 and 2.5 by the least-squares method, under the assumptions presented in Table 4.5.1. Flow charts of all the measured solutions are shown on Figure 4.4.16.

Table 4.5.1: *Assumptions for calculation of Power Law indexes.*

Parameter	Assumption
Infinite shear viscosity	$\mu\infty = \mu_{solvent}$
Zero shear viscosity	$\mu_0 > 1.5(\mu_{10\ 1/s})$
Power law index	$n < 1.0$

The rough estimate of the zero shear viscosity is due to the lack of viscosity measurements for shear rates below 10 1/s. Power Law indexes must be below unity since the solutions are non-Newtonian. Figure 4.5.1 presents both the PLM and CBY model compared to the measured viscosities.

As discussed in section *2.3.1 Non-Newtonian behaviour*, the shear thinning behaviour is caused by the equilibrium structure of the particles in solution being broken. The viscosity is decreasing as the polymer molecules are un-coiled and the number of inter-molecular associations is reduced. The resistance to un-coil is probably governed by the affinity between the particles, as strong attractive forces will resist splitting and vice versa. The power law

index *n* reflects the slope of the shear thinning region, and can therefore be seen as a measure for the affinity between the particles.

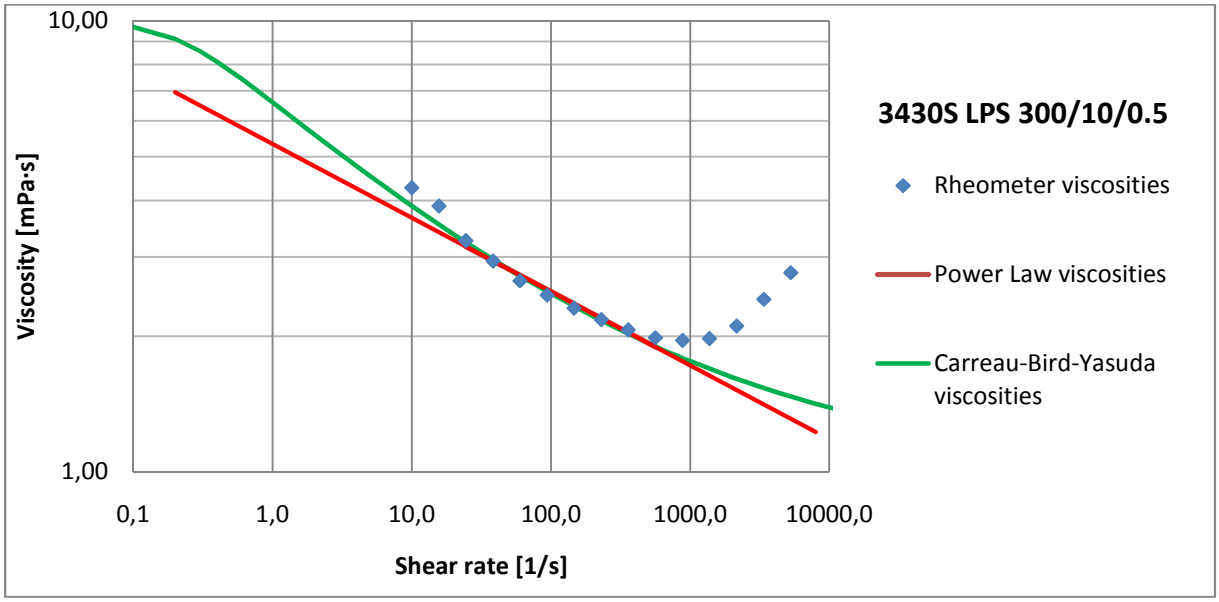

Figure 4.5.1: *Power Law-, Carreau-Bird-Yasuda- and measured viscosities for a 300/10/0.5 LPS of HPAM 3430S, as a function of shear rate.*

As seen on Figure 4.5.1, the PLM neglects the Newtonian- and the shear thickening region and has a constant slope approaching zero viscosity. The CBY model neglects the shear thickening region, but has a flattening slope towards the infinite shear viscosity. Figures for all applied solutions can be found in appendix A.8.

Due to the lack of viscosity measurements for shear rates below 10 1/s, μ_0 is set as a "free" variable under the assumption presented in Table 4.5.1. Therefore, neither μ_0 nor the time constant λ should not be emphasized. The constant K' is also set as a free variable to obtain a good fit for the Power law viscosities in the shear thinning region and cannot be used for interpretations.

Table 4.5.2: *Values for zero-shear viscosities, K', Power Law indexes, and λ, for LPS and polymer solutions of HPAM 3430S.*

Model	**Parameter**	**HPAM 3430S**					
		LPS (30:1 PtC-ratio)			**Polymer**		
		0.5%	**5 %**	**CeB 0.5/4.21**	**0.5%**	**5 %**	**CeB 0.5/4.21**
CBY	μ_0 [mPa·s]	9.84	5.84	12.15	6.00	3.60	3.60
Power Law	K'	5.33	3.87	5.98	5.39	2.70	2.99
Power Law	n	0.84	0.86	0.76	0.86	0.94	0.92
CBY	λ	5.00	3.66	3.98	0.64	12.65	2.24
CBY	n	0.71	0.74	0.59	0.76	0.88	0.83

As seen in Table 4.5.2, the Power law indexes are approximately equal for LPS and polymer when solved in 0.5% NaCl. When solved in 5% NaCl, both the polymer and LPS solution shows an increased *n*, where the increase for the polymer solution shows a slightly higher increase than the LPS solution. These trends are observed for both models. The trends suggest that increased ionic strength results in a slight increase in the affinity between polymer particles. This effect is even less for cross-linked polymer particles, this could be due to the difference in particle size for coils and x-coils.

For addition of calcium, LPS solutions have a significant reduction of *n*, while the polymer solutions have approximately unchanged *n*. The trends apply for both models. This suggests that Ca^{2+} results in reduced affinity between LPS particles, but has minor impact on the affinity between polymer particles. These results are seemingly contradictory to the findings presented in section *4.4.4 Variation of solvent composition*, which indicated that the observed enhanced Log-Jamming ability of LPS systems solved in calcium enriched brines could be due to higher affinity between the x-coils. The results may be explained by taking the differences in process into account. In rheological measurements, rotational forces will tear the particles apart. On the other hand, a filter-flood involves a pressure gradient that forces the particles through pores. The distance between particles may influence whether the interactions are repulsive or attractive, it is therefore possible that the applied method for characterization may influence the interpretation.

For a more precise determination of the discussed PLM- and CBY model parameters, viscosity measurements should be performed with an apparatus capable of measurements for shear rates lower than10 1/s, and as low as possible. This could have provided more consistent data for the magnitude of the zero-shear viscosity, and the vertex between the Newtonian and the shear thinning regime. In turn, this would have narrowed the free variables down to only the Power law exponent *n* in both the PLM and CBY-model.

Conclusion

The determination of Power law and CBY-parameters indicated that:

The affinity between particles in polymer solutions are increased for increased ionic strength, but shows little variation for addition of Ca^{2+}. The affinity between cross-linked particles

shows good resistance to increased ionic strength, but seems heavily dependent upon the presence of divalent ions.
Interpretations of data regarding the affinity between particles may be dependent upon the method applied to obtain the experimental data, and may therefore not be directly comparable.

4.5.2 Intrinsic viscosity and Huggins constant

As presented in section *2.3.3 Intrinsic viscosity and Huggins constant*, the quantities intrinsic viscosity ($|\eta|$), Huggins constant (K_H), and the critical overlap concentration (C*) may give useful information for characterization of the polymer itself, the solvent and the particles in the solution. Samples of all LPS/polymer systems solved in the applied brines where prepared in concentrations of 300, 900 and 1500 ppm. The 1500 ppm solutions have per definition too high polymer concentration to fall under the term "LPS", as discussed in section *1.Introduction.* Nevertheless, they are included to provide a sufficient span in concentrations for the experiments. The viscosities of the applied solutions where measured and plotted to calculate $|\eta|$, K_H, and C* from a plot of reduced viscosity versus concentration as shown in Figure 4.5.2.

The intrinsic viscosities were found by intersection of the linear regression of the data points with the y-axis, in accordance with Formula 2.6:

$$|\eta| = lim_{c\to 0}\frac{\eta-\eta_s}{\eta_s \cdot c} = lim_{c\to 0}\frac{\eta_{sp}}{c} \qquad \textbf{(2.6)}$$

Where η is the solution viscosity, $\eta_s$is the solvent viscosity, c is the polymer concentration, and η_{sp} is the specific viscosity.

Huggins constant was calculated by solving formula 2.7 for $K_{H.}$, i.e. K_H is dependent on the slope of reduced viscosity as a function of polymer concentration.

$$\eta_{sp} = |\eta|c + k_H|\eta|^2c^2 \qquad \textbf{(2.7)}$$

Where η_{sp} is the specific viscosity, $|\eta|$ is the intrinisc viscosity, and c is the polymer concentration.

Several models for estimation of C* directly from the intrinsic viscosity has been suggested. Sorbie [11] suggested that the critical overlap concentration could be estimated by the expression $C^* = \frac{1}{|\eta|}$, while Chauveteau[28] suggested that the relationship was $C^* = \frac{0.7}{|\eta|}$.

Figure 4.5.2 shows a plot of reduced viscosity versus polymer concentration for 3430S 300ppm LPS solutions at 30:1 PtC-ratio, solved in different brines. Plots for all fluid systems can be found in appendix A.2.

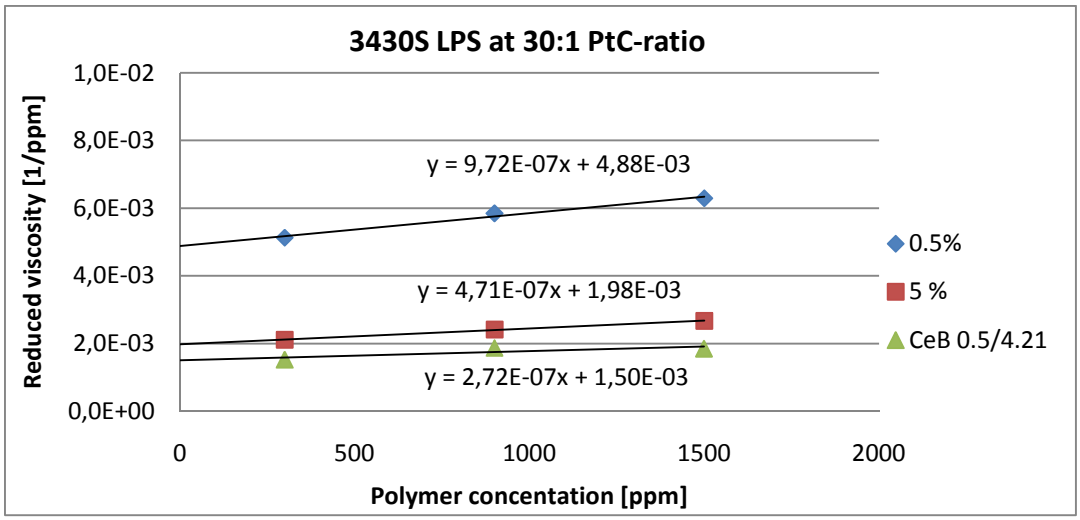

Figure 4.5.2: *Plot of reduced viscosity as a function of polymer concentration in HPAM 3430S LPS solutions at a fixed PtC-ratio, for the three solvents described in the legend. Viscosities are given at 22±0.1°C and a reference shear rate of 100 1/s.*

Addition of salts to a solution will partly screen the repulsive forces along the HPAM backbone, resulting in a progressively more spherical conformation compared to the conformation in a non-ionic solvent. This will result in a reduction of the polymers ability to viscosify the solution, thus a lower intrinsic viscosity. As seen in Tables 4.5.3 and 4.5.4, the intrinsic viscosity is lower for all systems solved in 5% NaCl than those in 0.5%. Even though the ionic strength for the brines is equal, the fluid systems solved in CeB 0.5/4.21 have lower intrinsic viscosities than those in 5% NaCl. This suggests that Ca^{2+} have a more detrimental effect on the intrinsic viscosity than Na^{+}, in accordance with previous findings by Sandvik and Maerker[39].

Table 4.5.3: *Estimated properties of HPAM 3430S. All LPS systems are at a 30:1 PtC ratio. Viscosities are compared at a reference shear rate of 100 1/s and 22±0.1°C.*

HPAM 3430S	**Solvent**	**Intrinsic viscosity**	**Huggins Constant**	**Critical overlap concentration**	
				C*= 1/ $\|\eta\|$	**C* = 0.7/$\|\eta\|$**
		[1/ppm]	**-**	**[ppm]**	**[ppm]**
Polymer	0.5% NaCl	0.0045	0.13	222	156
	5% NaCl	0.0018	0.52	556	389
	CeB 0.5/4.21	0.0012	0.79	833	583
LPS	0.5% NaCl	0.0049	0.04	204	143
	5% NaCl	0.0020	0.12	500	350
	CeB 0.5/4.21	0.0015	0.12	667	467

Table 4.5.4: *Estimated properties of HPAM 3630S. All LPS systems are at a 30:1 PtC ratio. Viscosities are compared at a reference shear rate of 100 1/s and 22±0.1°C.*

HPAM 3630S	**Solvent**	**Intrinsic viscosity**	**Huggins Constant**	**Critical overlap concentration**	
				C*= 1/ $\|\eta\|$	**C* = 0.7/$\|\eta\|$**
		[1/ppm]	**[-]**	**[ppm]**	**[ppm]**
Polymer	0.5% NaCl	0.0056	0.08	179	125
	5% NaCl	0.0034	0.12	294	206
	CeB 0.5/4.21	0.0023	0.28	435	304
LPS	0.5% NaCl	0.0049	0.08	204	143
	5% NaCl	0.0021	0.27	476	333
	CeB 0.5/4.21	0.0014	0.40	714	500

The Huggins constant characterizes the hydrodynamic interactions between dispersed particles during shear flow[27]. As seen in Tables 4.5.3 and 4.5.4, Huggins constant is increasing with ionic strength and addition of Ca^{2+} for all systems but the 3430S LPS, where the Huggins constant is equal for 5% NaCl and CeB 0.5/4.21. For the systems solved in 0.5% NaCl, K_H ranges between 0.04 and 0.13, indicating that 0.5% NaCl is a good solvent for the applied polymer types and concentrations. The systems solved in 5% NaCl has K_H ranging from 0.12 up to 0.52, which suggests that this solvent is good to neutral for the applied polymer types and concentrations. The systems solved in CeB 0.5/4.21 have K_H ranging between 0.12 up to 0.79, which indicates that CeB 0.5/4.21 is a good to neutral solvent. Chauveteau[4] suggests that increase of k_H is caused by relatively stronger attractive interactions between the colloidal particles. This interpretation suggests that addition of Ca^{2+}

to the solution increases the affinity between the cross-linked particles as discussed in section *4.4.4 Variation of solvent composition*.

The critical overlap concentrations, C*, are estimated by the approximations described initially and presented in Tables 4.5.3 and 4.5.4. The two approximations results in a certain span in C* for each fluid system, as seen in Figure 4.5.3.

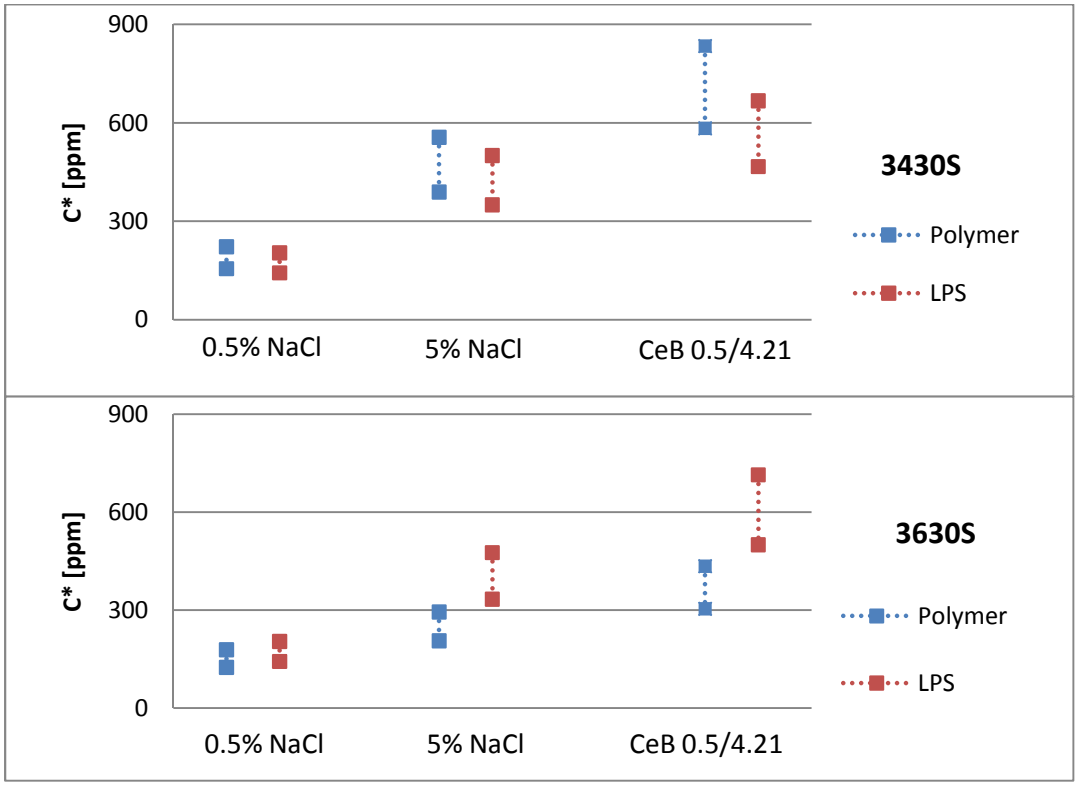

Figure 4.5.3: *Span in estimated C* by the two approximations, for all applied fluid systems..*

As seen on Figure 4.5.3, solutions solved in 0.5% NaCl has the lowest C*, solutions solved in 5% NaCl has intermediate C*, while the solutions solved in CeB 0.5/4.21 has the highest C*. These trends apply to both polymer types. By applying the Einstein relation (Formula 4.4) and the relationship between C* and $|\boldsymbol{\eta}|$, an increase of C* can be interpreted as a decrease in the specific volume of the particle. When comparing C* of solutions solved in 5% and CeB 0.5/4.21, it is therefore suggested that addition of Ca^{2+} decreases the particle size above the contribution of the ionic strength.

The filter-floods performed to investigate Qc has been carried out with a constant polymer concentration of 300 ppm. This means that all systems solved in 0.5% NaCl and 3630S polymers solved in 5% NaCl were above C*, whereas the rest of the applied systems was below C*. For estimation of Huggins constant/intrinsic viscosity, solutions of up to 1500ppm

were prepared for all solvents and both polymer types. Precipitation or gel formation may be a problem when AlCit or polyvalent ions are added to a polymer solution with a concentration above C*[9]. In spite of 1500ppm being significantly higher than C* for all solvents, none of the solutions showed visual signs of precipitations or gel formation. However, solutions should be filter-flooded to determine whether precipitates or gels may affect their flow performance. Some of the 300ppm LPS solutions solved in 0.5% NaCl that were prepared for filter-floods did cause plugging of the filters. Microgels or particles present due to incomplete hydration of the polymer granulate should have been removed during the pre-filter-flood filtration, so the plugging could be caused by the polymer concentration being above C*.

Conclusion

The intrinsic viscosities decreased for higher salinity of the solvent, and for addition of Ca^{2+}. This may be caused by the increased degree of coiling of the polymer molecules for higher ionic strength and the addition of divalent ions.

Huggins constant ranged between 0.04 up to 0.79, indicating that the applied brines ranges from good to neutral solvents within the experimental ranges. 0.5% NaCl had the lowest K_H, followed by 5% NaCl and CeB 0.5/4.21. For all systems but the 3430S LPS, addition of calcium under constant ionic strength resulted in increased K_H. In accordance with Chauveteau[4], this may indicate higher attractive forces between the particles.

C* was found to decrease for addition of Ca^{2+} under constant ionic strength. This suggests that Ca^{2+} results in smaller particles than those cross-linked by Al^{3+}. C* was found to be below 300ppm for LPS/polymer solutions solved in 0.5% NaCl. This may be the reason for observed plugging of filters during filter-floods of 300/10/0.5 LPS solutions.

Nordli[24] estimated $|\eta|$, K_H, and C* for HPAM 3630S solved in 0.5% and 5% NaCl. The obtained comparable data from this thesis concurs with the reported findings.

5. Overall conclusions

A novel method for characterization of LPS solutions by filter-flooding under variation of flow rate, combined with viscosity measurements, was evaluated and qualified. The method determined a critical rate, Qc, for a sudden increase in dP*(Q) for polymer and LPS solutions.

An applied model for non-Newtonian flow behaviour suggested that the increased dP*(Q) observed for polymer solutions could be explained by shear thickening behaviour. However, the increased dP*(Q) for LPS solutions could not be explained by shear thickening behaviour alone, but was also suggested caused by the Log-Jamming effect.

The LPS solutions where characterized under variation of polymer molecular weight, solvent salinity, and solvent composition. The Log-Jamming ability of LPS solutions seems to be reduced for higher ionic strengths, most likely due to enhanced coiling of the polymer molecules. Addition of 0.5% by weight $CaCl_2$ under constant ionic strength seemed to improve the Log-Jamming ability of LPS solutions. Viscosity measurements suggested no increase in the particle size, and this is interpreted as that Ca^{2+} either increases the density of x-coils, the number of x-coils, or the affinity between x-coils.

It is suggested that Ca^{2+} can cross-link polymer solutions without addition of a dedicated cross-linker. The experimental data indicates that addition of 0.5% by weight $CaCl_2$ to a 300ppm polymer solution under constant ionic strength gave equivalent Log-Jamming ability as a 300ppm LPS solution cross-linked by 10ppm Al^{3+} solved in 5% NaCl.

Addition of 1% by weight $CaCl_2$ to a polymer solution under constant ionic strength seemed to reduce the Log-Jamming ability of the solution, probably because of repulsion between the particles due to oversaturation of the negative sites on the polymer molecules.

6. Further work

The perhaps most interesting finding in this thesis was the increased Log-Jamming ability of LPS solutions observed for addition of 0.5% by weight $CaCl_2$ under constant ionic strength. A natural continuance of this clue, could be to extend the variables to include higher polymer concentrations and an equivalent increase in the $CaCl_2$ concentration (under constant ionic strength) to keep the Polymer-to-Ca^{2+} ratio constant. This could determine whether the improved Log-Jamming ability is reproducible for other systems.

An increase from 0.5 to 1.0% by weight $CaCl_2$ under constant ionic strength seemed to reduce the Log-Jamming ability of polymer solutions without Al^{3+}. Filter-floods and viscosity measurements involving a wider range of $CaCl_2$ concentrations under constant ionic strength and polymer concentration could be performed, to estimate the fringes in whether the $CaCl_2$ concentration improves or reduces the Log-Jamming ability.

Another approach to obtain experimental data regarding the attraction/repulsion between LPS particles in calcium enriched brines, could be to include Zeta-potential measurements. However, such measurements may be challenging for solutions with high ionic concentrations- Therefore, the applied solutions should have low ionic strengths, and equivalent reduced polymer concentrations.

With an offshore LPS application on the Norwegian continental shelf in mind, further investigation of the flow properties of systems solved in synthetic seawater (SSW) would be a possible approach. LPS solved in SSW with a net addition of $CaCl_2$ (not constant ionic strength) could also be implemented in such experiments to further investigate cross-linking without a dedicated cross-linker.

Further investigation of preparation of AlCit solutions could be performed, involving a buffer or addition of agents for pH-control of the solutions. LPS solutions prepared by pH-controlled AlCit solutions should also be characterized to investigate possible side-effects of the pH-controlling agents.

References

[1] Mack, J. C. and Smith, J. E. (1994). In-Depth Colloidal Dispersion Gels Improve Oil Recovery Efficiency.*Paper SPE 27780*, *Presented at the SPE/DOE Improved Oil Recovery Symposium, 17-20 April*, Tulsa, Oklahoma, USA.

[2] Chang, H. L.,Sui, X.,Xiao, L.,Liu, H.,Guo, Z.,Yao, Y.,Xiao, Y.,Chen, G.,Song, K., and Mack, J. C. (2004). Successful Field Pilot of In-Depth Colloidal Dispersion Gel (CDG) Technology in Daqing Oil Field.*Paper SPE 89460*, *Presented at the SPE/DOE Symposium on Improved Oil Recovery,17-21 April* Tulsa, Oklahoma, USA.

[3] Maleki, A.,Kjøniksen, A., and Nyström, B. (2005). Effect of shear on intramolecular and intermolecular association during cross-linking of hydroxyethylcellulose in dilute aqueous solutions. *J. Phys. Chem. B*: **109**, 12329-12336.

[4] Chauveteau, G.,Omari, A., and Tabary, R. (2003). Gelation of polymer solutions under shear flow. *Colloids and Surfaces A: Physicochemical and Engineering Aspects*: **225**, 37-48.

[5] Smith, J. (1989). The transition pressure: A quick method for quantifying polyacrylamide gel strength.*Paper SPE 18739*, *Presented at the SPE International Symposium on Oilfield Chemistry 8-10 February*, Houston, Texas, USA.

[6] Skauge, T., Djurhuus, K, Hetland S, Spildo, K, Skauge, A (2011). B17 Offshore implementation - LPS flooding. *Presented at the EAGE IOR Symposium 12.-14. April*, Cambrigde, UK.

[7] Spildo, K.,Skauge, A.,Aarra, M. G., and Tweheyo, M. T. (2009). A New Polymer Application for North Sea Reservoirs. *Paper SPE 113460*, *SPE Reservoir Evaluation & Engineering*: **12**, pp. 427-432.

[8] Smith, J. E. (1997). Aluminum citrate preparations and methods, *US pat. 5,654,261*,

[9] Bjørsvik, M.,Høiland, H., and Skauge, A. (2008). Formation of colloidal dispersion gels from aqueous polyacrylamide solutions. *Colloids and Surfaces A: Physicochemical and Engineering Aspects*: **317**, 504-511.

[10] Li, M.,Dong, Z.,Lin, M., and Wu, Z. (2004). A study on the size and conformation of linked polymer coils. *J. of Petroleum Science and Eng.*: **41**, 213-219.

[11] Sorbie, K. S.(1991). *Polymer-Improved Oil Recovery*, Blackie and Son Ltd, Glasgow, *ISBN 0216926939*.

[12] Smith, J. (1995). Performance of 18 polymers in aluminum citrate colloidal dispersion gels.*Paper SPE 28989*, *Presented at the SPE International Symposium on Oilfield Chemistry, 14-17 February*, San Antonio, Texas, USA.

[13] Wang, W. and Lu, X. (2009). Molecular Configuration and Flow Performance of Al3+ Cross-linked Polymer. *Petroleum Sci Tech.*: **27**, 699-711.

[14] Lake, L.(1989). *Enhanced oil recovery*, Prentine Hall, New Jersey, *OSTI ID 5112525*.

[15] Sydansk, R.,Xiong, Y.,Al-Dhafeeri, A.,Schrader, R., and Seright, R. (2004). Characterization of partially formed polymer gels for application to fractured production wells for water-shutoff purposes.*Paper SPE 89401*, *Presented at the SPE/DOE Symposium on Improved Oil Recovery, 17-21 April*, Tulsa, Oklahoma, USA.

[16] Bjørsvik, M. (2007). Physico-chemistry Characterization of Colloidal Dispersion Gels, *PhD thesis, University of Bergen - Dept. of Chem.*

[17] Aarra, M. G., M. Bjørsvik, H. Høiland, T. Skodvin, D. Standnes, A. Skauge. (2005). Linked Polymer Solutions for Improved Oil Recovery by Waterflooding. *Presented at the 13th European Symposium on Improved Oil Recovery, 25-27 April*, Budapest, Hungary.

[18] Wang, W.,Lu, X., and Xie, X. (2008). Evaluation of Intra-Molecular Cross-Linked Polymers.*Paper SPE 113760*, *Presented at the SPE Western Regional and Pacific Section AAPG Joint Meeting, 31 March- 2 April*, Bakersfield, California, USA.

[19] Ryles, R. (1988). Chemical stability limits of water-soluble polymers used in oil recovery processes. *Paper SPE 13585*, *SPE J. res.eng.*: **3**, 23-34.

[20] Smith, J.,Liu, H., and Guo, Z. (2000). Laboratory Studies of In-Depth Colloidal Dispersion Gel Technology for Daqing Oil Field.*Paper SPE 62610*, *Presented at the SPE/AAPG Western Regional Meeting, 19-22 June*, Long Beach, California, USA.

[21] Spildo, K.,Skauge, A., and Skauge, T. (2010). Propagation of Colloidal Dispersion Gels (CDG) in Laboratory Corefloods.*Paper SPE 129927*, *Presented at the SPE Improved Oil Recovery Symposium, 24-28 April*, Tulsa, Oklahoma, USA.

[22] Diaz, D.,Somaruga, C.,Norman, C., and Romero, J. L. (2008). Colloidal Dispersion Gels Improve Oil Recovery in a Heterogeneous Argentina Waterflood.*Paper SPE 113320*, *Presented at the SPE/DOE Symposium on Improved Oil Recovery, 20-23 April*, Tulsa, Oklahoma, USA.

[23] Skauge, T.,Spildo, K., and Skauge, A. (2010). Nano-sized Particles For EOR.*Paper SPE 129933*, *Presented at the SPE Improved Oil Recovery Symposium, 24-28 April*, Tulsa, Oklahoma, USA.

[24] Nordli, M. (2010). Kryssbundet polymerløsning (LPS) for anvendelse i saltholdige reservoar, *Masters thesis, University of Bergen - Dept. of Chem.*

[25] Schramm, G.(1994). *A practical approach to rheology and rheometry*, HAAKE, Karlsruhe, Germany.

[26] Hu, Y.,Wang, S., and Jamieson, A. (1995). Rheological and rheooptical studies of shear-thickening polyacrylamide solutions. *Macromolecules*: **28**, 1847-1853.

[27] Chauveteau, G.,Tabary, R.,Bon, C. l.,Renard, M.,Feng, Y., and Omari, A. (2003). In-Depth Permeability Control by Adsorption of Soft Size-Controlled Microgels.*Paper SPE 82228*, *Presented at the SPE European Formation Damage Conference, 13-14 May*, The Hague, Netherlands.

[28] Chauveteau, G.(1986). *Fundamental criteria in polymer flow through porous media*, ACS Publications, *ISBN 9780841209312*.

[29] Lien, J. R.(2009). *PTEK212 Reservoarteknikk I*, Uni. of Bergen, Bergen.

[30] Smith, F. W. (1970). The behaviour of partially hydrolysed polyacrylamide solutions in porous media. *Paper SPE 2422*, *J. Pet. Tech*: **22**, 148-156.

[31] Fallah, S., Skauge, A., MacKay, E. (2009). Pore Scale Modelling of Linked Polymer Solution (LPS) - A New EOR Process. *Presented at the 15th European Symposium on Improved Oil Recovery 27-29 April*, Paris, France.

[32] RezaeiDoust, A.,Puntervold, T.,Strand, S., and Austad, T. (2009). Smart Water as Wettability Modifier in Carbonate and Sandstone: A Discussion of Similarities/Differences in the Chemical Mechanisms. *Energy & Fuels*: **23**, 4479-4485.

[33] Rahman, S. S.,Arshad, A., and Chen, H. (1994). Prediction of Critical Condition for Fines Migration in Petroleum Reservoirs.*Paper SPE 28760*, *Presented at the SPE Asia Pacific Oil and Gas Conference, 7-10 November*, Melbourne, Australia.

[34] Martin, F. D. (1975). The Effect of Hyrolysis of Polyacrylamide on Solution viscosity, Polymer Retention and Flow Resistance Properties.*Paper SPE 5339*, *Presented at the SPE Rocky Mountain Regional Meeting, 7-9 April*, Denver, Colorado, USA.

[35] Morel, D.,Jouenne, S.,VERT, M., and NAHAS, e. (2008). Polymer Injection in Deep Offshore Field: The Dalia Angola Case.*Paper SPE 135735*, *Presented at the SPE Annual Technical Conference and Exhibition, 19-22 September*, Florence, Italy.

[36] McCormick, C.,Bock, J., and Schulz, D.(1989). *Encyclopedia of polymer science and engineering, vol. 17*, Wiley, New York, *ISBN 0471811815*

[37] Zaitoun, A.,Makakou, P.,Blin, N.,Al-Maamari, R.,Al-Hashmi, A. A.,Abdel Goad, M., and Al-Sharji, H. (2011). Shear Stability of EOR Polymers.*Paper SPE 141113*, *Presented at the SPE International Symposium on Oilfield Chemistry, 11-13 April*, The Woodlands, Texas, USA.

[38] Willhite, G. and Uhl, J. (1986). Correlation of the mobility of biopolymer with polymer concentration and rock properties in sandstone. *Polymeric Science and Engineering*: **55**, 577.

[39] Sandvik, E. and Maerker, J. (1977). Application of xanthan gum for Enhanced Oil Recovery. *Extracellular Microbial Polysaccharides, Am. Chem. Soc. series*: **45**, 242–264.

Appendix

A.1. Mixing procedures - Intensity distributions

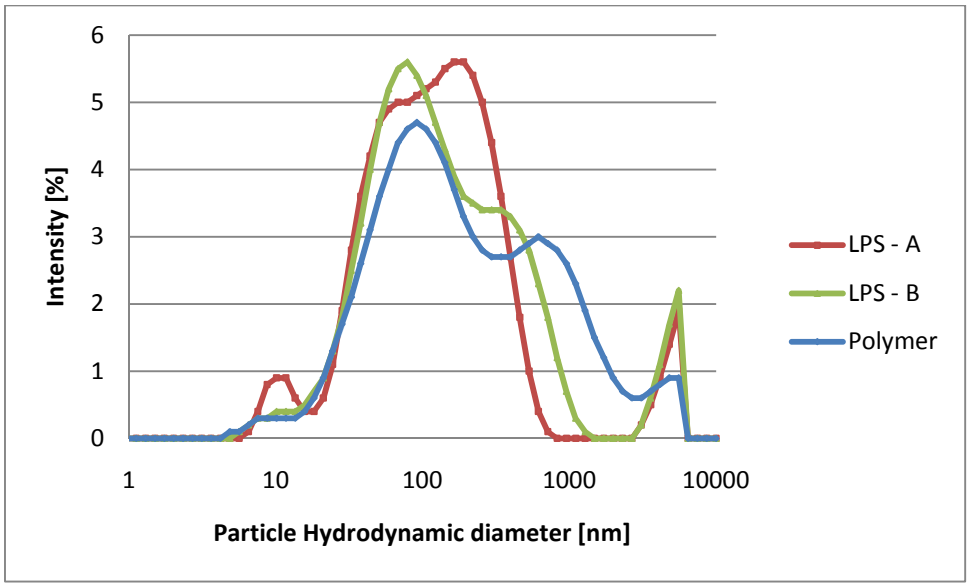

Figure A.1.1: *PSD-charts of 3630S 600/20/0.5 LPS solutions prepared by method A and B respectively, and the corresponding polymer solution, two hours after preparation.*

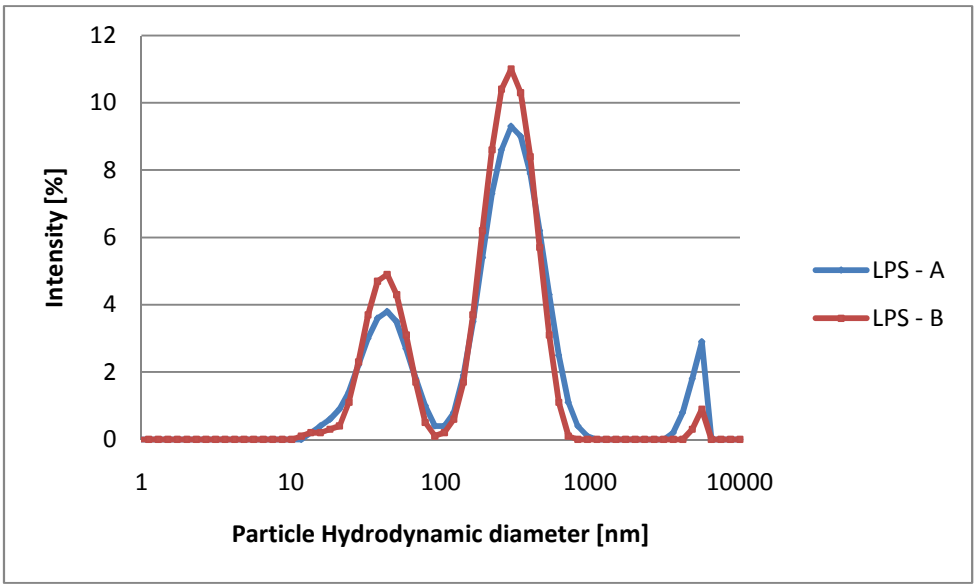

Figure A.1.2: *PSD-charts of 3630S 600/20/0.5 LPS solutions prepared by method A and B respectively, one day after preparation.*

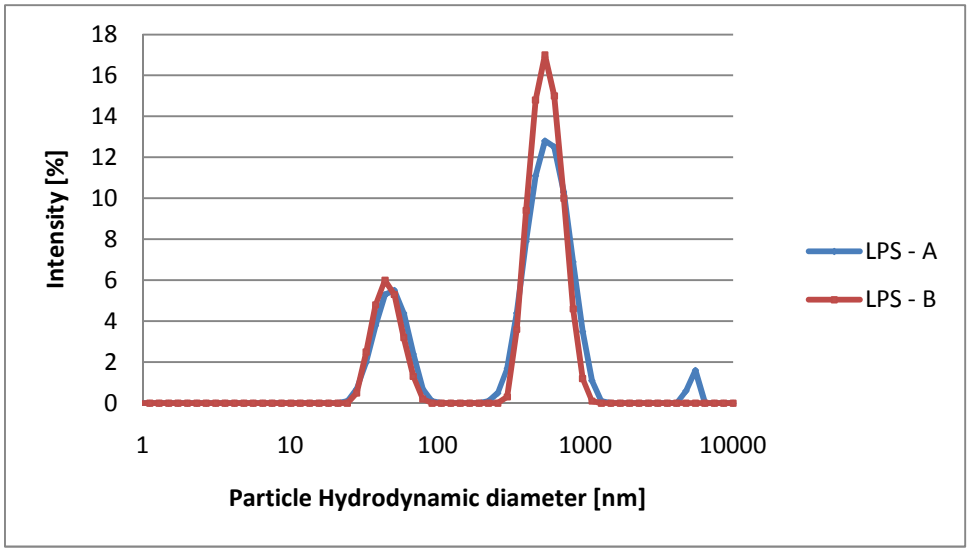

Figure A.1.3: *PSD-charts of 3630S 600/20/0.5 LPS solutions prepared by method A and B respectively, two days after preparation.*

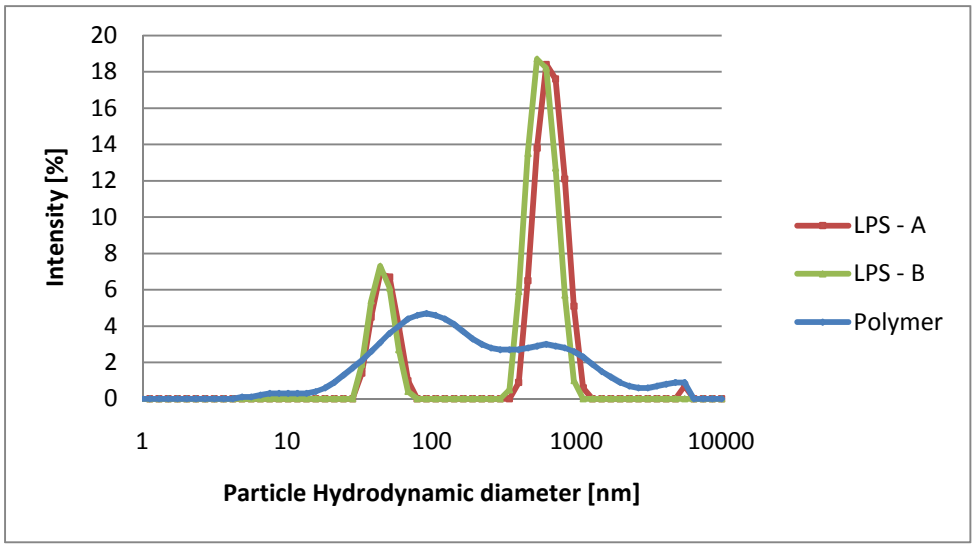

Figure A.1.4: *PSD-charts of 3630S 600/20/0.5 LPS solutions prepared by method A and B respectively, and the corresponding polymer solution, three days after preparation.*

A.2. Plots for estimation of intrinsic viscosity and Huggins constant

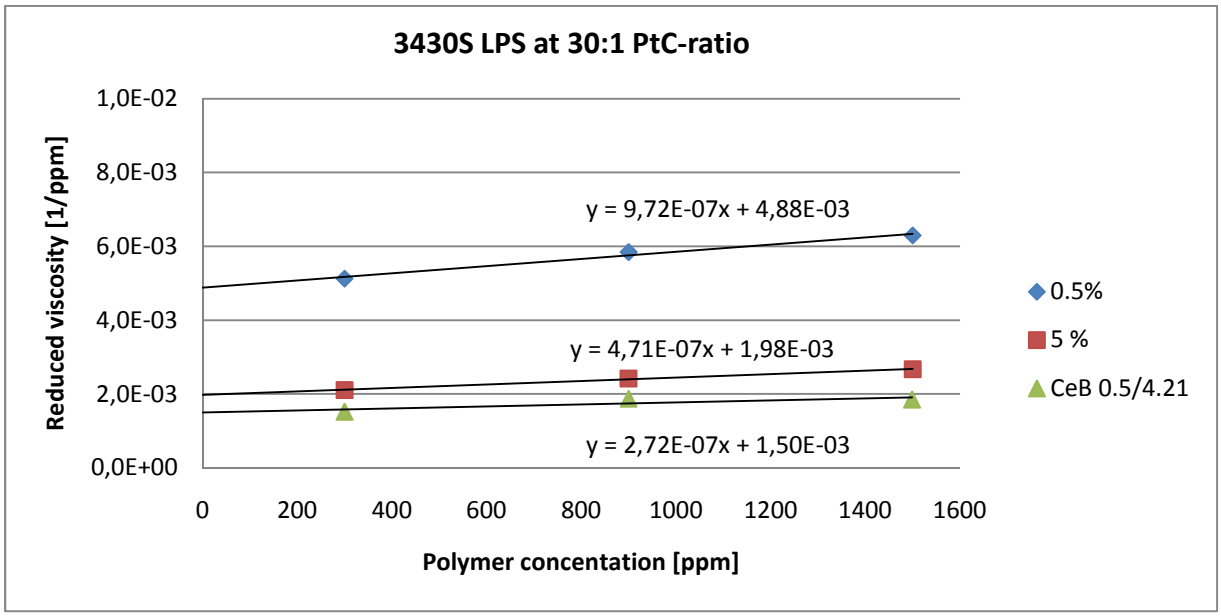

Figure A.2.1: *Reduced viscosity as a function of polymer concentration for 3430S 300/10 LPS solved in three different brines according to the legend.*

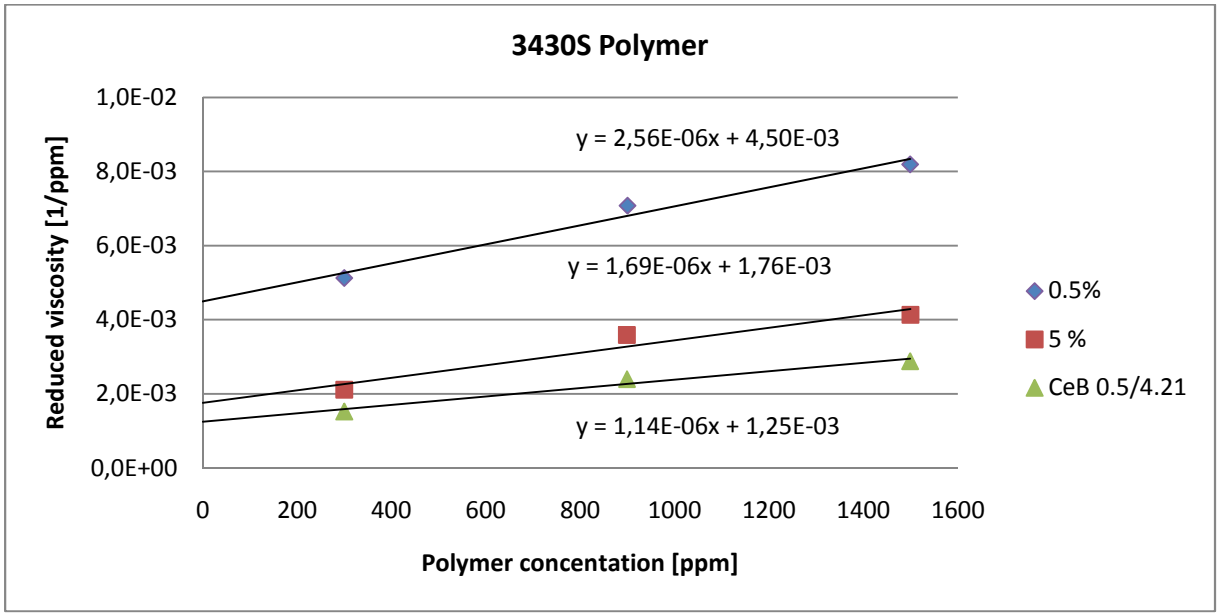

Figure A.2.2: *Reduced viscosity as a function of polymer concentration for 3430S 300 ppm polymer solutions solved in three different brines according to the legend.*

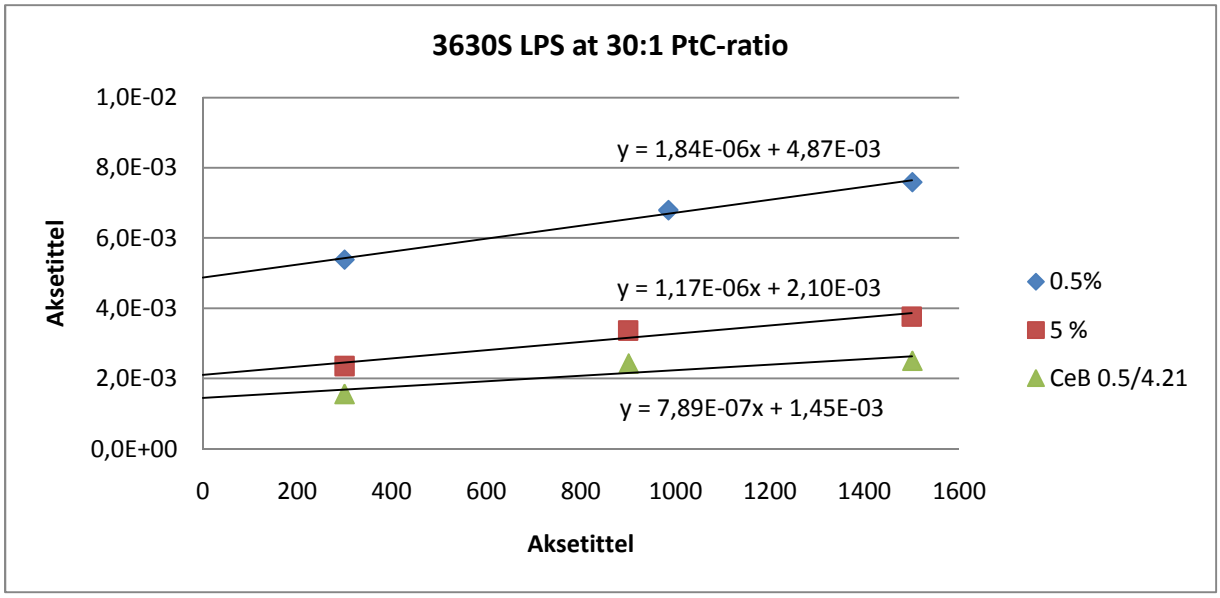

Figure A.2.3: *Reduced viscosity as a function of polymer concentration for 3630S 300/10 LPS solved in three different brines according to the legend.*

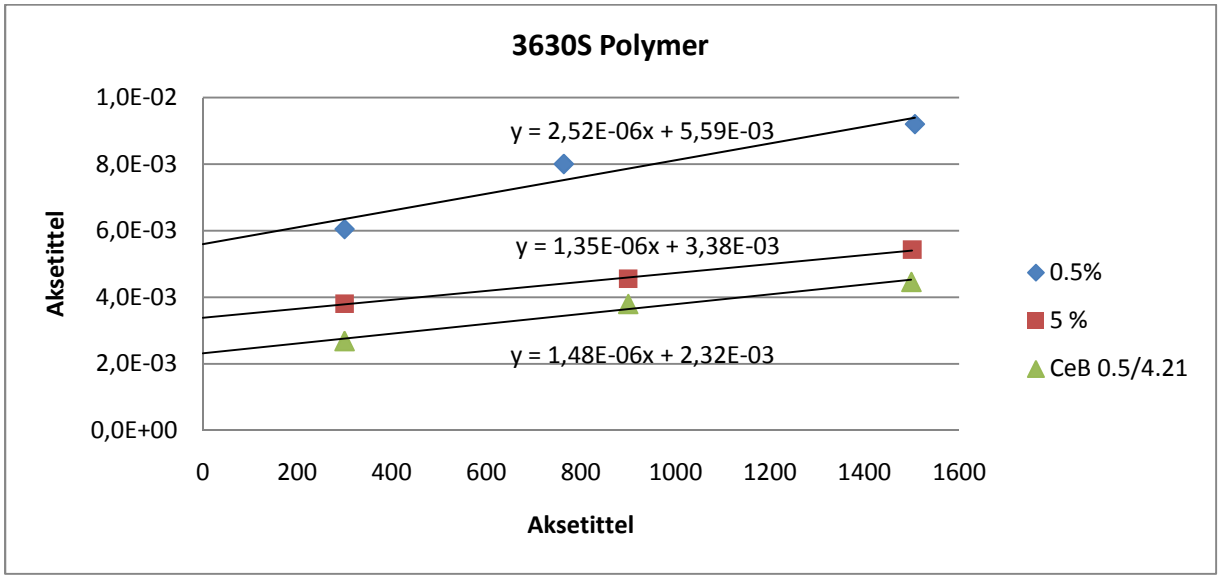

Figure A.2.4: *Reduced viscosity as a function of polymer concentration for 3630S 300 ppm polymer solutions solved in three different brines according to the legend.*

A.3. Estimation of filter permeabilities

Table A.3.1: *Measured differential pressures and estimated permeabilities for 0.5µm filters. Differential pressures are given relative the zero point of the measuring range, minus 100 mbar.*

0.5µm filter				
Q[ml/min]	dP_{Total} [mbar]	dP_{Bypass}[mbar]	dP_{Filter}	K [mD]
1.0	110.0	100.0	10.0	129.4
	108.5	100.0	8.5	158.4
	109.0	100.0	9.0	149.6
5.0	159.0	107.5	51.5	125.6
	151.0	107.5	43.5	154.8
	154.0	107.5	46.5	144.8
10.0	223.5	116.5	107.0	120.9
	204.0	117.0	87.0	154.8
	205.5	117.0	88.5	152.2
Average			**143.4 [mD]**	

Table A.3.2: *Measured differential pressures and estimated permeabilities for 2µm filters. Differential pressures are given relative the zero point of the measuring range, minus 100 mbar.*

2µm filter				
Q[ml/min]	dP_{Total} [mbar]	dP_{Bypass}[mbar]	dP_{Filter}	K [mD]
1.0	105.0	100.0	5.0	269.4
	104.0	100.0	4.0	336.7
	105.5	100.0	5.5	244.9
	104.5	100.0	4.5	299.3
	105.0	100.0	5.0	269.4
5.0	136.5	107.5	29.0	232.2
	130.0	107.5	22.5	299.3
	132.0	107.0	25.0	269.4
	134.0	107.0	27.0	249.4
	140.5	107.0	33.5	201.0
10.0	170.5	117.0	53.5	251.7
	163.5	117.0	46.5	289.6
	170.0	117.0	53.0	254.1
	179.5	117.0	62.5	215.5
	185.0	117.0	68.0	198.1
Average			**258.7 [mD]**	

Table A.3.3: *Measured differential pressures and estimated permeabilities for 7µm filters. Differential pressures are given relative the zero point of the measuring range, minus 100 mbar.*

7 µm filter				
Q[ml/min]	dP_{Total} [mbar]	dP_{Bypass}[mbar]	dP_{Filter}	K [mD]
1.0	102.0	100.0	2.0	647.0
	102.5	100.0	2.5	517.6
	102.0	100.0	2.0	647.0
	102.0	100.0	2.0	647.0
	102.0	100.0	2.0	647.0
5.0	119.0	107.0	12.0	539.1
	121.0	107.0	14.0	462.1
	118.5	107.0	11.5	562.6
	118.0	107.5	10.5	616.2
	117.5	107.5	10.0	647.0
10.0	140.5	117.0	23.5	550.6
	144.5	117.0	27.5	470.5
	143.0	117.0	26.0	497.7
	141.5	117.0	24.5	528.1
	141.0	117.0	24.0	539.1
Average			**567.9 [mD]**	

A.4. Viscosities of polymer stock solutions

Table A.4.1: *Measured viscosities of stock solutions of both polymer types at a reference shear rate of 100 1/s and 22±0.1°C.*

Solution	**HPAM type**	**Concentration** [ppm]	**Viscosity** [mPa·s]
A	3630S	4500	67.0
B	3630S	4528	67.5
C	3630S	4986	82.0
D	3430S	4977	77.5
E	3430S	5017	76.6
F	3630S	5042	81.7
G	3430S	5005	77.2
H	3630S	5011	77.6
I	3630S	5004	75.4

A.5. Raw data from filter-floods

Viscosities are given at 22±0.1°C and a reference shear rate of 100 1/s.

Table A.5.1: *Flow rates, normalized differential pressures, bypass differential pressure of the solvent and viscosities of all solutions tested in experimental matrix A*

Matrix A - 0.5µm filter							
LPS				**Polymer**			
3430S 300/10/0.5				**3430S 300/0/0.5**			
Q	**dP^*_{LPS}**	**Bypass dP_{brine}**	**Viscosity**	**Q**	**$dP^*_{Polymer}$**	**Bypass dP_{brine}**	**Viscosity**
[ml/min]	*[mbar/mPa·s]*	*[mbar]*	*[mPa·s]*	*[ml/min]*	*[mbar/mPa·s]*	*[mbar]*	*[mPa·s]*
0.35	120.22	0.57	2.39	0.35	58.50	0.16	2.59
0.50	141.16	-0.05	2.39	1.00	179.57	1.26	2.59
1.00	287.29	5.69	2.39				
2.00	652.34	4.54	2.39				

Table A.5.2: *Flow rates, normalized differential pressures, bypass differential pressure of the solvent and viscosities of all solutions tested in experimental matrix B.*

Matrix B- 2µm filter							
LPS				**Polymer**			
3430S 300/10/0.5				**3430S 300/0/0.5**			
Q	**dP^*_{LPS}**	**Bypass dP_{brine}**	**Viscosity**	**Q**	**$dP^*_{Polymer}$**	**Bypass dP_{brine}**	**Viscosity**
[ml/min]	*[mbar/mPa·s]*	*[mbar]*	*[mPa·s]*	*[ml/min]*	*[mbar/mPa·s]*	*[mbar]*	*[mPa·s]*
0.50	33.81	0.00	2.46	0.50	18.16	6.10	2.59
1.00	73.10	3.12	2.46	1.00	60.39	6.47	2.65
1.50	87.53	7.76	2.60	1.50	84.65	4.92	2.75
3.00	200.94	7.22	2.60	3.00	193.30	16.17	2.75
5.00	396.47	19.34	2.46	5.00	279.17	32.95	2.75
7.00	688.85	16.61	2.46	7.00	563.55	26.07	2.59
10.00	1206.27	18.39	2.39	10.00	983.84	18.80	2.59

Table A.5.3: *Flow rates, normalized differential pressures, bypass differential pressure of the solvent and viscosities of all solutions tested in experimental matrix C.*

Matrix C - 7µm filter							
LPS				**Polymer**			
3430S 300/10/0.5				**3430S 300/0/0.5**			
Q	**dP*$_{LPS}$**	**Bypass dP$_{brine}$**	**Viscosity**	**Q**	**dP*$_{Polymer}$**	**Bypass dP$_{brine}$**	**Viscosity**
[ml/min]	*[mbar/mPa·s]*	*[mbar]*	*[mPa·s]*	*[ml/min]*	*[mbar/mPa·s]*	*[mbar]*	*[mPa·s]*
4.00	157.75	14.97	2.37	4.00	132.16	20.03	2.59
10.00	444.54	17.43	2.37	15.00	704.79	26.85	2.67
15.00	654.57	24.12	2.37				
20.00	747.18	44.60	2.37				
25.00	1053.91	45.34	2.21				

Table A.5.4: *Flow rates, normalized differential pressures, bypass differential pressure of the solvent and viscosities of all solutions tested in experimental matrix D*

Matrix D- 2µm filter							
LPS				**Polymer**			
3630S 300/10/0.5				**3630S 300/0/0.5**			
Q	**dP*$_{LPS}$**	**Bypass dP$_{brine}$**	**Viscosity**	**Q**	**dP*$_{Polymer}$**	**Bypass dP$_{brine}$**	**Viscosity**
[ml/min]	*[mbar/mPa·s]*	*[mbar]*	*[mPa·s]*	*[ml/min]*	*[mbar/mPa·s]*	*[mbar]*	*[mPa·s]*
0.25	11.03	0.00	2.50	0.50	54.38	4.21	2.71
0.50	60.94	1.59	2.50	1.00	128.11	2.41	2.67
1.00	121.85	5.14	2.50				
2.00	809.99	6.23	2.50				
3.00	1997.04	2.96	2.50				

Table A.5.5: *Flow rates, normalized differential pressures, bypass differential pressure of the solvent and viscosities of all solutions tested in experimental matrix E.*

Matrix E - 7µm filter							
LPS				**Polymer**			
3630S 300/10/0.5				**3630S 300/0/0.5**			
Q	**dP*$_{LPS}$**	**Bypass dP$_{brine}$**	**Viscosity**	**Q**	**dP*$_{Polymer}$**	**Bypass dP$_{brine}$**	**Viscosity**
[ml/min]	*[mbar/mPa·s]*	*[mbar]*	*[mPa·s]*	*[ml/min]*	*[mbar/mPa·s]*	*[mbar]*	*[mPa·s]*
1.00	25.40	5.48	2.50	Q	dP*	Bypass DP	
2.00	83.11	4.32	2.50	1.00	55.52	3.50	2.71
3.00	141.65	8.15	2.50	5.00	392.38	10.40	2.67
4.00	316.81	9.17	2.50				
6.00	1924.35	15.52	2.50				

Table A.5.6: *Flow rates, normalized differential pressures, bypass differential pressure of the solvent and viscosities of all solutions tested in experimental matrix F.*

Matrix F - 0.5µm filter							
LPS				**Polymer**			
3430S 300/10/5				**3430S 300/0/5**			
Q	**dP^*_{LPS}**	**Bypass dP_{brine}**	**Viscosity**	**Q**	**$dP^*_{Polymer}$**	**Bypass dP_{brine}**	**Viscosity**
[ml/min]	*[mbar/mPa·s]*	*[mbar]*	*[mPa·s]*	*[ml/min]*	*[mbar/mPa·s]*	*[mbar]*	*[mPa·s]*
1.00	148.24	4.60	1.64	1.00	320.42	4.87	1.90
3.00	589.50	10.81	1.64	3.00	1170.72	8.42	1.90
5.00	939.48	4.46	1.64	5.00	2049.75	10.40	1.95
6.00	1327.06	14.86	1.66	6.00	2432.60	8.56	1.95
8.00	2711.00	13.61	1.66				

Table A.5.7: *Flow rates, normalized differential pressures, bypass differential pressure of the solvent and viscosities of all solutions tested in experimental matrix G.*

Matrix G- 2µm filter							
LPS				**Polymer**			
3430S 300/10/5				**3430S 300/0/5**			
Q	**dP^*_{LPS}**	**Bypass dP_{brine}**	**Viscosity**	**Q**	**$dP^*_{Polymer}$**	**Bypass dP_{brine}**	**Viscosity**
[ml/min]	*[mbar/mPa·s]*	*[mbar]*	*[mPa·s]*	*[ml/min]*	*[mbar/mPa·s]*	*[mbar]*	*[mPa·s]*
3.00	155.95	5.52	1.69	7.00	720.09	31.91	1.90
7.00	444.05	45.83	1.69	15.00	1767.33	31.63	1.90
15.00	1289.38	31.09	1.69				
25.00	2248.15	60.58	1.69				

Table A.5.8: *Flow rates, normalized differential pressures, bypass differential pressure of the solvent and viscosities of all solutions tested in experimental matrix H.*

Matrix H - 0.5µm filter							
LPS				**Polymer**			
3630S 300/10/5				**3630S 300/0/5**			
Q	**dP^*_{LPS}**	**Bypass dP_{brine}**	**Viscosity**	**Q**	**$dP^*_{Polymer}$**	**Bypass dP_{brine}**	**Viscosity**
[ml/min]	*[mbar/mPa·s]*	*[mbar]*	*[mPa·s]*	*[ml/min]*	*[mbar/mPa·s]*	*[mbar]*	*[mPa·s]*
0.50	157.51	7.60	1.69	1.00	361.06	2.14	2.16
1.00	205.16	4.38	1.69	3.00	1183.89	10.40	2.21
3.00	632.50	7.74	1.69				
5.00	1528.37	13.88	1.69				
6.00	1979.18	13.06	1.80				

Table A.5.9: *Flow rates, normalized differential pressures, bypass differential pressure of the solvent and viscosities of all solutions tested in experimental matrix I.*

Matrix I- 2µm filter							
LPS				**Polymer**			
3630S 300/10/5				**3630S 300/0/5**			
Q	**dP^*_{LPS}**	**Bypass dP_{brine}**	**Viscosity**	**Q**	**$dP^*_{Polymer}$**	**Bypass dP_{brine}**	**Viscosity**
[ml/min]	*[mbar/mPa·s]*	*[mbar]*	*[mPa·s]*	*[ml/min]*	*[mbar/mPa·s]*	*[mbar]*	*[mPa·s]*
3.00	167.25	5.89	1.73	3.00	344.48	14.43	2.16
7.00	608.89	16.34	1.73	7.00	1084.98	13.65	2.21
15.00	1672.50	36.82	1.73				
20.00	2269.98	48.29	1.73				

Table A.5.10: *Flow rates, normalized differential pressures, bypass differential pressure of the solvent and viscosities of all solutions tested in experimental matrix J*

Matrix J - 0.5µm filter							
LPS				**Polymer**			
3430S 300/10/CeB 0.5/4.21				**3430S 300/0/CeB 0.5/4.21**			
Q	**dP^*_{LPS}**	**Bypass dP_{brine}**	**Viscosity**	**Q**	**$dP^*_{Polymer}$**	**Bypass dP_{brine}**	**Viscosity**
[ml/min]	*[mbar/mPa·s]*	*[mbar]*	*[mPa·s]*	*[ml/min]*	*[mbar/mPa·s]*	*[mbar]*	*[mPa·s]*
0.50	53.19	-0.32	1.50	0.50	134.44	4.25	1.63
1.00	126.87	0.91	1.50	1.00	352.82	7.33	1.63
3.00	643.43	5.96	1.50	3.00	647.42	5.69	1.63
5.00	1397.77	11.22	1.50	5.00	1019.69	10.60	1.63
				7.00	1880.79	16.69	1.63

Table A.5.11: *Flow rates, normalized differential pressures, bypass differential pressure of the solvent and viscosities of all solutions tested in experimental matrix K.*

Matrix K - 2µm filter							
LPS				**Polymer**			
3430S 300/10/CeB 0.5/4.21				**3430S 300/0/CeB 0.5/4.21**			
Q	**dP^*_{LPS}**	**Bypass dP_{brine}**	**Viscosity**	**Q**	**$dP^*_{Polymer}$**	**Bypass dP_{brine}**	**Viscosity**
[ml/min]	*[mbar/mPa·s]*	*[mbar]*	*[mPa·s]*	*[ml/min]*	*[mbar/mPa·s]*	*[mbar]*	*[mPa·s]*
5.00	245.85	12.86	1.50	5.00	464.57	10.60	1.63
10.00	583.87	22.69	1.50	15.00	1703.83	33.95	1.63
20.00	1453.92	40.51	1.50				
22.00	3008.07	50.75	1.50				
25.00	2464.17	55.39	1.50				

Table A.5.12: *Flow rates, normalized differential pressures, bypass differential pressure of the solvent and viscosities of all solutions tested in experimental matrix L.*

Matrix L - 0.5µm filter							
LPS				**Polymer**			
3630S 300/10/CeB 0.5/4.21				**3630S 300/0/CeB 0.5/4.21**			
Q	**dP^*_{LPS}**	**Bypass dP_{brine}**	**Viscosity**	**Q**	**$dP^*_{Polymer}$**	**Bypass dP_{brine}**	**Viscosity**
[ml/min]	*[mbar/mPa·s]*	*[mbar]*	*[mPa·s]*	*[ml/min]*	*[mbar/mPa·s]*	*[mbar]*	*[mPa·s]*
0.50	16.52	3.23	1.52	1.00	248.80	4.05	1.85
1.00	184.89	5.36	1.52	3.00	825.92	9.95	1.85
6.00	1172.92	11.75	1.52				
10.00	1844.75	19.62	1.52				

Table A.5.13: *Flow rates, normalized differential pressures, bypass differential pressure of the solvent and viscosities of all solutions tested in experimental matrix M.*

Matrix M - 2µm filter							
LPS				**Polymer**			
3630S 300/10/CeB 0.5/4.21				**3630S 300/0/CeB 0.5/4.21**			
Q	**dP^*_{LPS}**	**Bypass dP_{brine}**	**Viscosity**	**Q**	**$dP^*_{Polymer}$**	**Bypass dP_{brine}**	**Viscosity**
[ml/min]	*[mbar/mPa·s]*	*[mbar]*	*[mPa·s]*	*[ml/min]*	*[mbar/mPa·s]*	*[mbar]*	*[mPa·s]*
3.00	216.10	5.28	1.52	3.00	326.52	5.28	1.85
10.00	767.14	21.91	1.52	7.00	992.77	17.43	1.85
15.00	1441.85	34.77	1.52				
20.00	2220.92	49.73	1.52				

Table A.5.14: *Flow rates, normalized differential pressures, bypass differential pressure of the solvent and viscosities of all solutions tested in experimental matrix N.*

Matrix L - 0.5µm filter			
Polymer			
3430S 300/0/CeB 1.0/3.42			
Q	**dP***	**Bypass dP**	**Viscosity**
[ml/min]	*[mbar/mPa·s]*	*[mbar]*	*[mPa·s]*
1.00	260.03	6.92	1.53
3.00	794.19	4.87	1.53
5.00	926.34	14.70	1.53
7.00	1247.06	14.43	1.53
9.00	2279.26	21.91	1.53

A.6. Plots for estimation of Qc

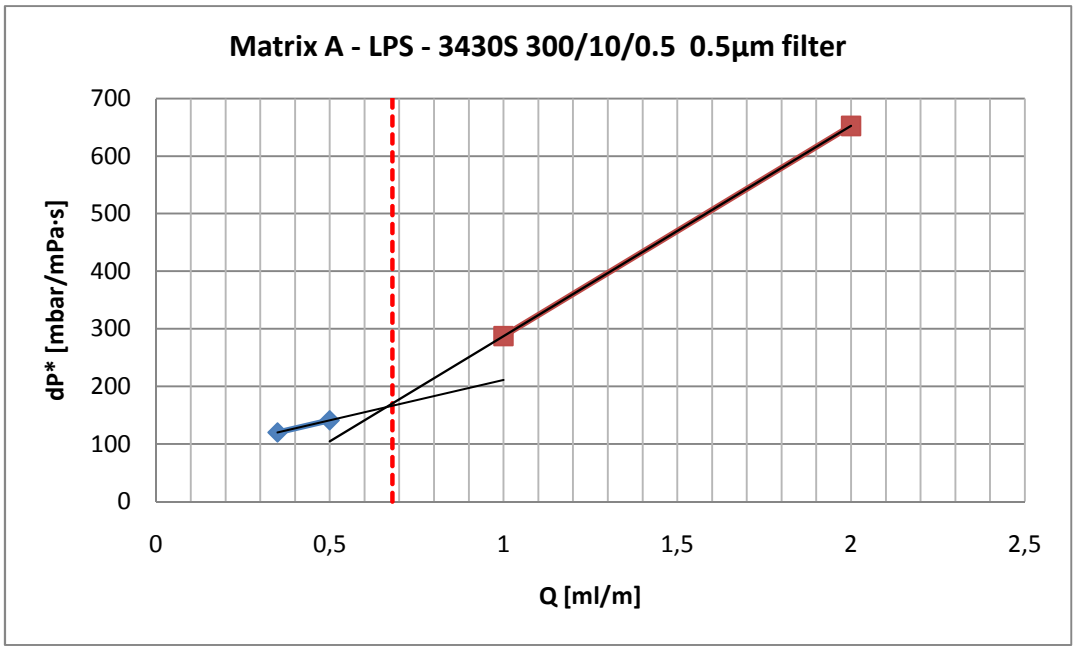

Figure A.6.1: *Determination of Qc by intersection of the linear extrapolations for each flow regime. The dotted red line indicates Qc.*

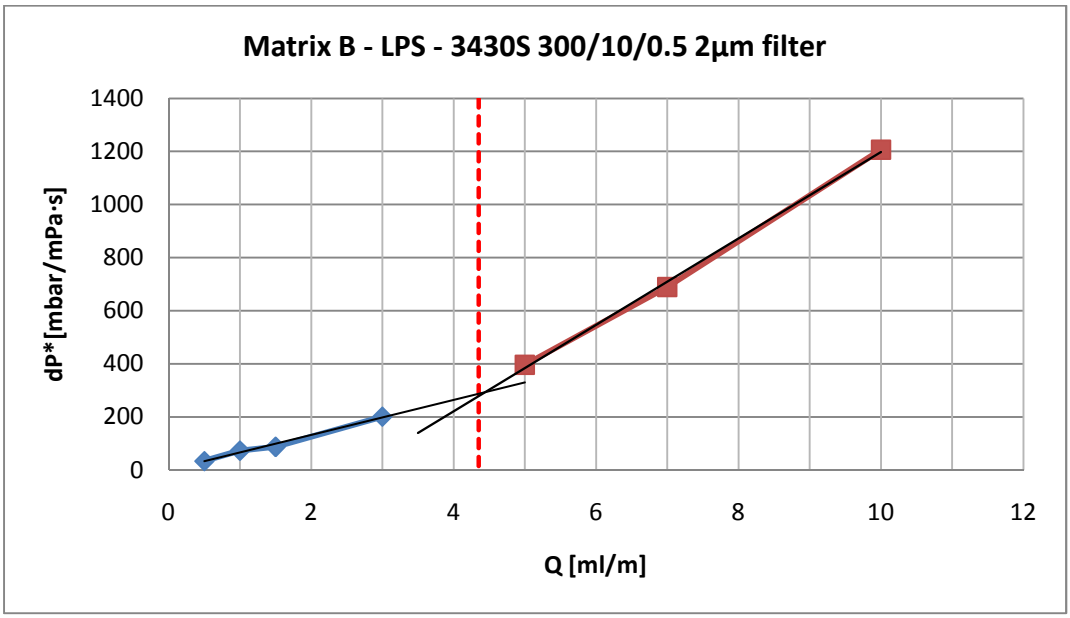

Figure A.6.2: *Determination of Qc by intersection of the linear extrapolations for each flow regime. The dotted red line indicates Qc.*

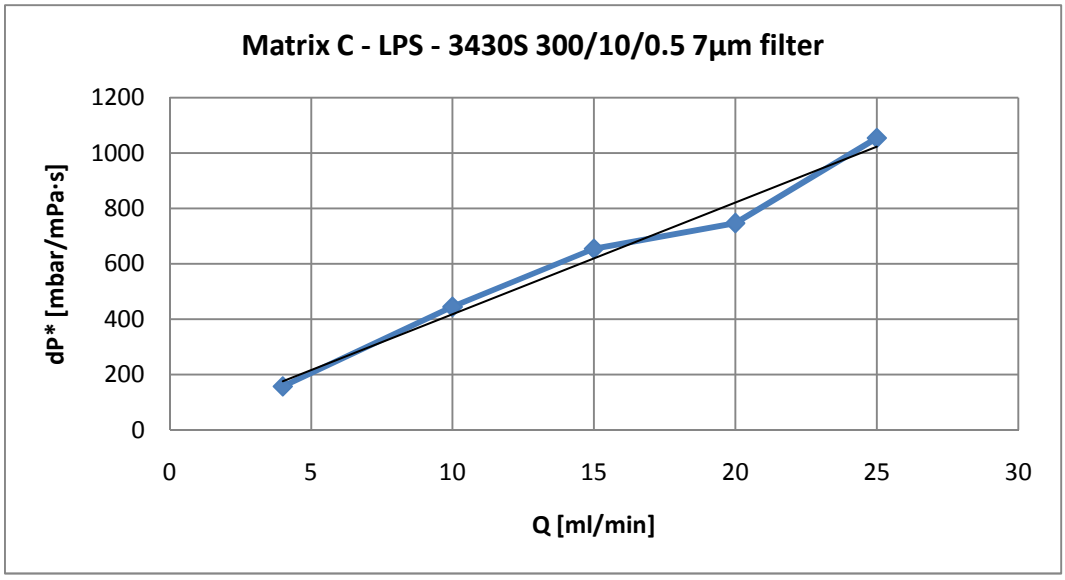

Figure A.6.3: *Determination of Qc by intersection of the linear extrapolations for each flow regime. Qc was not observed for this system.*

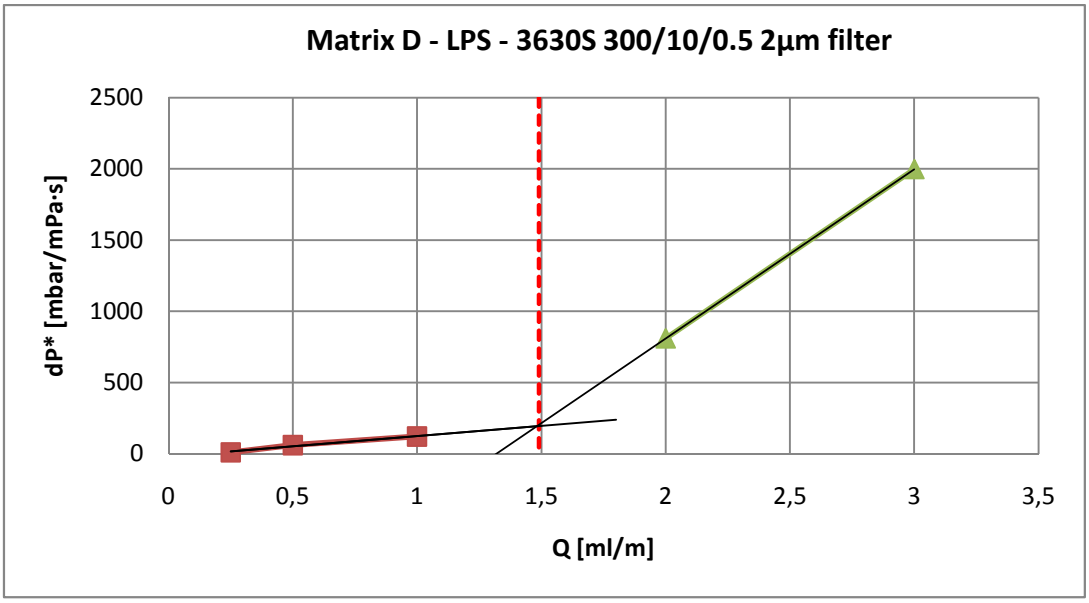

Figure A.6.4: *Determination of Qc by intersection of the linear extrapolations for each flow regime. The dotted red line indicates Qc.*

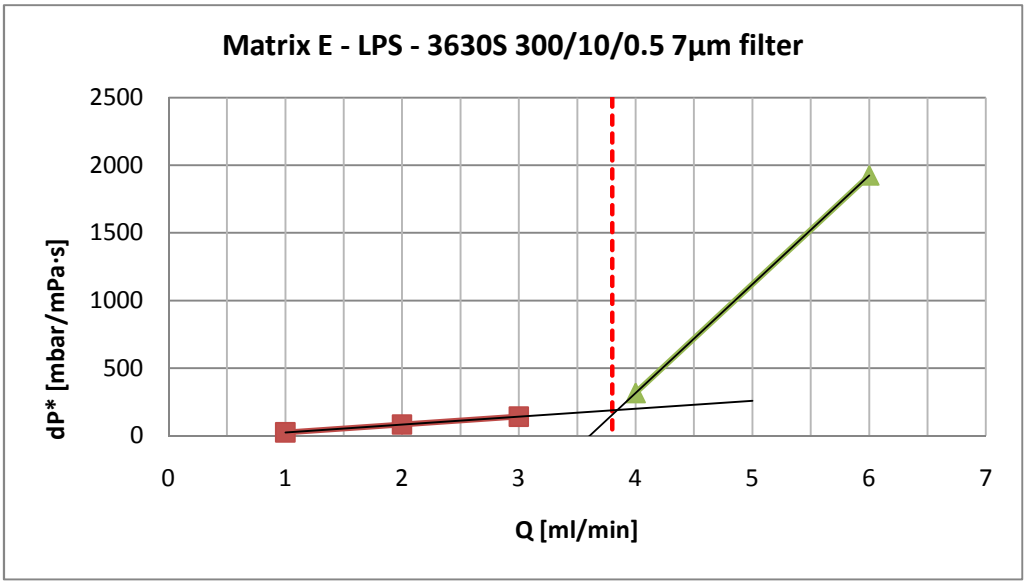

Figure A.6.5: *Determination of Qc by intersection of the linear extrapolations for each flow regime. The dotted red line indicates Qc.*

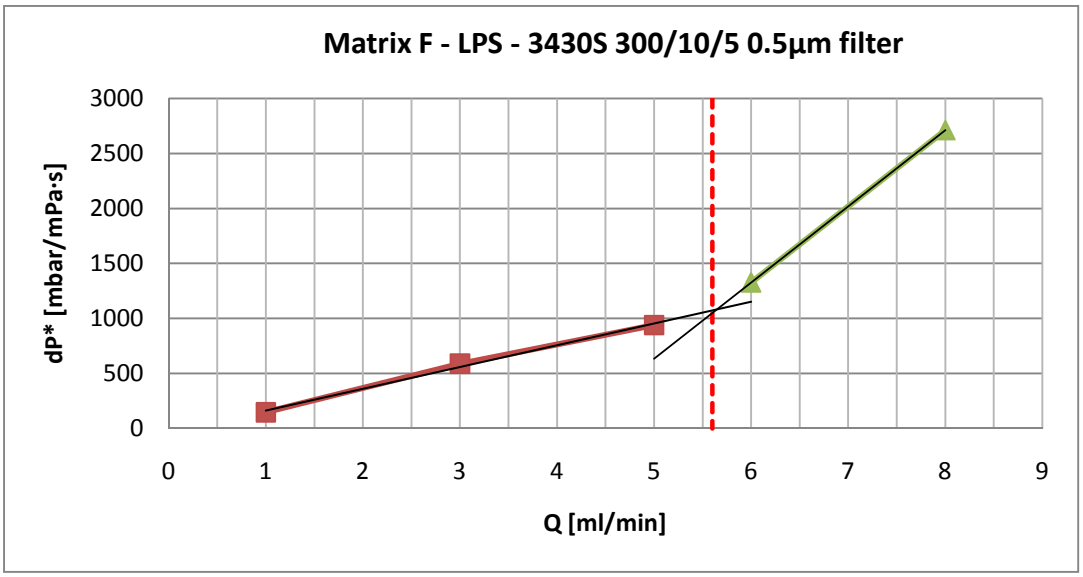

Figure A.6.6: *Determination of Qc by intersection of the linear extrapolations for each flow regime. The dotted red line indicates Qc.*

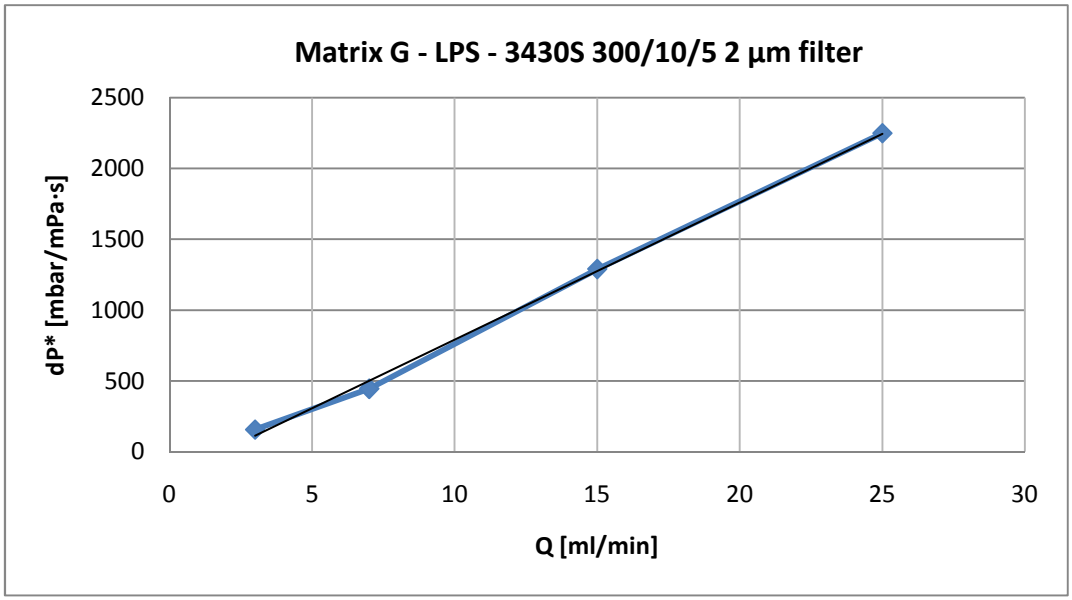

Figure A.6.7: *Determination of Qc by intersection of the linear extrapolations for each flow regime. Qc was not observed for this system.*

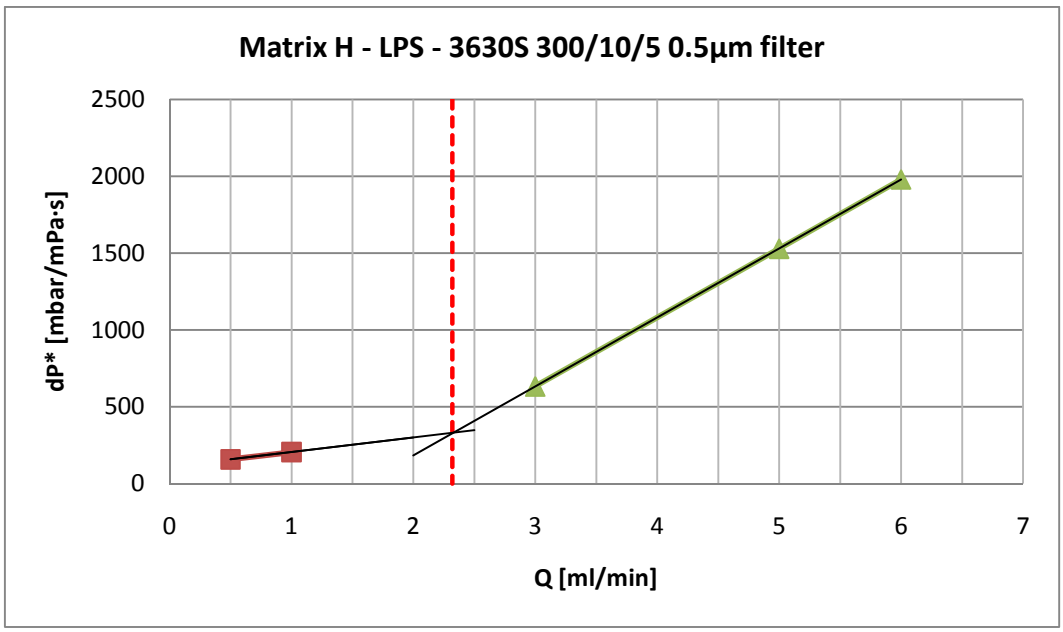

Figure A.6.8: *Determination of Qc by intersection of the linear extrapolations for each flow regime. The dotted red line indicates Qc.*

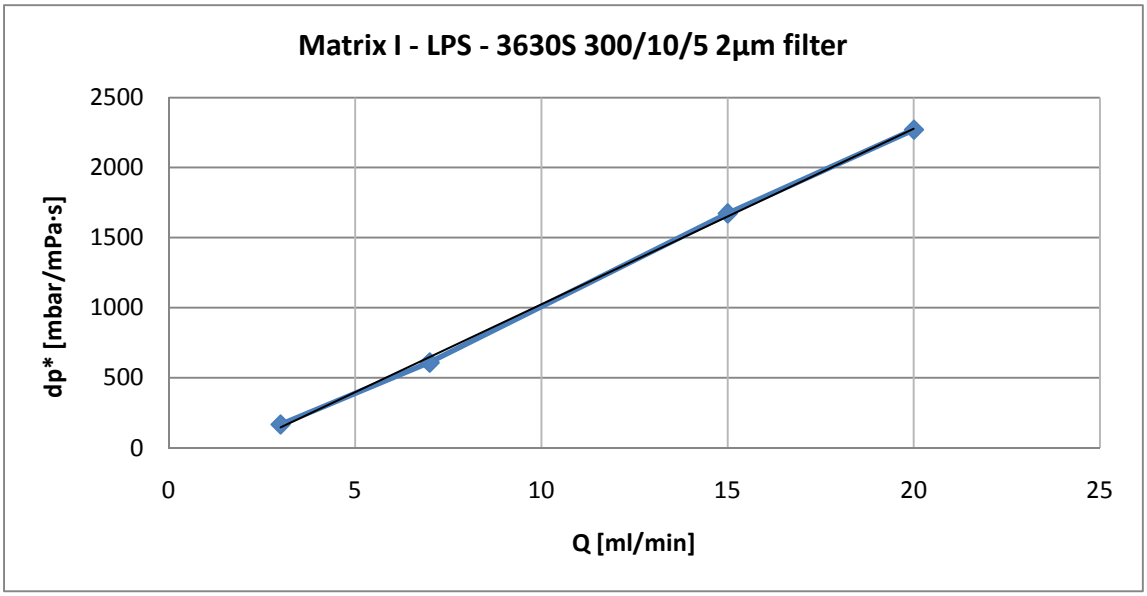

Figure A.6.9: *Determination of Qc by intersection of the linear extrapolations for each flow regime. Qc was not observed for this system.*

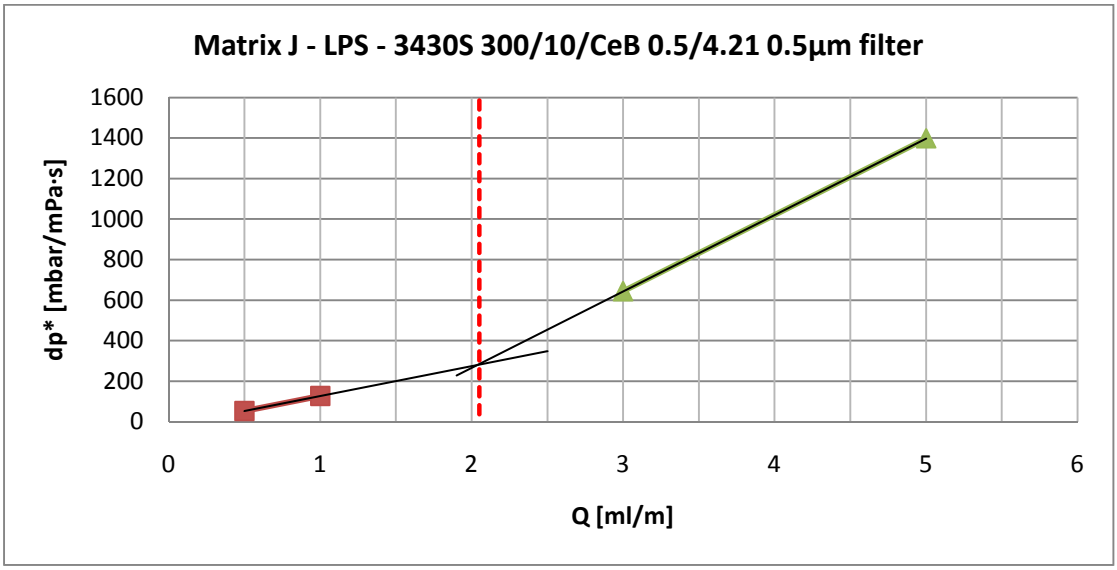

Figure A.6.10: *Determination of Qc by intersection of the linear extrapolations for each flow regime. The dotted red line indicates Qc.*

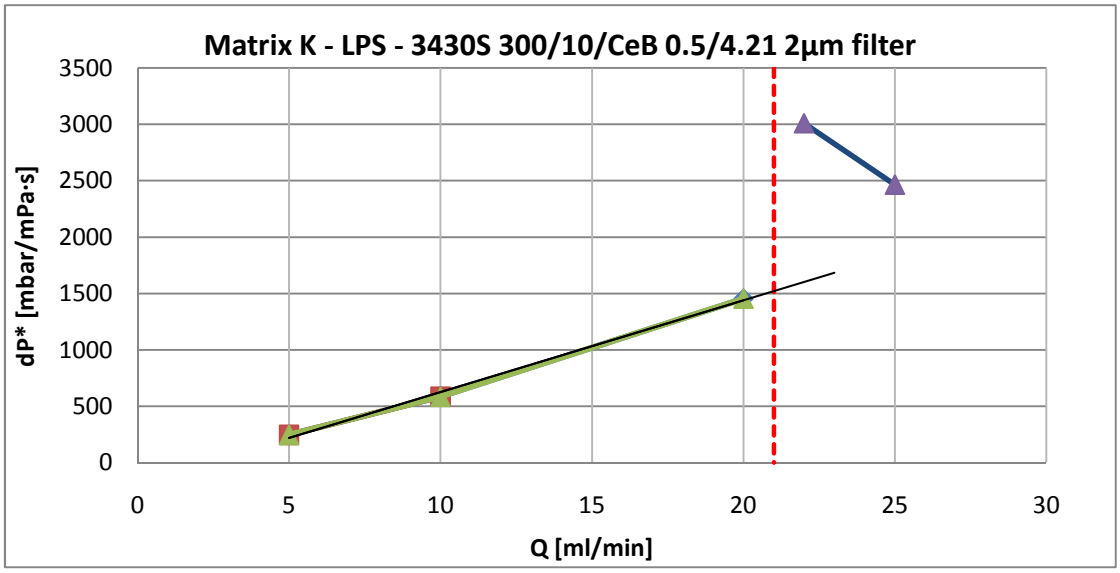

Figure A.6.11: *Determination of Qc by intersection of the linear extrapolations for each flow regime. No intersection was found for this matrix, thus Qc is estimated as the mean point between the two regimes. The dotted red line indicates Qc.*

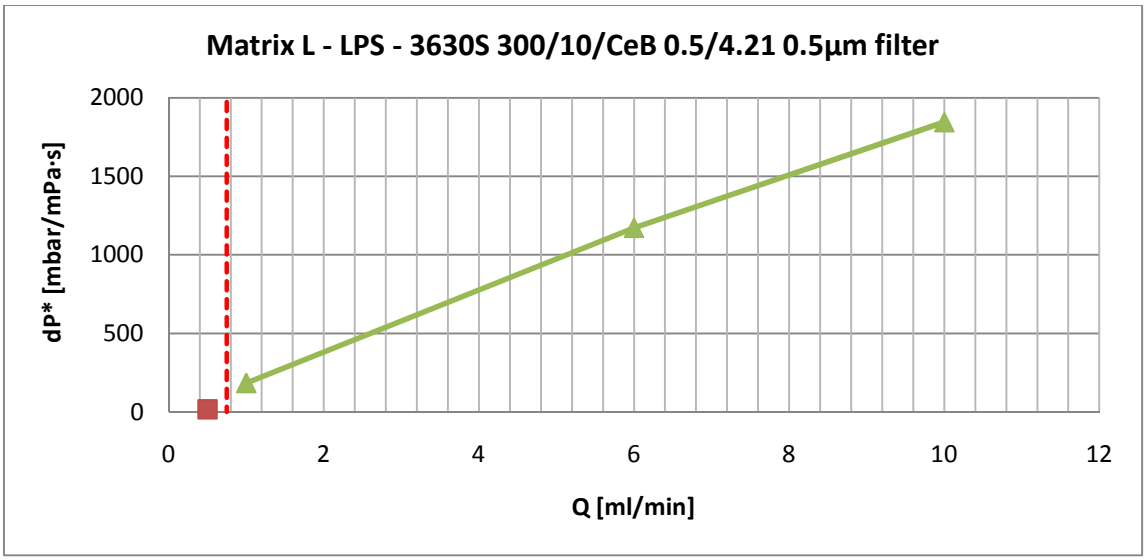

Figure A.6.12: *Determination of Qc by intersection of the linear extrapolations for each flow regime. No intersection was found for this matrix, thus Qc is estimated as the mean point between the two regimes. The dotted red line indicates Qc.*

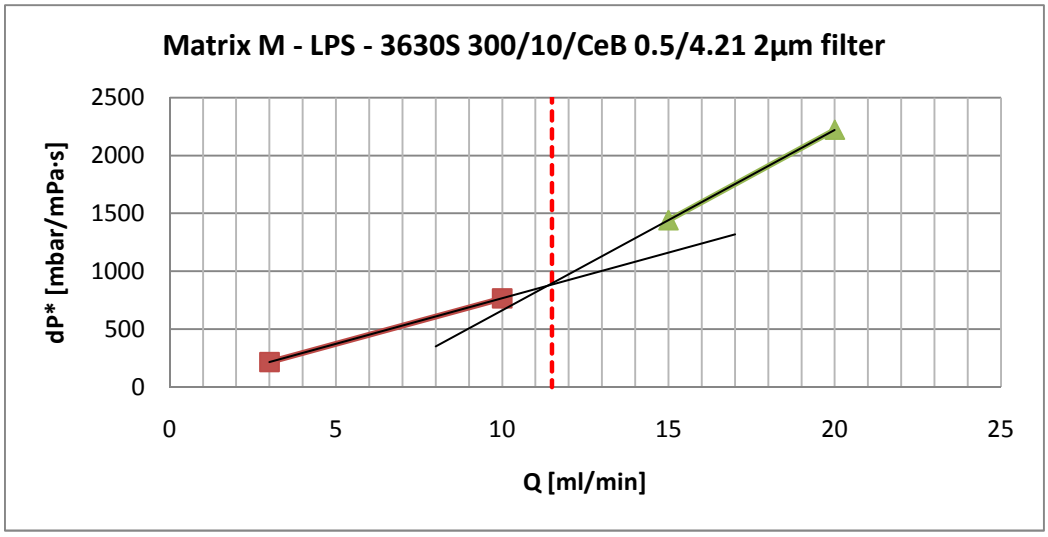

Figure A.6.13: *Determination of Qc by intersection of the linear extrapolations for each flow regime. The dotted red line indicates Qc.*

A.7. Relative differential pressures for constant- versus shear-dependent viscosity

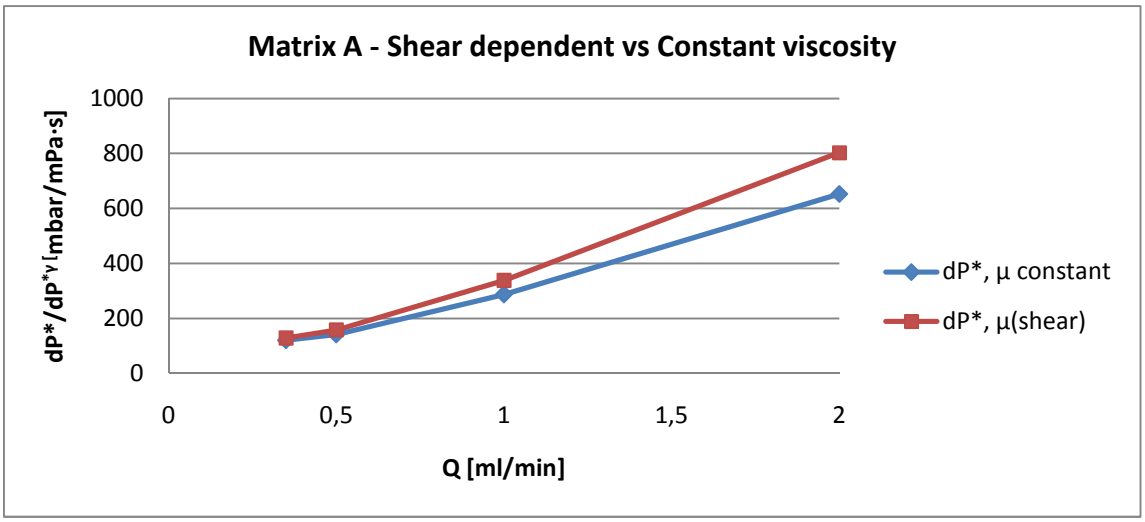

Figure A.7.1: *dP* and $dP^{*\gamma}$ as a function of flow rate for a 3430S 300/10/0.5 LPS solution injected over a 0.5µm filter.*

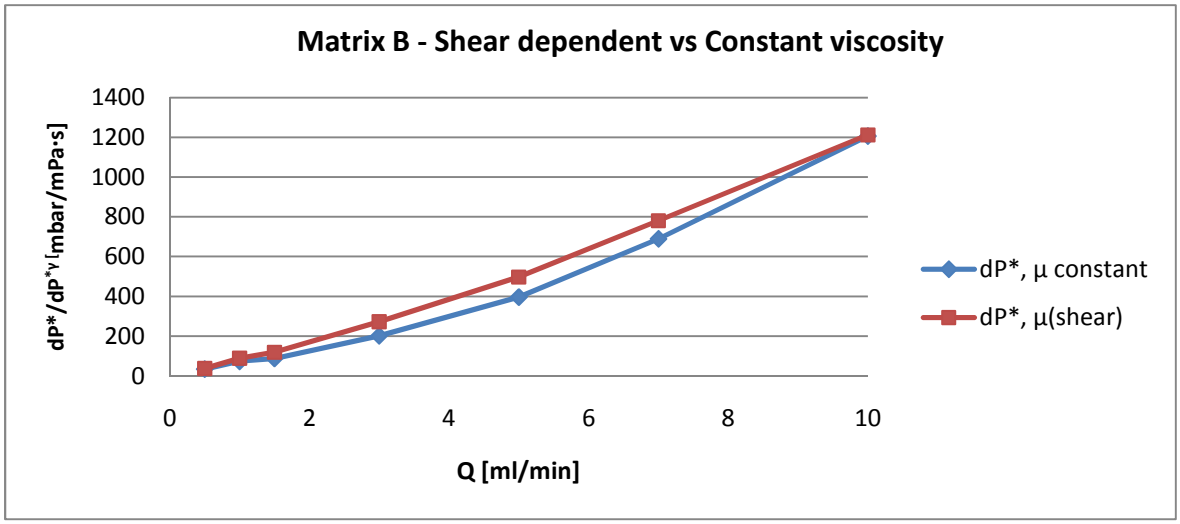

Figure A.7.2: *dP* and $dP^{*\gamma}$ as a function of flow rate for a 3430S 300/10/0.5 LPS solution injected over a 2µm filter.*

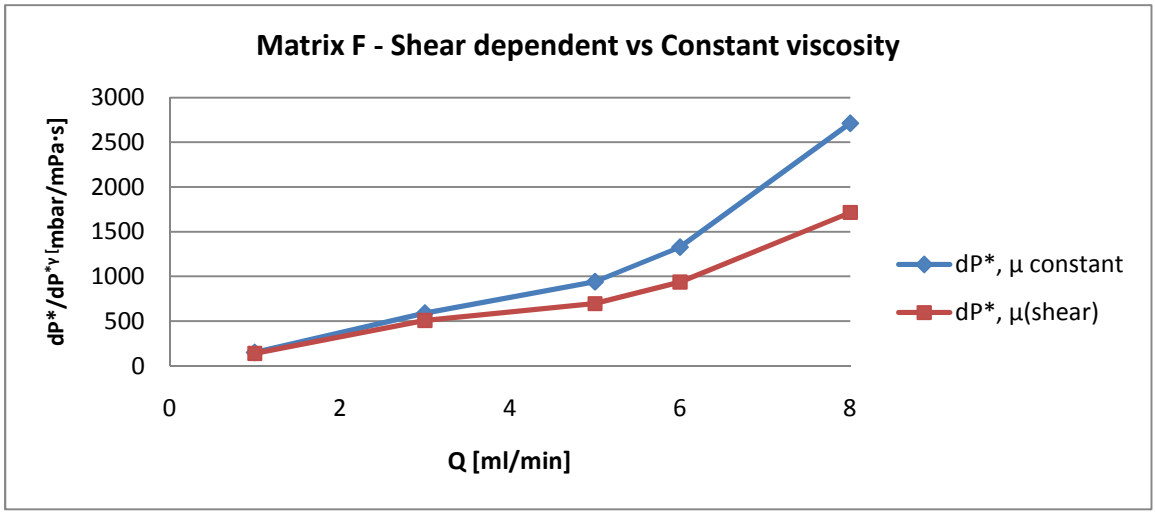

Figure A.7.3: *dP* and $dP^{*\gamma}$ as a function of flow rate for a 3430S 300/10/5 LPS solution injected over a 0.5µm filter.*

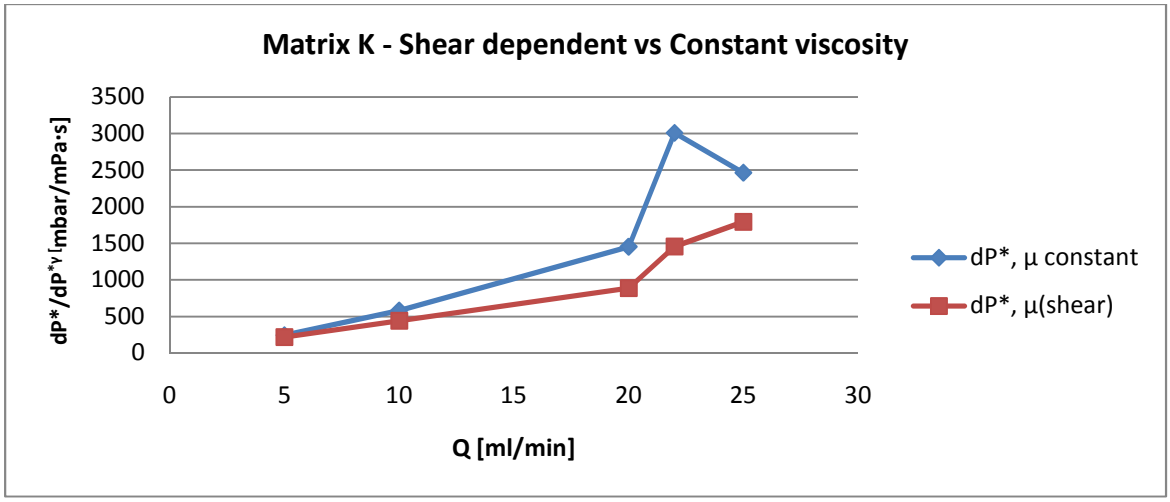

Figure A.7.4: *dP* and $dP^{*\gamma}$ as a function of flow rate for a 3430S 300/10/CeB 0.5/4.21 LPS solution injected over a 0.5µm filter.*

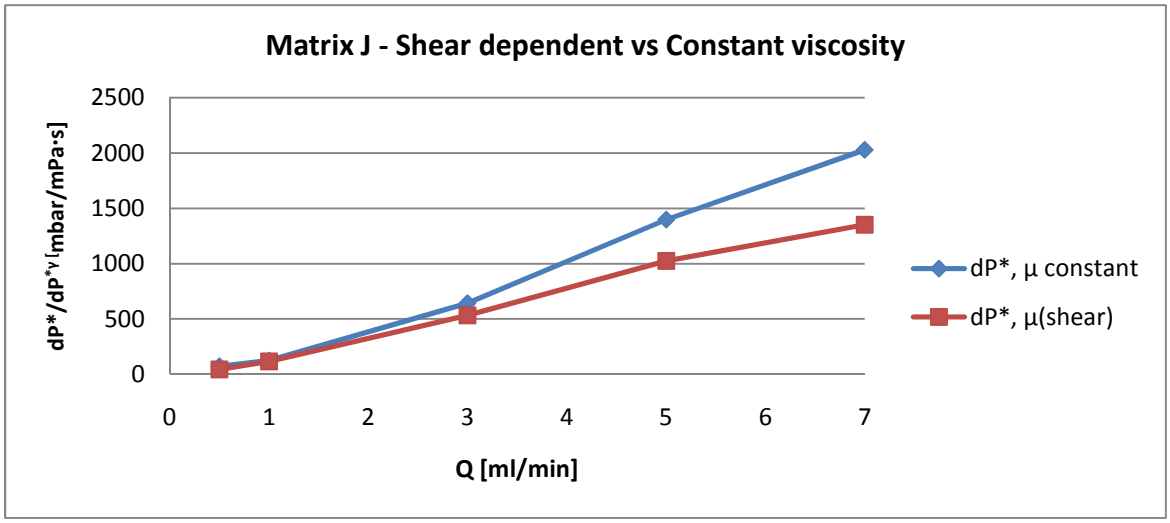

Figure A.75: *dP* and $dP^{*\gamma}$ as a function of flow rate for a 3430S 300/10/CeB 0.5/4.21 LPS solution injected over a 2μm filter.*

A.8. Models for non-Newtonian behaviour

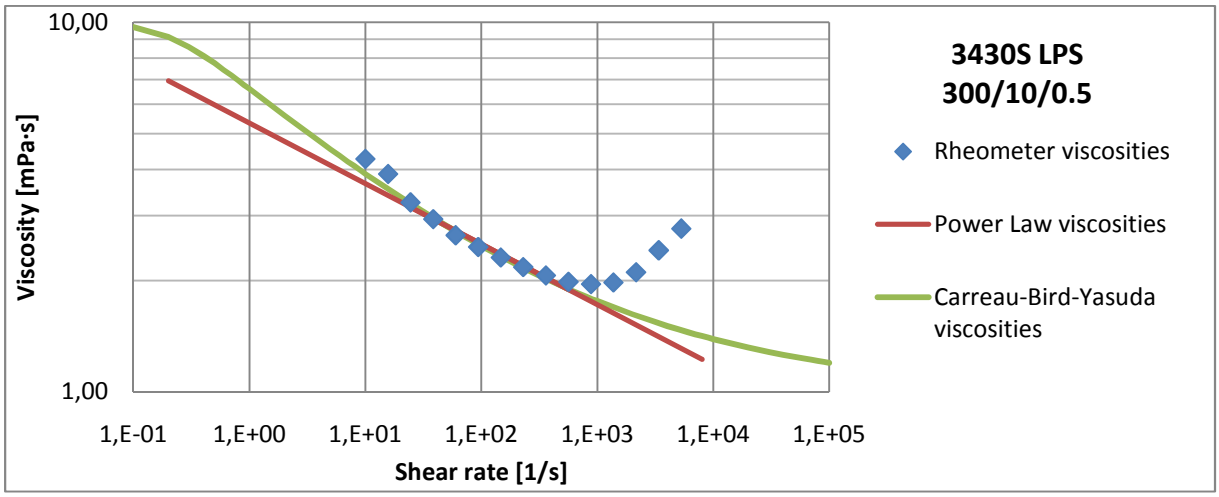

Figure A.8.1: *Measured viscosities compared to estimated viscosities by the Power Law- and Carreau-Bird-Yasuda models.*

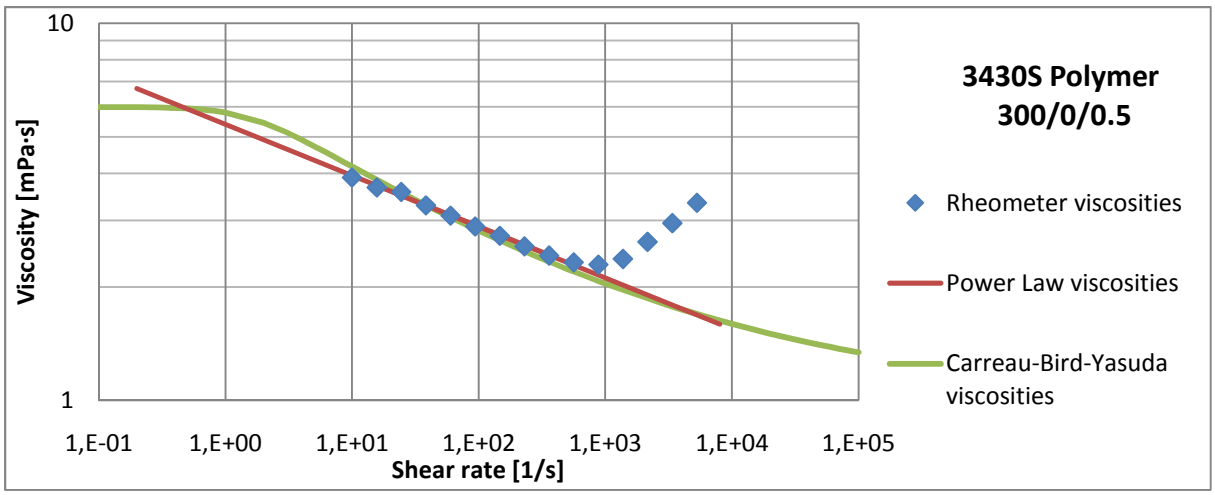

Figure A.8.2: *Measured viscosities compared to estimated viscosities by the Power Law- and Carreau-Bird-Yasuda models.*

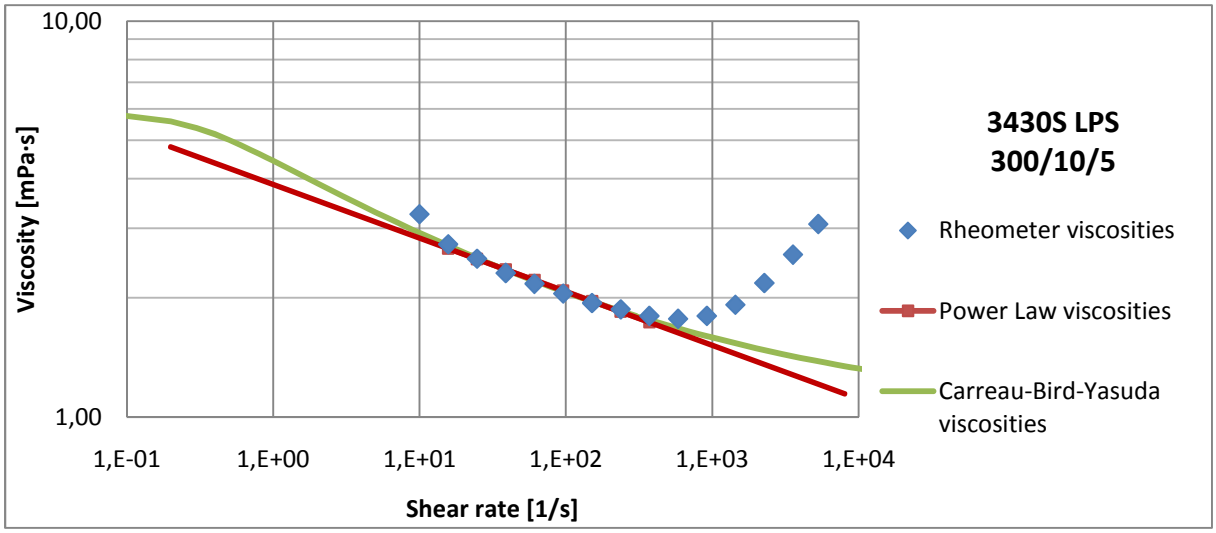

Figure A.8.3: *Measured viscosities compared to estimated viscosities by the Power Law- and Carreau-Bird-Yasuda models.*

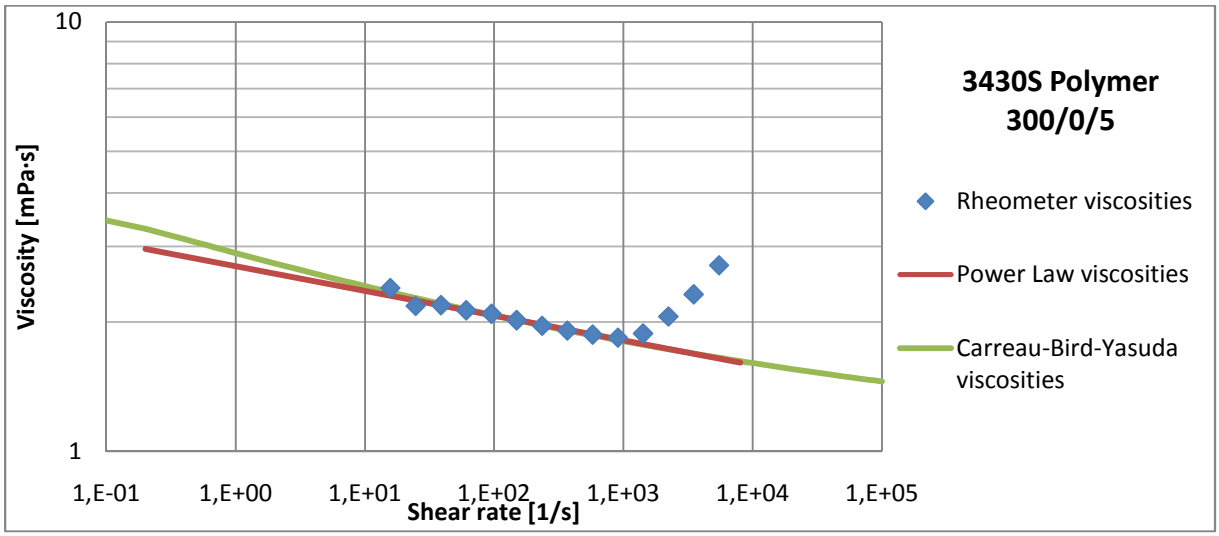

Figure A.8.4: *Measured viscosities compared to estimated viscosities by the Power Law- and Carreau-Bird-Yasuda models.*

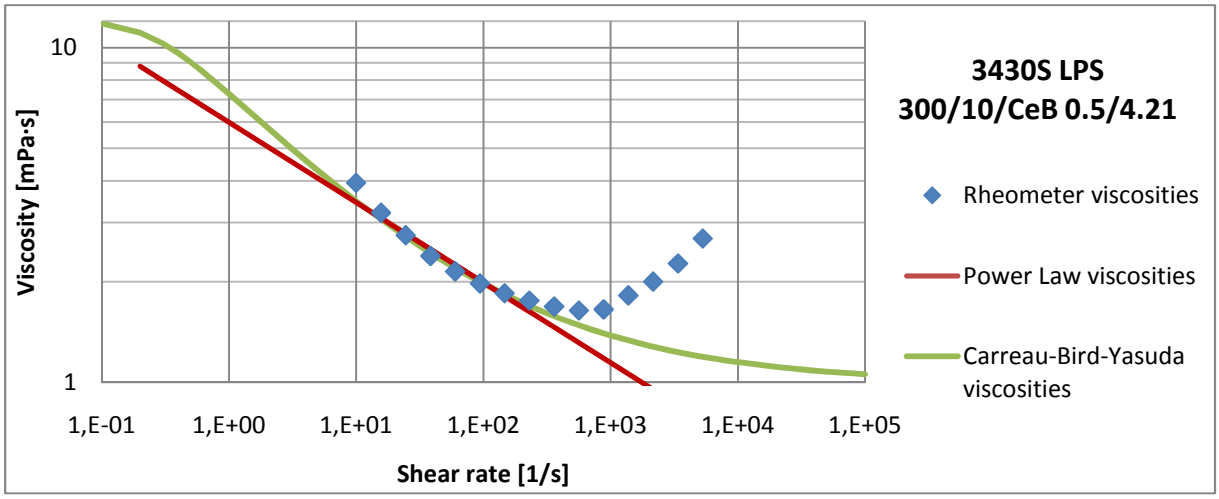

Figure A.8.5: *Measured viscosities compared to estimated viscosities by the Power Law- and Carreau-Bird-Yasuda models.*

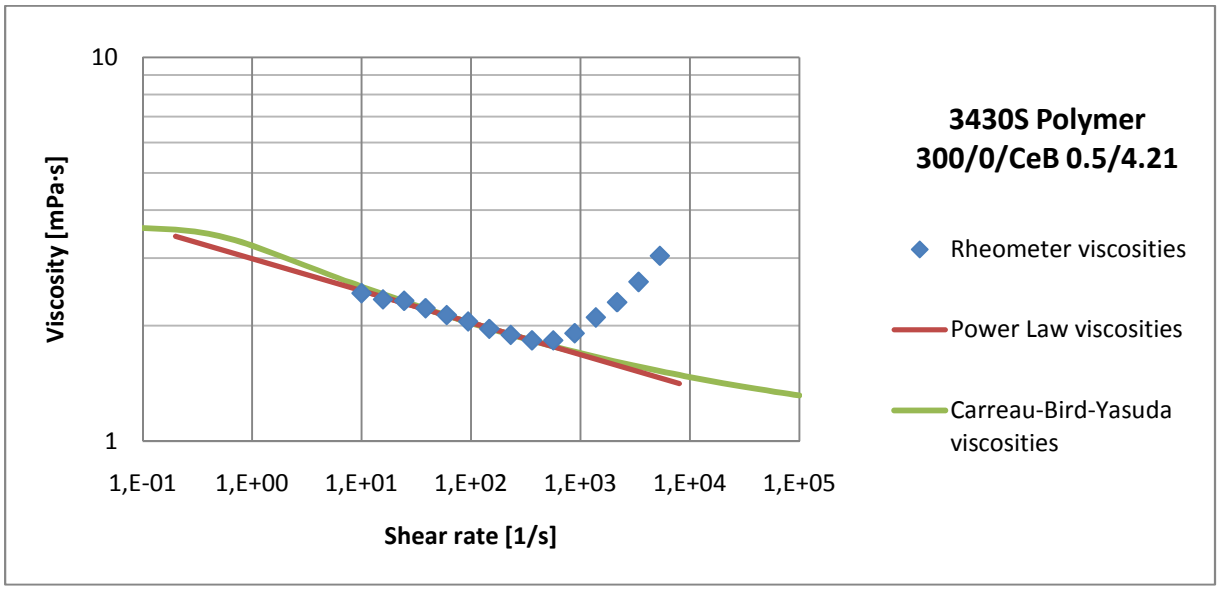

Figure A.8.6: *Measured viscosities compared to estimated viscosities by the Power Law- and Carreau-Bird-Yasuda models.*